Geophysical Journal International

Paleomagnetism from multi-orogenic terranes is "not a simple game": Pyrenees' Paleozoic warning

Journal:	*Geophysical Journal International*
Manuscript ID	GJI-21-0257
Manuscript Type:	Research Paper
Date Submitted by the Author:	16-Mar-2021
Complete List of Authors:	Pastor-Galán, Daniel; Tohoku Daigaku, Frontier Research Institute for Interdisciplinary Scieces; Universidad de Granada, Geodinánmica Groenhof, Oscar; Utrecht University Izquierdo-Llavall, Esther; LFCR Dinarès-Turell, Jaume; Istituto Nazionale di Geofisica e Vulcanologia Pueyo, Emilio L.; Instituto Geológico y Minero de España, Unidad de Zaragoza; www.igme.es/zaragoza/default.htm Dekkers, Mark; Utrecht University, Paleomagnetic Laboratory Fort Hoofddijk, Department of Earth Sciences
Keywords:	Palaeomagnetism < GEOMAGNETISM and ELECTROMAGNETISM, Remagnetization < GEOMAGNETISM and ELECTROMAGNETISM, Crustal structure < TECTONOPHYSICS, Folds and folding < TECTONOPHYSICS, Rock and mineral magnetism < GEOMAGNETISM and ELECTROMAGNETISM
Note: The following files were submitted by the author for peer review, but cannot be converted to PDF. You must view these files (e.g. movies) online.	
SF3.pub	

Paleomagnetism from multi-orogenic terranes is "not a simple game": Pyrenees' Paleozoic warning

Daniel Pastor-Galán[1,2,3], Oscar Groenhof[4], Emilio L. Pueyo[5], Esther Izquierdo-Llavall[6], Jaume Dinarès-Turell[7], Mark J. Dekkers[4]

[1]Frontier Research Institute for Interdisciplinary Science, Tohoku University, Japan

[2]Center for North East Asian Studies, Tohoku University, 980-8576, 41 Kawauchi, Aoba-ku, Sendai, Miyagi, Japan

[3]Department Earth Science, Tohoku University, Japan

[4]Paleomagnetic Laboratory 'Fort Hoofddijk', Utrecht University, The Netherlands

[5]Instituto Geológico y Minero de España. Unidad de Zaragoza. Spain

[6]Université de Pau et des Pays de l'Adour, E2S UPPA, CNRS, TOTAL, LFCR, Pau, France

[7]Istituto Nazionale di Geofisica e Vulcanologia, Roma, Italy

Summary

Paleomagnetism is a versatile tool in the Earth sciences: it provides critical input to geological time scales and plate tectonic reconstructions. Despite its undeniable perks, paleomagnetism is not without complications. Remagnetizations overprinting the original magnetic signature of rocks are frequent, especially in orogens which tend to be the areas with better rock exposure.

Unraveling the magnetic history of the rocks is a complicated task, especially in areas that underwent several orogenic pulses. In turn, constraining the timing of remagnetization represents an opportunity to solve post-magnetization structural and tectonic kinematics. Here, we evaluate the magnetization history of Silurian-Devonian carbonates from the Pyrenees (Spain). The Pyrenees are a multi-orogenic mountain belt where Silurian-Devonian rocks have seen the Variscan collision (late Paleozoic), the opening of the Atlantic-Biscay bay (early Cretaceous) and the Alpine orogeny (late Cretaceous to Miocene). Our results show widespread remagnetization(s) of the Silurian-Devonian series of the Pyrenees. The majority of the samples likely acquired their magnetization during waning episodes of the Variscan orogeny, i.e. late Carboniferous and early Permian times, although some apparently were subsequently remagnetized during the Alpine orogeny. The paleomagnetic results constrained that theVariscan orogeny was responsible for their main folding event, whereas the Alpine orogeny produced the thrusting and antiformal stacking of the Paleozoic rocks. In addition, we observed a general clockwise rotational pattern which could be related with the formation of the Cantabrian Orocline and/or rotations associated with the Alpine orogeny. The Silurian-Devonian carbonates are thus useful to understand the tectonic evolution of the Pyrenean mountain range after a systematic combination of paleomagnetism with structural and petrological observations. In contrast, the secondary character of magnetization and complications associated with the Variscan tectonics indicate that a reassessment of Siluro-Devonian poles from the Variscan elsewhere in Europe might be appropriate.

Keywords

Remagnetization, Pyrenees, Variscan, Alpine, Silurian-Devonian, orocline

1. Introduction

The Earth's magnetic field has left a remnant signature in the geological record through eons. These magnetic signals in the rock archive have been crucial to almost any field of Earth Sciences, from the development of plate tectonics (e.g., Vine and Matthews, 1963), to the development of global time scales (e.g., Kuiper et al., 2008) or the origin and evolution of the core (e.g., Biggin et al., 2015). Paleomagnetism is still the only available technique that can quantify pre-Jurassic paleolatitudes (Domeier and Torsvik, 2019), intensities of the past magnetic field, or global reference times through reversals. The paleomagnetic imprint in rocks can last billions of years but may be also fragile. For example, remagnetizations that overprint or even delete the original magnetic signature are ubiquitous, especially in orogenic belts (e.g., Pueyo et al. 2007, 2016a; Van der Voo and Torsvik, 2012; Huang et al. 2017). The majority of the studies associated with the preservation and reacquisition of a magnetic remanence in rocks are relatively recent. Remagnetizations were initially recognized already during the 1960's and remarked its importance in the 1980's (McCabe et al., 1983; McCabe and Elmore, 1989). However, they have been studied in particular detail only from the first two decades of the 21st century onward (c.f. van der Voo and Torsvik, 2012), when paleomagnetists and rockmagnetists realized to the full that a plethora of chemical and physical processes are capable of resetting the magnetic signature in a rock (e.g., Jackson et al., 1993; Weil and van der Voo., 2002; Dekkers, 2012; Pastor-Galán et al., 2017; Aubourg et al., 2019; Huang et al., 2020). Many paleomagnetic studies were performed before our current understanding of remagnetization processes. However, for a given region, time frame, or lithology, those older paleomagnetic data may be the only data available. There is an evident need to review and critically reassess such paleomagnetic information: regional and even global geologic interpretations are still grounded in them.

Remagnetization is often deemed a problem because it interferes with paleogeographic reconstructions that rely on the analysis of primary natural remanent magnetization (NRM), i.e. the age of the NRM is the same as the age of the sampled rock unit. However, despite the perceived loss of information, remagnetized rocks do represent valuable sources of geological information when it is possible to retrieve precisely the timing of the resetting of the orginal NRM acquisition, i.e. the remagnetization. Remagnetized rocks have been successfully used to unravel paleolatitudes of orogenic processes, orogenic kinematics, as geothermometers, to reconstruct inverted basins, … (e.g., Dinarès-Turell and García-Senz, 2000, Huang et al., 2015; Villalaín et al., 2016; Auburg et al., 2019; Izquierdo-Llavall et al., 2020). Rocks with complex orogenic histories – the rule in many orogens – present a myriad of complications including the timing of their NRM acquisition. In such settings, paleomagnetism can be an excellent tool to understand multiphase orogenic systems if wisely used in concert with other geologic tools.

In this paper, we reappraise the paleomagnetism from Silurian-Devonian limestones in the Pyrenean mountain belt, from which only three rather limited studies have been previously published (Tait et al., 2000; Gil-Peña et al., 2006; Izquierdo-Llavall et al., 2020). Our results, together with an enhanced geologic and paleomagnetic knowledge of the orogen, show that the sampled Silurian-Devonian carbonates were completely remagnetized during the late Carboniferous and Early Permian, when they experienced significant clockwise vertical axis rotations. These rocks were partially overprinted yet another time during the Cenozoic times, and experienced tilting and vertical axis rotations related to both the opening of the Bay of Biscay in the Late Mesozoic and the Cenozoic building of the Alpine chain in the Pyrenees. The magnetization history of the Pyrenees is a warning for paleomagnetists beautifully illustrated in Chris Scotese's anagram: PALEOMAGNETISM = NOT A SIMPLE GAME (Van der Voo, 1993).

2. The Pyrenean mountain belt

The Pyrenees are a mountainous barrier that separates the Iberian Peninsula from the rest of Eurasia. They are a prime example of the superposition of different tectonic events: (1) the multiphase late Paleozoic Variscan orogeny; (2) the Jurassic and early Cretaceous major extension during the opening of the Atlantic Ocean and the formation of the Bay of Biscay; (3) the opening of a seaway including the exhumation of the mantle between the Neotethys and Atlantic Oceans along the current Pyrenees; (4) the subduction of this previously opened seaway in the late Cretaceous; and (5) the final collision between Iberia and Eurasia during the Cenozoic (Muñoz, 1992; 2019 and references therein).

2.1 Paleozoic History: Variscan cycle

The tectonic evolution of the Paleozoic era was dominated by the progressive amalgamation of most continents into Pangea (e.g., Domeier and Torsvik, 2014; Domeier, 2016), the latest supercontinent (Pastor-Galán et al., 2019a). In western Europe the Pangean amalgamation history is recorded in the Variscan orogen, which sutured the continents of Gondwana and Laurussia along with a variable number of smaller plates that likely drifted away from Gondwana (e.g., Nance et al., 2010). On the basis of paleomagnetic data, Iberia has been considered part of a ribbon continent (usually named Armorica, Galatia, or Hun) that detached from Gondwana and drifted to the north or northwest in the Late Silurian or Early Devonian (e.g., van der Voo, 1993; Tait et al., 2000; Tait, 1999; Stampfli et al., 2013; Domeier and Torsvik, 2014). Other authors, however, place Iberia along the passive margin of Gondwana throughout the Paleozoic based on the fossil record or the provenance of detrital zircons (e.g., Robardet, 2003; Pastor-Galán et al., 2013a). Convergence leading up to the Variscan orogen started ca. 420 Ma (e.g., Franke et al., 2017) and continued until the complete consumption of the Rheic ocean and other minor oceanic basins that existed between Gondwana and Laurussia at ca. 280 Ma; (e.g., Pastor-Galán, 2020). The final continent–continent collision was diachronic and became progressively younger westwards (in present-day coordinates) with Devonian continent–continent collision along the eastern boundary of the Variscan orogen, progressing to earliest Permian ages in the westernmost sector (e.g., Pastor-Galán et al., 2020 and references therein).

Iberia has the largest exposure of the Variscan orogen in Europe, and an almost continuous cross section of the orogen (e.g., Azor et al., 2019). The majority of the Paleozoic outcrops in Iberia contain Gondwanan affinity rocks (e.g., Pastor-Galán et al., 2013a; Casas et al., 2019) and only a little sector of Southwest Iberia shows Laurussian affinity (e.g., Pérez-Cáceres et al., 2017). Geographically, the external zones of the Gondwana margin are nested to the north into the core of the Cantabrian Orocline (Fig. 1A), whereas the hinterland zones are to the west, center and northeast of Iberia (Fig. 1A; e.g., Azor et al., 2019). The stratigraphy of the Gondwanan authochton consists of Neoproterozoic arc rocks (e.g., Fernández-Suárez et al., 2014), which evolved to a rift-to-drift sequence during the Cambrian to early Ordovician and then to an Ordovician to late Devonian passive margin basin sequence (e.g., Gutiérrez-Alonso et al., 2020). During the Carboniferous and early Permian, the rocks recorded up to 6 phases of deformation (e.g., Dias da Silva et al., 2020; Pastor-Galán et al., 2020 and references therein), metamorphism (e.g., Ribeiro et al., 2019) and synorogenic sedimentation processes that evolved to post-orogenic and intracontinental style basins during the Permian (e.g., Oliveira et al., 2019).

The trend of the Variscan belt in Iberia follows a “S” shape; to the north and convex to the west is the Cantabrian Orocline, and to the center-south and convex to the east is the Central Iberian curve (e.g., Pastor-Galán et al., 2020). To the north, the Cantabrian Orocline displays a curvature of approximately 150°. In eastern Iberia the Cantabrian Orocline seems isoclinal, but this is likely the product of a retightening during the Alpine orogeny (e.g., Pastor-Galán et al., 2011; Leite Mendes et al., 2021; Fig. 1A). All kinematic data studied so far support a model in which the Cantabrian Orocline formed due to secondary vertical-axis rotation in a period of time later than 315 Ma and earlier than 290 Ma. Overall, the southern limb of the orocline rotated counterclockwise (CCW) and the northern limb clockwise (CW; e.g., Weil et al., 2013). Orocline formation postdates the main Variscan orogenic phases (e.g., Pastor-Galán et al., 2015a). The development of the Cantabrian Orocline implies the existence of a roughly linear orogenic belt during the early Variscan closure of the Rheic Ocean (with an approximately N–S orientation in present-day coordinates), which was subsequently bent in map-view into an orocline during the late stages of Pangea's amalgamation. This interpretation is grounded in extensive paleomagnetic, structural and geochronological studies (e.g., Weil et al., 2001; Pastor-Galán et al., 2014; Shaw et al., 2015; Gutiérrez-Alonso et al., 2015). The more southern Central Iberian curve has a similar magnitude, but opposite curvature compared to the Cantabrian Orocline (Fig. 1A), although its exact geometry is uncertain because this structure is largely covered by Mesozoic and Cenozoic basins (e.g., Pastor-Galán et al., 2020; Fig. 1A). The curvature is most recognizable at the boundary between the Galicia–Tras-os-Montes and Central Iberian zones (e.g., Aerden, 2004; Martínez Catalán, 2012). The most recent geometric and kinematic investigations suggest that the Central Iberian curve is not a structure formed by differential vertical-axis rotation as the Cantabrian Orocline, but one formed as a consequence of several complex, complementary and successive tectonic processes (e.g., Pastor-Galán et al., 2018).

The Palaeozoic rocks of the Pyrenees form the backbone of the chain and crop out in two areas (the Axial Zone and the Basque Massif, to the east and west, respectively) that define an E-W elongated strip unconformably overlain by Mesozoic and Cenozoic rocks (Fig. 1A and B). These outcrops are geographically disconnected from neighboring Paleozoic outcrops of the Catalan Coastal Range and

Balearic to the southeast, the Mouthoumet and Montagne Noire (southern French Central massifs) to the north, Corsica-Sardinia to the east and the Iberian Massif to the west and southwest. The pre-Permian rocks of the Pyrenees recorded a polyphase deformation during the Variscan orogeny with metamorphism that ranges from absent to high grade (e.g. Casas et al., 2019). So far, no relics of early Variscan deformation and/or subduction related high pressure metamorphism have been found. Most palaeogeographic reconstructions suggest that the Pyrenean Paleozoic outcrops (Fig. 1) may be equivalent to the northern branch of the Cantabrian Orocline (e.g. García-Sansegundo, 2011; Pastor-Galán et al., 2020). Deformation, structural style and metamorphic grade show important differences along strike in the Pyrenees (Autran and García-Sansegundo, 1996; Debon and Guitard, 1996). The superposition of the later Mesozoic extension and subsequent Alpine orogeny markedly complicate an integral interpretation of the Variscan portions of the Pyrenees (see Casas et al., 2019). As a consequence, a comprehensive scheme integrating all the available data is lacking despite decades of geological research (e.g., de Sitter and Zwart, 1959; Kleinsmiede, 1960; Zwart, 1979; 1986). In general terms, the Silurian, Devonian and Carboniferous successions show no to low-grade metamorphism and are composed of carbonates and shales (e.g., Casas et al., 2019). During the Carboniferous and Early Permian, the Pyrenees recorded an intense igneous activity including syn- to post-kinematic plutonism and volcanism (Fig. 1B; e.g., Gleizes et al., 1997, 2003; Denèle et al., 2011, 2014; Porquet et al., 2017), sometimes interpreted as subduction related (e.g., Pereira et al., 2014).

2.2 Mesozoic to present day evolution: Alpine cycle

The final break-up of Pangea is marked with the opening of the Central and South Atlantic from late Triassic times onward (e.g., Müller et al., 2019). During the Jurassic, Iberia was attached to Europe and North America as another piece of Laurasia. In the Cretaceous, the breakup and spreading in the North Atlantic led to the separation of the Iberian microplate from Eurasia, North America and Africa (e.g., Vissers and Meijer, 2012). During the North Atlantic breakup, the Bay of Biscay opened, leading to approximately 35° of counterclockwise (CCW) rotation of Iberia (Van der Voo, 1969; Neres et al., 2013) probably during the Aptian (Juárez et al., 1998; Gong et al., 2008). The opening of the Bay of Biscay to the west got recorded in the Pyrenees with the formation of a hyperextended margin with mantle exhumation during the Albian–Cenomanian (e.g. Lagabrielle et al., 2010). The rotation of Iberia, together with the increased convergence between Africa and Eurasia culminated in the collision between Iberia and Eurasia to form the Pyrenean range during Late Cretaceous-Miocene in the frame of the Alpine orogeny (e.g., Muñoz, 2019).

Paleozoic rocks in the Spanish Pyrenees occur in three main Alpine thrust sheets (Muñoz 1992, 2019; Barnolas et al., 2019) that provoked over 100 km of N-S shortening. So, the original position of the Palaeozoic rocks should be located northward from their present-day arrangement. The outcrops of Paleozoic rocks in the Axial Zone have witnessed more than 7000 meters of basement stacking (measured between the Balaitous peak and the San Vicente drill core; Fig. 1B; Lanaja, 1987). The geometry and kinematics of the thrust units affecting the Paleozoic rocks are not fully understood because of the complex superposition of deformation events and the unclear relationships with cover units where syntectonic sedimentation plays a key role to assign kinematic ages (Oliva-Urcia, 2018). Numerous structural studies (e.g., Muñoz et al., 1986, 2019; Muñoz, 1992; Puigdefábregas et al., 1992; Teixell, 1996, Millán et al., 2000; Martínez-Peña and Casas, 2003; Casas et al., 2003; Millán et al., 2006; Labaume et al., 2016; Labaume and Teixell, 2018) have identified a general Alpine piggy-back thrust sequence affecting the Paleozoic rocks (Fig. 2). Besides, numerous fission-track data on granites (Fitzgerald et al., 1999; Jolivet et al., 2007), on detrital rocks (Beamud et al., 2011; Bosch et al., 2016; Labaume et al., 2016) as well as $^{40}Ar/^{39}Ar$ and U/Pb dating of samples directly taken from fault planes (Abd Elmola et al., 2018) and calcite veins (Hoareau et al., 2021), see also recent reviews by Oliva-Urcia, 2018 and Calvet et al., 2020, and references therein), have improved the chronology of emplacement and exhumation of the basement units and their relationship with the cover ones. Basement thrusts partly reactivated previous Variscan, late-Variscan and/or Mesozoic structures. The Alpine structure defines an imbricate thrust system (Fig 2) with a progressively increasing vertical overlap between the basement units from west (Fig. 2A) to east where thrusts define an antiformal stack (Fig. 2C). Basement units in the west include three thrusts in the central sector: Millares (Paleocene), Bielsa (Eocene) and Gavarnie (Eocene-Oligocene); and an undetermined number in the western sector (for example Lakora-Eaux Chaudes (Upper Cretaceous-Paleocene- even Eocene); Gavarnie (Eocene); Guara-Gedré (Eocene-Oligocene), Fiscal-Broto(Oligocene), and Guarga (Oligocene-Miocene, not indicated in Fig. 2). In the eastern sector main basement units are recognized, from the North to the South: Nogueras (emplaced in the Paleocene), Orri (Eocene), and Rialp (Oligocene). In the South Pyrenean Zone, all these basement units connect with an imbricate fold-and-thrust system with different Mesozoic and Cenozoic décollements (Cretaceous shales, Eocene marls and Upper/Middle Triassic evaporites); their geometry is controlled by salt-tectonics and Mesozoic inheritance (Millán et al., 2000; Huyghe et al., 2009; Labaume et al., 2016; Oliva-Urcia, 2018; Labaume and Teixell, 2018; Calvín et al., 2018; Santolaria et al., 2020; Muñoz et al., 2021).

Thrusting was associated with important foreland flexure and foreland succession deposition both in the Northern Pyrenees (France; Biteau et al., 2006) and the Southern Pyrenees (Spain; Puigdefàbregas, 1975). Foreland deposits partly covered the Paleozoic units of the Axial Zone in the early orogenic stages and were subsequently exhumed and eroded (Beamud et al., 2011; Fillon and Van der Beek, 2012). The early, maximum burial conditions in the sampled portion of the Axial Zone are partly constrained by paleothermal studies in the overlying Meso-Cenozoic cover units (Izquierdo-Llavall et al., 2013; Labaume et al., 2016). They indicate Cenozoic-age, maximum temperatures of 160-190 ºC in the Upper Cretaceous units of the western Axial Zone (Izquierdo-Llavall et al., 2013) that increase up to ~250 ºC in the Eocene tubidites to the center of the Southern Pyrenean Zone. These values indicate that maximum temperatures in the underlying Paleozoic rocks were higher than 200-250 ºC during the Cenozoic. They are in agreement with thermal modelling results of the Panticosa intrusion (Bosch et al., 2016) that indicate peak burial temperatures of ~300 ºC during the Oligocene. In the central Axial Zone, thermal models for the Paleozoic units of the Gavarnie and Orri units reveal peak temperatures below 300ºC that were attained during the Early Paleogene (Waldner, 2019). Cenozoic burial favored the development of Alpine cleavage in the western Axial Zone (Choukroune and Séguret, 1972; Matte et al., 2000). Conversely, in the central Axial Zone Alpine cleavage developed only locally, the main cleavage being Variscan in age (Muñoz, 1992).

2.3 Paleomagnetism in the Pyrenees

Paleomagnetic investigations in the Pyrenees commenced with the pioneering studies of Van der Lingen (1960) and Schwarz (1963) in some Paleozoic rocks from the center of the Pyrenees. The available database has grown substantially during the following decades due to the excellent outcrop conditions (including world class stratigraphic sequences), the general exposure of synorogenic material throughout the chain allowing an accurate dating of deformation, the existence of well-exposed zones of lateral transference of deformation, etc. At present, the Pyrenean chain represents one of the most densely and homogeneously sampled paleomagnetic databases worldwide (Pueyo et al., 2017). Despite the quality and amount of paleomagnetic data in the Pyrenees, the Pyrenean Paleozoic rocks have remained largely unexplored. In the Axial Zone, very few data are known from sites older than Permian–Triassic red beds (Van Dongen, 1967; McClelland and McCaig, 1988, 1989; Keller et al., 1994; Tait et al., 2000; Gil-Peña et al., 2006; Izquierdo-Llavall et al., 2014, 2020; Ramón et al., 2016). And, to our knowledge, in the Pyrenees only three paleomagnetic studies collected and analyzed a limited number of sites dating from older than late Carboniferous (Stephanian) age: Tait et al. (2000), Gil-Peña et al. (2006), and Izquierdo-Llavall et al. (2020). The two latter studies found the rocks remagnetized in the Late Carboniferous and Paleogene, respectively. Previous studies in late Carboniferous and early Permian rocks (Izquierdo-Llavall et al., 2014) revealed shallow inclinations and clockwise rotations of ~40°. Gil-Peña et al. (2006) showed analogous rotations (~50° CW) for the Ordovician rocks that remagnetized during these times.

The relatively good paleomagnetic control on undeformed areas in the vicinity of the Pyrenees (e.g., Garcés et al., 2020; Oliva-Urcia and Pueyo, 2019) allows to define a reliable reference paleomagnetic direction and to understand the post-Variscan (late Permian to Eocene) magnetization and tectonic history during the Alpine orogeny in the Pyrenees. In the South Pyrenean Zone, significant rotations both CW and CCW (40-60°) derived from proven primary paleomagnetic records from rocks of ages ranging from Permo-Triassic (e.g., Larrasoaña et al., 2003) to Oligocene (e.g., Sussman et al., 2004) are found in the most external cover units in relation to lateral ramps in thrust sheets. These rotations are especially evident nearby the boundaries of the so-called South Pyrenan Central Unit (e.g., Sussman et al., 2004; Mochales et al., 2012, 2016; Muñoz et al., 2013; Rodriguez-Pintó et al., 2016) but also in the most external thrust units (Pueyo et al., 2021a, 2021b). Other moderate vertical axis rotations (15-25° CW and CCW) occur in the Permo-Mesozoic structural units immediately to the south of the Axial Zone: The Internal Sierras (Larra-Monte Perdido units; Oliva-Urcia and Pueyo, 2007a, 2007b; Oliva-Urcia et al., 2008; Izquierdo-Llavall et al., 2015), the Nogueras thrust unit (McClelland and McCaig, 1988, 1989; Dinarès et al., 1992; Oliva-Urcia et al., 2012; Izquierdo-Llavall et al., 2018) and in the eastern Cadi unit (Dinarès et al., 1992; Keller et al., 1994; Pueyo et al., 2016b). In the North Pyrenean Zone (France, Fig. 1B), paleomagnetic data are scarcer and evidence strong (over 70° CW in Aptian-Albian rocks, Oliva-Urcia et al., 2010; Rouvier et al., 2012) to null (Izquierdo-Llavall et al., 2020) vertical axis rotations in different areas.

Early Cretaceous remagnetizations are only described, so far, in the out of the Axial Zone, in the Southwestern Pyrenees (Larrasoaña et al., 2003) and in the Cotiella Massif (Garcés et al., 2016). These remagnetizations are relatively common in the deformed Cretaceous basins to the south of the Axial Zone. They are local and affect compartimentalized and highly subsident basins developed under high thermal gradient conditions (e.g., Lagabrielle et al., 2010) which played a key role to chemically remagnetize these rocks (e.g., Dinarès-Turell and García-Senz, 2000; Gong et al., 2008; 2009). On top of that, Cenozoic remagnetizations have been described in the Meso-Cenozoic units just above the Axial Zone (Oliva et al., 2008; 2012; Izquierdo-llavall et al., 2015). These Cenozoic remagnetizations likely occurred due to the burial associated with the development of the Pyrenean orogenic wedge. The wedge generated important lithostatic and tectonic load in the internal units until the final collision, continentalization and exhumation of the Paleozoic rocks during Oligocene-Miocene times.

Most of the paleomagnetic data to the south of the Axial Zone recorded, at least partially, Eocene secondary magnetizations (pre, syn and postfolding). Remanent magnetization in the Mesozoic units immediately to the North of the Axial Zone is in general terms post-folding and has been interpreted as a Cenozoic chemical (Oliva-Urcia et al., 2010) or thermal (Izquierdo-Llavall et al., 2020) remagnetization.

3. Sampling, methods and results

We drilled in 19 limestone sites from the Silurian or Devonian, one site of a late Carboniferous-early Permian granite (OG01, Panticosa intrusion) and one Permian dyke that intruded the surroundings of site OG12 (OG12dyke; Fig. 1B; Table 1) with a petrol-powered drill, in total 240 cores. We also collected 6 oriented hand samples (from the OG07 and OG08 sites, three samples each). Sites are distributed along–strike the southern and central Axial Zone from the Gallego valley in the west to the Valira valley in the east in eight different valleys (Figs. 1B; the kml file sample_locations.kml with exact locations is in the Supplementary material). Sites BN1 and OR15 were collected in the same area of sites published in Tait et al. (2000). Several sites allowed field tests: five site-scale fold-tests could be obtained (OG2; OG11; OG13; OG14; OG19); two tilt tests between sites within the same thrust unit (OG3-4; BN1-OR15), and two sites with a baked contact test (OG12 and OG17). We performed all analyses at Paleomagnetic Laboratory Fort Hoofddijk, Universiteit Utrecht, The Netherlands.

Our sample collection comes from fresh, non metamorphic and weakly or non-internally deformed sites. Most limestone sites contained variable amounts of organic matter visible while drilling. A few of these sites show a spaced solution cleavage and evidence of recrystallization. We collected the bedding orientation and, when observable, that of the pressure-solution cleavage (Table 1). The sampled rocks were affected by both Variscan and Pyrenean orogenies. The large scale Pyrenean (Alpine) thrusting can be distinguished from the Variscan because its emplacement produced kilometric-scale folding of the basement that is well recorded by the Mesozoic units unconformably overlying the Paleozoic rocks. Basement folding resulted in dominantly southward and northward tilts in the southern and northern part of the Axial Zone, respectively, but not producing significant plunging axes (<15°). To provide a detailed kinematic reconstruction separating the Variscan and Alpine events we inferred the approximate value of these Mesozoic-Cenozoic Alpine tilts from the surface or reconstructed orientation of the Mesozoic units that overlay the basement . To this end, we used geological maps and regional-scale cross sections where sampling sites were projected (Fig. 2; Table 1).

3.1 Methods

Knowing when and how rocks magnetized is crucial towards an appropriate interpretation of paleomagnetic results, especially in terms of plate and structural kinematics. In this paper we combined rock magnetic, paleomagnetic and structural geology analyses to unravel the magnetization history of the rocks.

Rock magnetism studies the magnetic properties of rocks and their magnetic minerals. The different magnetic properties of rocks, such as magnetic hysteresis, susceptibility and its anisotropy, magnetization vs. temperature (thermomagnetic analysis), can inform about the mineral(s) carrying the magnetic remanence and their crystal structure and grain size. This information is the most important to understand the geological proceses involved in the magnetization of the rocks, and eventually also a key to unravel magnetization timings. In this research we have performed a series of rock magnetic analyses to fully characterize the magnetic mineralogy of the studied samples as a step towards understanding the magnetization process and timing. We measured 18 high-field thermomagnetic runs in an in-house-built horizontal translation-type Curie balance with a sensitivity of approximately $5*10^{-9}Am^2$ (Mullender et al., 1993) and in an AGICO KLY-3 susceptibility bridge with a CS2 furnace attachment with nominal sensitivity ($5*10^{-7}$ SI) and air forced into the tube. We also analyzed 20 magnetic hysteresis loops and one first order reversal curve (FORC) diagram. They were measured at room temperature with an alternating gradient force magnetometer (MicroMag Model 2900 with 2 Tesla magnet, Princeton Measurements Corporation, noise level 2×10^{-9} Am^2). Finally, we obtained 88 isothermal remanent magnetization (IRM) acquisition curves from our Pyrenean limestone samples. Curves were obtained with the robotized magnetometer system of Utrecht University (Mullender et al., 2016).

Our paleomagnetic analyses were focused towards determining the Natural Remanent Magnetization (NRM) of the rocks. NRM provides information about ancient latitudes (inclination of the magnetic remanence) and rotations (declinations with respect to the past north) so that we can constrain the magnetization timing. The NRM of the sample collection was investigated through alternating field (AF) demagnetization and thermal demagnetization. AF demagnetization was carried out using the aforementioned robotic 2G-SQUID magnetometer, through variable field increments (4–10 mT) up to 70–100 mT. In all limestone samples, where high-coercitivity, low-blocking temperature minerals (i.e. goethite, titano-hematite) were expected, heating step to 150 °C was performed previous to the AF demagnetization. At the same time this enhances the distinction between secondary and characteristic NRM components determined with AF demagnetization (van Velzen & Zijderveld, 1995). In samples demagnetized thermally, a stepwise thermal demagnetization was carried through 10–100 °C increments up to complete demagnetization. Principal component analysis (Kirschvink, 1980) was used to calculate magnetic component directions from orthogonal vector end-point demagnetization diagrams (Zijderveld, 1967) with the online open-source software Paleomagnetism.org (Koymans et al., 2016; 2020).

Anisotropy of magnetic susceptibility (AMS) measures the induced magnetization in a rock when applying a magnetic field in different directions, defining an ellipsoid. The shape of the AMS ellipsoid depends on the crystallographic preferred orientation of the minerals; the shape, size, and preferred orientation of mineral grains; the occurrence of microfractures, its distribution and size… Frequently it is a good proxy for sedimentary and tectonic fabrics that are not visually obvious, but it is also a powerful method to investigate the effect of deformation on the NRM. We determined the composite fabric of the paramagnetic, diamagnetic and ferromagnetic grains by measuring the AMS of 148 samples from our collection with an AGICO MFK1-FA susceptometer (nominal sensitivity $2*10^{-8}$ SI).

3.2 Rock magnetism results

3.2.1 Thermomagnetic analyses

We place between 50–100 mg of powdered sample material from representative samples into quartz glass cup holders that hold the sample with quartz wool. We programmed stepwise thermomagnetic runs with intermittent cooling between successive heating steps. The heating and cooling segments were 150, 100, 250, 200, 300, 250, 400, 350, 520, 450, 620, 550, 700º C and finally back to 25° C, respectively. Heating and cooling rates were 10° C min^{-1}. Many samples show a paramagnetic contribution, sometimes uniquely (OG19; Supplementary File SF1), sometimes with a more or less noteworthy alteration reaction at about 400–450° C. This indicates the presence of non-magnetic sulfides (likely pyrite) that oxidize to magnetite during the thermomagnetic run (Fig. 3; OG14; Supplementary File SF1). Some samples show a small but sharp decay between 500 and 600° C, indicating the presence of magnetite (Fig. 3, OG13), others show the presence of pyrrhotite with a sudden increase at ~300°-320° C followed by a sharp decrease afterwards (OG8 in Fig. 3; OG06 and OG07 in SF1), all samples showing pyrrhotite contained a less important, but observable, content of pyrite. In the susceptibility vs. temperature curve (Fig. 3, BN1), pyrrhotite is observable during cooling but it likely formed as a secondary mineral during heating.

3.2.2 Magnetic hysteresis

Representative samples with masses ranging from 20 to 50 mg were measured using a P1 phenolic probe. Hysteresis loops were measured to determine the saturation magnetization (Ms), the saturation remanent magnetization (Mrs), and the coercive force (Bc). These parameters were determined after correcting for the paramagnetic contribution. The maximum applied field was 0.5 T. The field increment was 10 mT and the averaging time for each measurement was 0.15 s. We found different loop shapes (Fig. 4, SF-2): (i) Loops that do not saturate at 0.5 T with a pseudo-single-domain like shape which points to the presence of a relatively hard magnetic carrier likely pyrrhotite (Fig. 4, OG08) and (ii) typical magnetite-like pseudo-single domain loops (Fig. 4, OG19). We performed a first order reversal curve (FORC) diagram (Fig. 4, BN1-3) that shows a mixture between superparamagnetic and single domain behaviour.

3.2.3 Isothermal Remanent Magnetization (IRM)

Before the actual IRM acquisition, samples were AF demagnetized with the static 3-axis AF protocol with the final demagnetization axis parallel to the subsequent IRM acquisition field, a procedure that generates IRM acquisition curves with a shape as close to a cumulative-lognormal distribution as possible (Egli, 2004; Heslop et al., 2004). IRM acquisition curves consist of 61 IRM levels up to 700 mT. The shape of IRM curves is approximately a variably skewed cumulative log-Gaussian function in which may contain more than one coercivity phase. IRM component analysis enables a semi-quantitative evaluation of different coercivity components (magnetic minerals or particle sizes) to a measured IRM acquisition curve. Every skewed log-normal curve is characterized by four parameters: (1) The field ($B_{1/2}$) corresponding to the field at which half of the saturation isothermal remanent magnetization (SIRM) is reached; (2) the magnitude of the phase (Mri), which indicates the contribution of the component to the bulk IRM acquisition curve; (3) the dispersion parameter

(DP), expressing the width of the coercivity distribution of that mineral phase and corresponding to one standard deviation of the log-normal function (Kruiver et al. 2001; Heslop et al. 2002); and (4) the skewness of the gaussian curve (Maxbauer et al., 2016). IRM curve unmixing was performed with IRM MaxUnmix package (Maxbauer et al., 2016). The interpretation of the coercivity components in terms of mineralogy and grain size is usually done in concert with thermomagnetic curves.

Results from individual samples are characterized by two main IRM components: (a) a relatively soft component (C1 in Fig 5A) with $B_{1/2}$ between a minimum value of 23 and a maximum of 74 mT, but generally ~40 mT and dispersion parameter (DP) of ~ 0.33 and 0.38 (log units); and (b) a high coercivity component (C2) with a high $B_{1/2}$ > 200 mT and DP ~0.5 (log units). Both components are present in all samples but in varying proportions (Fig. 5A) of the SIRM. We performed end-member modeling in all of the same lithology Silurian-Devonian samples (following the steps of Gong et al. (2009a) but without a 150 °C preheating of the samples) to fully characterize the IRM set of samples. The program (Heslop and Dillon, 2007) to interpret the IRM acquisition curves uses the algorithm developed by Weltje (1997). End-member modeling assumes that the measured data can be represented by a linear mixture of a number of invariant constituent components, which are referred to as endmembers. The algorithm dictates that input IRM acquisition curves are monotonic; the curves were smoothed when appropriate to enforce them being monotonic. By least-squares minimization calculated normative compositions are optimized to the measured IRM acquisition curves, eliminating the need for prior knowledge of end-member properties (cf. Weltje, 1997). For further information about this technique in the framework of remagnetization see the review by Dekkers (2012). We found that a two end-member model shows an acceptable r^2 value of 0.6. Models with 3 to 9 end members show slightly better fits (r^2 = 0.73 to 0.88 respectively) although improvement is not deemed that significant (see discussion). The two end members are a soft (42 mT component with a DP = 0.36) and a hard (a 200mT component and DP = 0.35) component, analogous to C1 and C2 in the individual IRM curves analyzed (Fig. 5C).

3.3 Paleomagnetism results

A minimum of five demagnetization steps was considered to characterize a remnant component. In specimens where directions were difficult to isolate, we used the approach of McFadden and McElhinny (1988) in combining great circles and linear best fits (set points). The Virtual Paleomagnetic Directions (VPD) software was also used (Ramón et al., 2017) at the site level (stacking routine, linearity spectrum analysis, and the virtual direction methods by Scheepers and Zijderveld (1992); Schmidt (1982) and Pueyo (2000), respectively) to confirm the means derived from PCA analyses of individual specimens. Representative Zijderveld diagrams are shown in Fig. 6. For the complete analyses, the reader can check the paleomagnetism.org files associated with this paper (check persistent identifier -PID- in the acknowledgements).

Mean directions and uncertainties of each component were evaluated using Fisher's statistics (1953) of virtual geomagnetic poles (VGPs). We applied a fixed 45° cut-off to the VGP distributions of each site. In addition, we used the Deenen et al. (2011) criteria to evaluate the scatter of VGPs. As a general rule, if scatter is—mostly—due to paleosecular variation (PSV) of the geomagnetic field, the associated VGP distribution is roughly circular in shape. However, internal deformation, vertical axis rotation or inclination shallowing may add anisotropy to the scatter. In such cases, VGP distributions will show a certain degree of elongation or are otherwise not spherically uniform. Many samples show a NRM component with very low unblocking temperatures and low coercivities (100–180 °C or 10–12 mT). We consider this component as a viscous remanent magnetization (VRM), because of its similarity to the recent field (Fig. 7).

After VRM removal, the samples show a single NRM component (Fig. 6), generally pointing to the origin, regardless of the mineral, magnetite (usually fully demagnetized at 40-60 mT and 500-580° C) and/or pyrrhotite (fully demagnetized at 330° C and little to barely demagnetized in AF). This characteristic remanent magnetization (ChRM) clusters well in all the sites (concentration parameter $k > 8$, but generally over 15; Table 2) with the exceptions of sites OG02 and OG08 (Figs. 8 and 9; Table 2). In addition, there are three sites with less than seven samples passing the 45° cut-off (OG05, OG06, OG14) and therefore their statistical parameters are not reliable. These five sites were excluded from further interpretation. The remaining 15 sites show quite variable ChRM declinations and inclinations which appear to be only comparable between sites within the same thrust unit (Figs. 2, 8 and 9, Table 2). To account for the different events of deformation we have used bedding corrections (Table 2) and fold tests (Fig. 10). In addition, we also performed inclination only statistics (Enkin and Watson, 1996; Arason and Levi, 2010) to eliminate clustering problems related to vertical axis rotations using both the bedding parameters and our inferred Alpine corrections (see top of section 3) (Table 3).

In geographic coordinates the considered sites show clusterings that range from k (concentration parameter) ~ 8 (OG10 and 11) to k ~188 (OG19). Site average declinations range from 125° to 297°, the majority of them in the south quadrants with sites OG15 and BN1-OR15 (combined sites separated by 100 m) being the only exceptions (Fig. 8 and 9; Table 2). Inclinations range from -50° to 50°. Bedding correction significantly changes the distribution of the site averages, but the scattering in declinations (from 111° to 289°) and inclinations (-65° to 56°) remains (Table 2), which means that magnetization timing is not the same for all samples and/or structural complications are larger than folding.

All fold-tests whose samples passed the aforementioned quality criteria (Fig. 10; OG03-04; OG11; OG13 and OG19) were performed in folds with weakly plunging axes (Table 1; Fig. 11) with the exception of OG11, which in turn is the only one that is not negative (Fig. 10). OG11 shows a better clustering ($\tau1$) after tilt correction, however, the fold-axis in site OG11 is steeply plunging (the only case; Fig. 10). After back-tilting the plunging-axis (azimuth/plunge = 005/42), the fold test remains indeterminate, in this case with a greater clustering ($\tau1$) before tilt correction (Figs. 10 (structural correction panel) and 11). The statistics of all sites that pass our quality criteria ($n \geq 7$ and $k > 8$) yield close to random distributions both considering all specimens ($k = 1.63$ and $K = 1.65$; Supplementary File SF3) and the mean of site averages ($k = 1.95$ and $K = 2.5$; Table 4). As expected from the negative within-site fold-tests, the concentration parameter does not change after bedding correction neither in all specimens together ($k = 1.51$ and $K = 1.59$; Supplementary File SF3) nor the mean of site averages ($k = 1.57$ and $K = 1.64$; Table 4).

Inclination only statistics are independent to differential vertical axis rotations since declinations are not taken into account (e.g. Enkin and Watson, 1996). Inclination only statistics were performed on site averages to avoid weighting based on number of specimens (Table 4). The concentration parameter (k) equals to 0 in geographic coordinates and 2.17 in tilt corrected coordinates both figures representing very poor clusterings. k becomes close to 4 if we do not account for OG3 and OG4, which follow a different trajectory and may represent a different magnetization event. In contrast, when correcting the studied samples exclusively for our inferred Alpine tilt, the inclination only concentration parameter is ~4, but becomes ~14 when excluding OG3 and OG4 (Table 4). An inclination only tilt test without OG3 and OG4 shows a best fit for a 110% correction, both using the Enkin and Watson, 1996 approach (with a maximum clustering around k ~12) and a stepwise untilting following Arason and Levi (2010) inclination only statistics with a maximum at k ~15 to

(Fig. 12). OG3 and OG4 share a common true direction in geographic coordinates and their Alpine tilt correction does not change them too much (Fig. 13)

3.4 Anisotropy of the Magnetic Susceptibility (AMS) results

In pyrrhotite, the magnetic easy direction is confined to the basal crystallographic plane which implies an intrinsically strong anisotropy because of the 'hard' crystallographic c-axis (Schwarz and Vaughan, 1972; Schwarz, 1974). When pyrrhotite grows oriented in a preferred fabric (e.g. S1), the direction of the magnetic remanence can be biased towards the fabric plane (Fuller, 1963). The studied samples occasionally show pressure solution cleavage and a widespread presence of pyrrhotite as a partial or main carrier of the NRM. An inspection of the AMS fabrics can reveal whether pyrrhotite is oriented according to the S1 fabric.

We measured the magnetic anisotropy in 148 samples from most sites to explore possible causes for the variety of ChRM directions found (Table 2). The degree of anisotropy (P) appears to be generally low (< 1.05; Fig. 14, Supplementary file SF4) although some individual samples showed up to 1.5. The samples' three principal ellipsoid axes (Kmax, Kint, and Kmin) follow the bedding (S0) in six sites (OG09, 15, 16, 17, 18, 19); in three samples the AMS ellipsoid corresponded to the foliation S1 (OG06, 10 and 13); and others showed a quasi-random pattern (OG03, 05, 11, 14) both in geographic and tectonic coordinates (Fig. 14). No observed AMS fabric (not Kmax, Kint, or Kmin axes) from the datasets studies coincides with the ChRM directions, implying that NRM and ChRM are not biased by rock fabric.

4. Discussion

The paleomagnetic and rock magnetic results obtained from the Silurian-Devonian limestones in the Pyrenees certify that the Paleozoic rocks from this mountain belt have been subject to at least one widespread remagnetization event. Many samples contain a VRM that is similar to the recent geoaxial dipole for recent times in the Pyrenees (Fig. 7). Apart from this VRM, all rocks, regardless of their magnetic mineralogy, show a single stable component heading to the origin, with the exception of samples not delivering results (Fig. 6 and 8). This component is not deviated toward bedding/cleavage planes (as inferred from AMS patterns, Fig. 14) and displays negative fold tests (Fig. 10; perhaps a syn-folding fold test in the case of site OG11).

4.1 Rock magnetism

Rock magnetic analyses show that both pyrrhotite and magnetite are the magnetic carriers in the Silurian-Devonian limestones whereas magnetite is the carrier in the Panticosa late Carboniferous-Permian granite (OG1) and sampled dyke (OG12dyke). All limestone sites contain variable amounts of pyrrhotite and magnetite both in thermomagnetic curves (Fig. 3), in IRM acquisition curves and during NRM demagnetization (Figs. 5 and 6). We applied the IRM end-member modeling technique in an attempt to discriminate between different remagnetization events in the Pyrenees. The two end-member model with a reasonably high r^2 value of 0.65 is our preferred model. Models with 3 to 9 end members evidently show slightly better fits (r^2 = 0.73 to 0.88 respectively). However, neither the fit improves significantly, nor the shape of the end members shows more or less anticipated IRM acquisition curves for any particular mineralogy (Fig. 5B). In addition, most of the additional end members seem to represent the variable coercivity windows of magnetite (4 endmember example in Fig. 5B: 3 endmembers (EM1-3) all represent magnetite and do not deliver meaningful results). All samples contain a significant amount of those additional endmembers (varying from 10% to 60%) indicating that a variable grain-size or compositional magnetite is present in virtually every sample. The two end-member model further distinguishes a 42 mT component with a DP = 0.36 (C1), which is typical for magnetite and a 200mT component and DP = 0.35 (C2), which we interpret as pyrrhotite (Fig. 5C). The two end members are in agreement with individual sample fits, but end-member IRM acquisition curves describe much better the IRM properties of each magnetic phase (Fig. 5). We interpret the soft component (C1) as magnetite varying from coarse to very fine grained (i.e. lower and higher coercivity respectively) as supported by hysteresis loops (Fig. 4 and SF2). It is reasonable that the high coercivity component (C2) reflects the observed pyrrhotite in the thermomagnetic curves as SD pyrrhotite has a rather high coercivity.

The presence of variable amounts of pyrrhotite and magnetite in all Silurian-Devonian samples studied suggests that this is a common feature for the Paleozoic sedimentary and metasedimentary units of the mountain belt. Pyrrhotite is a stable mineral in low-grade metamorphic rocks under reducing conditions (e.g. Aubourg et al., 2012) such as the Pyrenean Silurian-Devonian limestones. Similar to the Pyrenees, pyrrhotite is the most common magnetic carrier in other limestone formations of the Iberian Variscides heavily affected by late Carboniferous magmatism (Pastor-Galán et al., 2015a; 2016; 2017; Fernández-Lozano et al., 2016).

In general terms, the occurrence of pyrrhotite in limestones is a sign of their remagnetization. Pyrrhotite is a frequent secondary mineral which is formed in limestones under anchimetamorphic and low-grade metamorphic conditions (Crouzet et al., 2001; Aubourg et al., 2019; Izquierdo-Llavall et al., 2020) or in the presence of non oxidizing magmatic fluids (Pastor-Galán et al., 2016). The ocurrence of pyrrhotite has been used as a geothermometer; increasing burial enhances the transformation of magnetite to pyrrhotite and the progressive replacement of magnetite-carried magnetizations by pyrrhotite-carried remagnetizations (e.g. Aubourg et al., 2019). In clay-rich rocks, magnetite and pyrrothite coexist at burial temperatures <340 ºC whereas at ~350 ºC the concentration of magnetite decreases drastically and pyrrothite becomes the dominant magnetic mineral (Aubourg et al., 2019). Izquierdo-Llavall et al. (2020) estimated the peak temperatures (~350 – 450 °C) in the North Pyrenean Zone (in the northermost side of cross section 2c in Fig. 1) following the magnetite –pyrrhotite transformations. The temperature estimates for the south Pyrenees (Izquierdo-Llavall et al., 2013; Labaume et al., 2016) are much lower, in contrast to the North Pyrenean Zone. Taking that into account, we suggest that in our samples pyrrhotite was formed by a fluid induced chemical remagnetization during the latest stages of the Variscan orogeny. However, our westernmost sampled units (OG1-OG4) could surpass the Curie temperature of pyrrhotite (~320° C; e.g. Dekkers, 1989) during the Cenozoic burial, and possibly represent a Cenozoic TRM.

4.2 Paleomagnetism and timing of remagnetization

We only consider sites for interpretation with at least 7 specimens passing the VGP's 45° cut-off criterion and with the concentration parameter $k > 8$. Sites OG02, 05, 06, 08, 14 and the dyke in OG12 do not pass these criteria and are not considered for further interpretation (Table 2). The rest of the sites show k values that range from barely above 8 in geographic coordinates (OG10 and 11), which could be expeted also from sedimentary magnetizations, to over 40 (OG12, OG15, OG17-OG19) in geographic coordinates, which is unlikely in primary magnetizations of sediments (e.g., Deenen et al., 2011). Site averages point generally to ESE-WSW with both positive and negative inclinations in geographic coordinates with the only exceptions of OG15 and BN1-OR15 which point WNW (Fig. 8 and 9; Table 2), something that does not change after bedding correction. With the exception of OG11, we have documented post-folding magnetizations. Importantly, the fabrics do not show consistency with NRM directions (particularly AMS fabric coincident with S1 does not occur) precluding any bias caused by a preferred orientation of pyrrhotite particles. Therefore, a post Variscan folding (i.e. late Carboniferous) is the oldest possible age for the magnetization since no earlier folding event has been described in the Pyrenees. The OG11 fold, which has a steep plunging axis (Fig. 11), yielded an inconclusive fold-test, but shows better clustering after tilt correction (Fig. 10). Classical fold-tests assume horizontal axes and performing them in plunging axis' folds introduces spurious rotations and false positive/negative foldtests (e.g. Pueyo et al., 2016a). Pre-correcting the plunge of the fold axis may help to unravel the relative timing of magnetization, but in turn the declination may not be reliable, introducing spurious rotations. In the case of OG11, pre-correcting the fold axis plunge produces another inconclusive result (Fig. 10). However, declinations in geographic, standard bedding correction, and Alpine tilt correction remain around 200° (Table 2 and 3) and inclinations are in all cases relatively shallow (between -9 and 20), suggesting that OG11 acquired its NRM during a reversed chron during a time when Iberia was at equatorial latitude: during late Carboniferous or Permian times (e.g. Pastor-Galán et al., 2018).

When considering all site paleomagnetic directions, we found that declinations and inclinations are only compatible in geographic coordinates for those sites within the same tectonic unit (Figs. 1, 2, 8, 9; Table 2). Such a directional pattern may be indicative of (a) different timing of NRM acquisition for each tectonic unit, (b) differential vertical axis rotations between units, (c) post-magnetization differential tilting between units or (d) a combination of the previous processes. To distinguish between these options inclination only statistics are appropriate (e.g. Enkin and Watson, 1996). Inclination only statistics do not consider declinations and therefore are independent of variations due to differential vertical axis rotations. In order to evaluate potential timing of magnetization we performed statistical analyses in geographic coordinates, after bedding correction, and also after correction of the tilt related to the emplacement of Alpine basement thrusts (Figs. 2, 12, 13; Tables 3 and 4). The concentration parameter of inclination data (k) is 0 in geographic coordinates (Table 4), which could mean that (i) sites magnetized at significantly different geological times when Iberia was at very different latitudes, and/or (ii) Alpine tilting postdates the magnetization and therefore it has a strong influence on the inclinations. Inclination only k is still too low (minimum k ~ 8 to consider an acceptable clustering) after bedding correction (~2) but also after Alpine tilt correction (~4).

Two sites from the Gavarnie nappe (OG03 and OG04; Fig. 8 and 13, geographic coordinates) move in a very different direction both during bedding and Alpine tilt corrections. In contrast, OG01 (Panticosa granite, late Carboniferous-Permian, Denèle et al., 2012), which is in the same Gavarnie nappe, correlates well with the rest of the sites in all thrust units after Alpine tilt correction but not with the neighboring OG03 and OG04. Thus, those sites might have acquired their magnetization at a significantly different time than the rest. After removing OG03 and OG04, the inclination only concentration parameter still indicates poor clustering after bedding correction (k ~ 4). However, when correcting only for the Alpine tilt k becomes 14.42 and a positive inclination only tilt test with a maximum in a 110% untilting (95% bwtween 58 and 150; Fig. 12; Table 4). After the Alpine tilt correction, the mean inclination is 5° ± 11 (Table 4) and all included sites show SW to SE declinations (Fig. 12). Despite the positive result, our Alpine tilt correction should be taken cautiously. We considered only regional tilt values, which were inferred from the average values of the overlying Mesozoic and thrust slopes in cross-sections (Fig. 2). Our estimated values took into account the kilometric-scale, thrust-related folding of the basement but can not consider the potential contribution of Alpine, outcrop-scale folding of the Paleozoic strata.

We believe, however, that the inclination only k value of 14.42 together with the obtained shallow inclinations and southerly declinations are sufficiently convincing to argue for a common timing of NRM acquisition for the samples included in the tilt test (Fig. 12). The results imply a postfolding but a pre-Alpine tilt NRM. The shallow inclinations suggest that Iberia was located at equatorial latitudes and the southerly declinations suggest that this occurred during a reverse chron. We therefore suggest that all samples that passed the quality criteria, with the exception of sites OG03 and OG04, magnetized during the latest Carboniferous to middle Permian times during the Kiaman reverse superchron, when Iberia was indeed located at equatorial latitudes (Weil et al., 2010). The late Carboniferous and early Permian times in the Pyrenees are characterized by widespread intrusions and volcanism (Panticosa granite, for example, OG01; Gleizes et al., 1998). We hypothesize that the remagnetization mechanism in the Pyrenees was triggered by fluids associated to the magmatic activity analogously to the remagnetizations observed in the Central Iberian Zone of west Iberia (e.g. Fernández-Lozano et al., 2016; Pastor-Galán et al., 2016; 2017).

OG03 and OG04 show a negative fold test (Fig. 10) and a common true mean direction in geographic coordinates (Fig. 13). Their paleomagnetic direction is, however, significantly different from OG01 that is a late Carboniferous-early Permian site located in the same thrust sheet. OG03 and OG04 show declinations to the south (both in geographic coordinates and after Alpine tilt correction) and upward inclinations of -43° and -48° (geographic coordinates) or -60° and -68º (after the restoration of the inferred Alpine tilt respectively). Both geographic and Alpine tilt corrected data indicate a remagnetization when Iberia was located at latitudes between 25°and 50° during a reverse chron. These results fit best to a remagnetization during late Cretaceous times, after the Cretaceous normal superchron (e.g. Izquierdo-Llavall et al., 2015 and references therein). Considering the steep >55° inclinations, we tentatively favor a late orogenic (Eocene) post Alpine tilting remagnetization. Such inclinations of >55° (after tilt correction) otherwise would only be possible after a remagnetization fairly long after the Alpine orogeny, when Iberia was located at similar latitudes as at present. We anticipate less remagnetization events long after the orogeny. Most structural units just above the basement units are remagnetized by tardi-orogenic burial remagnetizations (post-, syn- and pre- Alpine folding) that affected all kinds of rocks (limestones, calcarenites, redbeds...) (Dinarès et al., 1992; Dinarès, 1994; Keller et al., 1994; Oliva-Urcia and Pueyo, 2007b; Izquierdo-Llavall et al., 2015, Mujal et al., 2017 etc.) In addition, the burial temperature of OG03 and OG04 seem to have been sufficiently elevated to trigger a remagnetization after tilting during the unroofing of the Alpine orogeny.

4.3 Tectonic significance

The hypothesis of a detachment and northward drift of a peri-Gondwana microntinent (Armorica s.l.) during the late Silurian or early Devonian (e.g. Torsvik et al., 2012; Stampfli et al., 2013; Domeier and Torsvik., 2014; Franke et al., 2017) is grounded largely on the basis of paleomagnetic data from the Silurian and Devonian rocks of the Pyrenees (Tait et al., 2000), Brittany (Tait et al., 1999) and Bohemian Massif (Tait et al., 1994). Our results show that pervasive remagnetizations have affected the Silurian-Devonian limestones of the Pyrenees during, at least, two episodes: late Carboniferous-Early Permian and at the end of the Alpine orogeny. Our site BN1-OR15 was collected in the vicinity of those from Tait et al. (2000) and shows the same direction in geographic coordinates (Fig. 9), but within-site clustering worsens after bedding correction (Table 2). After Alpine tilt correction, however, a very good fit results with the majority of our Silurian-Devonian collection. In addition, site BN1-OR15 contains pyrrhotite (Fig. 3), a feature common to all the other samples studied (Fig. 9) and a secondary mineral in (meta)sediments indicative of remagnetization (e.g. Pastor-Galán et al., 2017; Izquierdo-Llavall et al., 2020). We therefore conclude that the originally published data by Tait et al. (2000) also reflect a remagnetization. Since the other paleomagnetic results from the putative Armorican s.l. continent are similar to those from the Pyrenees and come from areas with intense Carboniferous deformation and enhanced thermal activity, we suspect that they could be remagnetized as well. We request using those paleolatitudes (Tait et al., 1994; 1999) with caution; their paleomagnetic veracity warrants to be reassessed.

Despite the inherent loss of information due to the remagnetization, especially regarding the potential paleolatitudinal constraints, the Silurian-Devonian rocks of the Pyrenees do provide interesting insights. Based on the inclination data we interpret that the sampled rocks mostly remagnetized during late Carboniferous and Permian times when Iberia was located around the equator, thus previous to the Alpine orogeny. Our paleomagnetic results show a positive inclination only fold test when correcting the Alpine tilt inferred from the cross-sections but negative outcrop scale fold tests when using the bedding parameters. Thus, paleomagnetism in combination with detailed structural analysis, is a reliable tool to unravel the deformation style of multi-phase orogens like the Pyrenees. With our paleomagnetic data we now can separate the effects of Alpine and Variscan orogeny in the Silurian-Devonian carbonate series, something that classically is deemed challenging (e.g. Casas et al., 2019). With our data we can say that the Variscan orogeny was responsible for the main folding event observed in the Silurian and Devonian rocks since all remagnetizations are post-folding (Figs. 10 and 12). In contrast, our data supports that the tilting observed in the main Pyreneean thrusts postdates the late Carboniferous-Permian remagnetization. Consequently, those structures formed during the Alpine orogeny.

After the Alpine tilt correction, we obtained a relatively good agreement in inclinations, but declinations are still really scattered from SE to SW. Alpine vertical axis rotations in the Pyrenees are frequent and very variable with magnitudes ranging from a few degrees to up to 80° both clockwise and counterclockwise (e.g. Sussman et al., 2004; Rodríguez et al., 2016). Although it is plausible that the basement also underwent significant vertical axis rotations, very little is known about the rotational activity of Pyrenean basement thrusts during the Alpine orogeny. The declinations observed in the Silurian-Devonian rocks of the Pyrenees are generally clockwise with respect to the Permian reference pole for stable Iberia (Weil et al., 2010; Oliva et al., 2012) ranging from a few degrees to ca. 90° (Fig. 1). We note that such results are in line with the paleomagnetic results from Carboniferous and Permian igneous rocks in the Pyrenees and Catalan coastal ranges (Edel et al., 2018). The Pyrenees lay in the northern branch of the Cantabrian Orocline, which rotated clockwise during the Late Carboniferous and Early Permian (e.g. Pastor-Galán et al., 2015b; Pastor-Galán, 2020). Edel et al. (2018) interpreted their results as consistent with the rotations expected in the northern branch of the of the Cantabrian Orocline. Izquierdo-Llavall et al. (2014) also found similar data in late Carboniferous and Early Permian rocks of the Pyrenees and interpreted them as an Alpine rotation. Therefore, we would like to remain wary about their meaning. The variety of rotations found might be reflecting: (i) Differential timing of the remagnetization which occurred widely during the Cantabrian Orocline formation as observed in other areas of Iberia (e.g. Pastor-Galán et al., 2017; 2020); (ii) Vertical axis rotations associated with the Alpine orogeny (Izquierdo-Llavall et al., 2014); or (iii) a combination of both processes where the Alpine rotations may be opposite to and/or in the same sense as the late Carboniferous clockwise rotations.

4.4 A blessing in disguise

The Pyrenees are a multi-orogenic mountain mountain range whose kinematics is often complicated due to the superposition of different deformation events. Accumulation of geological processes, many of them involving relatively high temperatures and fluid percolation increases the chances of remagnetization for the rocks involved in the orogenies. In fact, we suspect that the majority of the Silurian-Devonian carbonate series of the Pyrenees won't preserve a primary and syn-sedimentary magnetization. This makes the Pyrenees, despite the great outcrop quality and quantity a bad candidate to study pre-Variscan plate motions and kinematics. However, we found generally strong magnetizations containing with univocal ChRMs. Our paleomagnetic data, in combination with detailed structural observations, has proven the best way so far to unravel the complex tectonic evolution of the Axial Zone of the Pyrenees. We think that at least the Devonian carbonate rocks, but likely other Paleozoic series and igneous rocks are excellent targets to study: (1) the Variscan - Alpine structural relationships, (2) the Alpine rotational history of the basement thrusts; and perhaps (3) the late Variscan deformation events leading to the final amalgamation of Pangea.

5. Conclusions and caution for paleomagnetists

- The Silurian-Devonian carbonate series of the Pyrenees show varying amounts of pyrrhotite, a secondary magnetic mineral, and negative fold tests using bedding parameters, which indicate widespread remagnetization(s).
- The majority of sites that passed the quality criteria ($n = 7$ and $k > 8$) show a positive inclination only fold test when correcting the Alpine tilt (with the exceptions of OG03 and OG04). The obtained inclinations are southerly and very shallow; they constrain the remagnetization to a reverse chron when Iberia was around the equator, only possible during late Carboniferous or early Permian times.
- Sites OG03 and OG04 (Western Pyrenees, Gavarnie thrust sheet) were likely remagnetized after the main Alpine thrusting, during a pervasive burial remagnetization widely observed in the Internal Sierras and other along-strike equivalent units (Bóixols, Cadí).
- Paleomagnetism from the Silurian and Devonian rocks suggest that the Variscan orogeny was responsible for their main folding event, whereas the Alpine orogeny produced their thrusting and antiformal stacking.

743 • Our results also show general clockwise rotations which may be consistent with the northern
744 branch of the Cantabrian Orocline. These rotations may as well represent Alpine vertical axis
745 rotations or a combination of both.
746 • Given the generally good paleomagnetic quality of the Devonian carbonates, they could be
747 targeted to study the Alpine imprint on Paleozoic rocks and thus, unravelling the rotational
748 history of basement thrusts.
749 • The widespread remagnetizations found in the Paleozoic of the Pyrenees indicate that
750 paleolatitudes inferred from Silurian and Devonian are very unlikely original and should be
751 taken very cautiously. We urge a reassessment of Siluro-Devonian poles from the Variscan in
752 Europe.
753 • Paleomagnetism from multi-orogenic areas is NOT A SIMPLE GAME. However, the
754 systematic combination of paleomagnetism with detailed structural observations, seems to
755 be a foremost way to unravel complex tectonic evolutions.

756

757 Acknowledgements

758 This work was funded by postdoctoral (ISES) grant from NWO to DPG and the projects
759 DR3AM, MAGIBER II and UKRIA4D (CGL2014-54118-C2-2, CGL2017-90632-REDT and
760 PID2019-104693GB-I00/CTA) from the Spanish Ministry of Science. We thank Mat Domeier
761 for providing help with the inclination only statistics. DPG thanks Edward Lodewijk Van Halen
762 for all times making him jump, we will keep on jumping.

763

Data availability statement

All data is included in the paper and supplementary materials. In Addition, paleomagnetic data is stored in paleomagnetism.org under the persisitent identifier (PID) 1871091757a6ef9d46ac59bb9f35c7a6387bc8fcece7bf0715eaba29164fbc7e and can be accessed in the link https://www.paleomagnetism.org/library/.

Figure and Table captions

Figure 1: A) Simplified map of the Iberian Peninsula showing the main Paleozoic outcrops and the areas affected by the Alpine orogeny (after Pastor-Galán et al., 2020). B) Geological map of the Pyrenees (modified from Barnolas et al., 2008 according to Choukroune and Seguret, 1973) showing our sampling locations (red dots) and the extensive paleomagnetic studies in the Pyrenees focused mainly on Permo-Triassic rocks (blue dots). Lines show the trend of the cross sections in figure 2.

Figure 2: Cross sections through the Pyrenees with projected positions of our sampling sites.

Figure 3: Selected magnetization vs. temperature curves (OG8, OG13, OG14) and susceptibility vs. temperature (BN1). Note that magnetic and non magnetic sulfides are common. All measurements performed are available in supplementary file SF1.

Figure 4: Selected slope corrected hysteresis loops and FORC diagram (plotted with FORCINEL (Harrison and Feinberg, 2008, smoothing factor 13). All measurements performed are available in supplementary file SF2.

Figure 5: A) Unmixing of IRM acquisition curve for three samples showing different proportions of a ‘soft’ mineral that saturates below 75 mT (magnetite) and a ‘harder’ one that saturates over 200 mT (pyrrhotite). B) Results from the endmember modeling showing our preferred two end-member solution (left) and the four end-member solution (right). C) Unmixing of the IRM synthetic acquisition curve from the two end members showing the same two magnetic mineralogies as in the forward modeling of different samples: magnetite to the left and pyrrhotite to the right.

Figure 6: Examples of ‘Zijderveld’ (Zijderveld, 1967) vector-end point plots for selected samples. All samples plotted in geographic coordinates. Close-open circles represent declination and inclination projections respectively. Complete analyses are available in paleomagnetism.org through the Persistent identifyer PID given in the acknowledgements.

Figure 7: Viscous remanent magnetization (VRM) from all samples is compatible with the present-day field (geographic coordinates). Red dots are those that fall outside of the 45° cut-off. Uncertainty envelope is in both cases VGP A95. The rather large scattering is likely due to the small number of demagnetization levels containing the VRM (3-4) and the possible migration of the VRM during transport, storage and analysis.

Figure 8: Directional and VGP results in geographic coordinates of sites OG01 to OG11. Uncertainty envelope is in both cases VGP A95. Red dots are those that fall outside of the 45° cut-off. Sites OG02, 05 and 08 did not provide statistically meaningful results and were not interpreted.

Figure 9: Directional and VGP results in geographic coordinates of sites OG12 to OG19 and BN1-OR15. Uncertainty envelope is in both cases VGP A95. Red dots are those that fall outside

of the 45° cut-off. Sites OG02, 05 and 08 did not provide statistically meaningful results and were not interpreted.

Figure 10: Within-site fold tests. All are negative but OG11, which is inconclusive.

Figure 11: Pi diagrams for the studied folds. Only OG11 shows a steeply plunging axis.

Figure 12: Results after the inferred Alpine tilt correction. Permian reference declination for Iberia is after Weil et al. (2010). The results show a positive inclination only tilt test following the methodology of Enkin and Watson (1996) (selected bootstraps in thin gray lines) and Arson and Levi (2010) approach (dashed line).

Figure 13: OG03 and OG04 show a common true mean bootstrapped direction (after Tauxe, 2010) in geographic (and Alpine tilt corrected) coordinates.

Figure 14: Results from the anisotropy of the magnetic susceptibility analyses. Magnetic fabrics represent bedding or S1 cleavage. Magnetic fabric directions do not coincide with the paleomagnetic directions, which allows us to discard an internal deformation control of the paleomagnetic remanence.

Table 1: Site Location and key structural data from each site.

Table 2: Paleomagnetic results for all sites in geographic and tilt (bedding) corrected coordinates.

Table 3: Paleomagnetic results after the Alpine tilt correction (tilt associated to the emplacement of the thrusts).

Table 4: Concentration parameters of inclination only statistics from the mean values of the sites.

Supplementary Files:

SF1: All thermomagnetic curves analyzed.

SF2: All Hysteresis loops analyzed.

SF3: Synthesis of the paleomagnetic results (can be opened with paleomagnetism.org).

SF4: KMZ file (Google Earth) with the sampled locations.

SF5: Zip file containing all obtained raw results.

References added by Emilio, Esther and Jaume

Abd Elmola, A., Buatier, M., Monié, P., Labaume, P., Trap, P., & Charpentier, D. (2018). 40Ar/39Ar muscovite dating of thrust activity: a case study from the Axial Zone of the Pyrenees. Tectonophysics, 745, 412-429.

Arason, þ. & Levi, S. (2010) Maximum likelihood solution for inclination-only data in paleomagnetism. *Geophysical Journal International*, **182**, 753–771. doi:10.1111/j.1365-246X.2010.04671.x

Aubourg, C., & Pozzi, J. P. (2010). Toward a new< 250 C pyrrhotite–magnetite geothermometer for claystones. Earth and Planetary Science Letters, 294(1-2), 47-57.

Aubourg, C., Pozzi, J.-P. & Kars, M. (2012) Burial, claystones remagnetization and some consequences for magnetostratigraphy. *Geological Society, London, Special Publications*, **371**, 181–188. doi:10.1144/SP371.4

Aubourg, C., Jackson, M., Ducoux, M., & Mansour, M. (2019). Magnetite-out and pyrrhotite-in temperatures in shales and slates. *Terra Nova*, *31*(6), 534-539.

Autran A, García-Sansegundo J (1996) Tectonique hercynienne. Carte structurale (moitié occidentale). In: Barnolas A, Chiron JC (eds) Synthèse géologique at géophysique des Pyrénées, vol 1. BRGM-ITGE, Orléans-Madrid

Azor, A., Dias da Silva, Í., Gómez Barreiro, J., González-Clavijo, E., Martínez Catalán, J.R., Simancas, J.F., Martínez Poyatos, D., *et al.* (2019) Deformation and Structure. in *The Geology of Iberia: A Geodynamic Approach* Regional Geology Reviews eds. Quesada, C. & Oliveira, J.T., pp. 307–348, Cham: Springer International Publishing. doi:10.1007/978-3-030-10519-8_10

Barnolas, A., Gil-Peña, I., Alfageme, S., Ternet, Y., Baudin, T., & Laumonier, B. (2008). Mapa geológico de los Pirineos a escala 1:400 000. IGME/BRGM ISBN: 978-2- 7159-2168-9.

Beamud, E., Muñoz, J. A., Fitzgerald, P. G., Baldwin, S. L., Garcés, M., Cabrera, L., & Metcalf, J. R. (2011). Magnetostratigraphy and detrital apatite fission track thermochronology in syntectonic conglomerates: constraints on the exhumation of the South-Central Pyrenees. Basin Research, 23(3), 309-331.

Biggin, A.J., Piispa, E.J., Pesonen, L.J., Holme, R., Paterson, G.A., Veikkolainen, T. & Tauxe, L. (2015) Palaeomagnetic field intensity variations suggest Mesoproterozoic inner-core nucleation. *Nature*, **526**, 245–248. doi:10.1038/nature15523

Bosch, G. V., Teixell, A., Jolivet, M., Labaume, P., Stockli, D., Domènech, M., & Monié, P. (2016). Timing of Eocene–Miocene thrust activity in the Western Axial Zone and Chaînons Béarnais (west-central Pyrenees) revealed by multi-method thermochronology. Comptes Rendus Geoscience, 348(3-4), 246-256.

Casas, J.M., Álvaro, J.J., Clausen, S., Padel, M., Puddu, C., Sanz-López, J., Sánchez-García, T., *et al.* (2019) Palaeozoic Basement of the Pyrenees. in *The Geology of Iberia: A Geodynamic Approach* Regional Geology Reviews eds. Quesada, C. & Oliveira, J.T., pp. 229–259, Cham: Springer International Publishing. doi:10.1007/978-3-030-10519-8_8

Calvet, M., Gunnell, Y., & Laumonier, B. (2020). Denudation history and palaeogeography of the Pyrenees and their peripheral basins: an 84-million-year geomorphological perspective. Earth-Science Reviews, 103436.

Calvín, P., Santolaria, P., Casas, A. M., & Pueyo, E. L. (2018). Detachment fold vs. ramp anticline: a gravity survey in the southern Pyrenean front (External Sierras). Geological Journal, 53(1), 178-190.

Casas, J. M., Domingo, F., Poblet, J., & Soler, A. (1989). On the role of the Hercynian and Alpine thrusts in the Upper Paleozoic rocks of the Central and Eastern Pyrenees. Geodinamica Acta, 3(2), 135-147.

Casas, A. M., Oliva, B., Román-Berdiel, T., & Pueyo, E. (2003). Basement deformation: tertiary folding and fracturing of the Variscan Bielsa granite (Axial zone, central Pyrenees). Geodinamica acta, 16(2-6), 99-117.

Choukroune, P., & Séguret, M. (1973). Carte structurale des Pyrénées, 1/500.000, Université de Montpellier – ELF Aquitaine

Crognier, N., Hoareau, G., Aubourg, C., Dubois, M., Lacroix, B., Branellec, M., ... & Vennemann, T. (2018). Syn-orogenic fluid flow in the Jaca basin (south Pyrenean fold and thrust belt) from fracture and vein analyses. *Basin Research*, *30*(2), 187-216.

Crouzet, C., Stang, H., Appel, E., Schill, E., & Gautam, P. (2001). Detailed analysis of successive pTRMs carried by pyrrhotite in Himalayan metacarbonates: an example from Hidden Valley, Central Nepal. Geophysical Journal International, 146(3), 607-618.

Deenen, M.H.L., Langereis, C.G., Hinsbergen, D.J.J. van & Biggin, A.J. (2011) Geomagnetic secular variation and the statistics of palaeomagnetic directions. *Geophysical Journal International*, **186**, 509–520. doi:10.1111/j.1365-246X.2011.05050.x

Debon and Guitard (1996) Métamorphisme at plutonisme hercyniens. Carte de synthèse. In: Barnolas A, Chiron, JC (eds) Synthèse géologique et géophysique des Pyrénées, vol 1. BRGM-ITGE, Orle´ans-Madrid

Dekkers, M. J. (1989) Magnetic properties of natural pyrrhotite. II. High- and low-temperature behaviour of Jrs and TRM as function of grain size. *Physics of the Earth and Planetary Interiors*, **57**, 266–283. doi:10.1016/0031-9201(89)90116-7

Dekkers, Mark J. (2012) End-member modelling as an aid to diagnose remagnetization: a brief review. *Geological Society, London, Special Publications*, **371**, 253–269. doi:10.1144/SP371.12

Denèle Y, Paquette JL, Olivier Ph, Barbey P (2011) Permian granites in the Pyrenees: the Aya pluton (Basque Country). Terra Nova 00:1–9

Denèle, Y., Laumonier, B., Paquette, J. L., Olivier, P., Gleizes, G., & Barbey, P. (2014). Timing of granite emplacement, crustal flow and gneiss dome formation in the Variscan segment of the Pyrenees. *Geological Society, London, Special Publications*, *405*(1), 265-287.

Dias da Silva, Í., González Clavijo, E. & Díez-Montes, A. (2020) The collapse of the Variscan belt: a Variscan lateral extrusion thin-skinned structure in NW Iberia. *International Geology Review*, **00**, 1–37, Taylor & Francis. doi:10.1080/00206814.2020.1719544

Dinarès-Turell, J. (1994). Remagnetizations associated to diagenesis and their relationship with thrust sheet emplacement in the Southern Pyrenees. Geogaceta, 15, 105-108.

Dinares-Turell, J., & Garcia-Senz, J. (2000). Remagnetization of Lower Cretaceous limestones from the southern Pyrenees and relation to the Iberian Plate geodynamic evolution. Journal of Geophysical Research, 105(B8), 19-19,418. doi:10.1029/2000JB900136.

Dinarès, J., McClelland, E., & Santanach, P. (1992). Contrasting rotations within thrust sheets and kinematics of thrust tectonics as derived from palaeomagnetic data: an example from the Southern Pyrenees. In *Thrust tectonics* (pp. 265-275). Springer, Dordrecht.

Domeier, M. (2016) A plate tectonic scenario for the Iapetus and Rheic Oceans. *Gondwana Research*, **36**, 275–295, Elsevier.

Domeier, M. & Torsvik, T.H. (2014) Plate tectonics in the late Paleozoic. *Geoscience Frontiers*, **5**, 303–350, Elsevier Ltd. doi:10.1016/j.gsf.2014.01.002

Domeier, M. & Torsvik, T.H. (2019) Full-plate modelling in pre-Jurassic time. *Geological Magazine*, **156**, 261–280, Cambridge University Press. doi:10.1017/S0016756817001005

Edel, J.B., Schulmann, K., Lexa, O. & Lardeaux, J.M. (2018) Late Palaeozoic palaeomagnetic and tectonic constraints for amalgamation of Pangea supercontinent in the European Variscan belt. *Earth-Science Reviews*, **177**, 589–612, Elsevier. doi:10.1016/j.earscirev.2017.12.007

Egli, R. (2004) Characterization of individual rock magnetic components by analysis of remanence curves. *Physics and Chemistry of the Earth*, **29**, 851–867. doi:10.1016/j.pce.2004.04.001

Enkin, R. J., & Watson, G. S. (1996). Statistical analysis of palaeomagnetic inclination data. Geophysical Journal International, 126(2), 495-504

Fernández-Lozano, J., Pastor-Galán, D., Gutiérrez-Alonso, G. & Franco, P. (2016) New kinematic constraints on the Cantabrian orocline: A paleomagnetic study from the Peñalba and Truchas synclines, NW Spain. *Tectonophysics*, **681**, 195–208, Elsevier B.V. doi:10.1016/j.tecto.2016.02.019

Fernández-Suárez, J., Gutiérrez-Alonso, G., Pastor-Galán, D., Hofmann, M., Murphy, J.B. & Linnemann, U. (2014) The Ediacaran-Early Cambrian detrital zircon record of NW Iberia: Possible sources and paleogeographic constraints. *International Journal of Earth Sciences*, **103**, 1335–1357. doi:10.1007/s00531-013-0923-3

Fillon, C., & van der Beek, P. (2012). Post-orogenic evolution of the southern Pyrenees: Constraints from inverse thermo-kinematic modelling of low-temperature thermochronology data. Basin Research, 24(4), 418-436.

Fisher, R. (1953) Dispersion on a Sphere. *Proceedings of the Royal Society A: Mathematical, Physical and Engineering Sciences*, **217**, 295–305. doi:10.1098/rspa.1953.0064

Fitzgerald, P. G., Muñoz, J. A., Coney, P. J., & Baldwin, S. L. (1999). Asymmetric exhumation across the Pyrenean orogen: implications for the tectonic evolution of a collisional orogen. Earth and Planetary Science Letters, 173(3), 157-170.

Franke, W., Cocks, L.R.M. & Torsvik, T.H. (2017) The Palaeozoic Variscan oceans revisited. *Gondwana Research*, **48**, 257–284. doi:10.1016/j.gr.2017.03.005

Fuller, M. D. (1963). Magnetic anisotropy and paleomagnetism. *Journal of Geophysical Research*, *68*(1), 293-309.

Garcés, M., López-Blanco, M., Valero, L., Beamud, E., Muñoz, J. A., Oliva-Urcia, B., ... & Cabrera, L. (2020). Paleogeographic and sedimentary evolution of the South Pyrenean foreland basin. *Marine and Petroleum Geology*, *113*, 104105.

García-Sansegundo, J., Poblet, J., Alonso, J.L. & Clariana, P. (2011) Hinterland-foreland zonation of the Variscan orogen in the Central Pyrenees: comparison with the northern part of the Iberian Variscan Massif. *Geological Society, London, Special Publications*, **349**, 169–184, Geological Society of London. doi:10.1144/SP349.9

Gil-Peña, I., Oliva, B., Pueyo, E. L., Barnolas, A., 2005. Datos preliminares de la remagnetización Estephaniense del Ordovícico Superior del Pirineo Centro-meridional, implicaciones estructurales. Ordovícico Catalán. MAGIBER-IV (Vigo), 47- 50.

Gil-Peña, I.; Oliva, B.; Pueyo, E. L.; Barnolas, A. Remagnetización Stefaniense-Pérmica del Ordovícico de la Zona Axial meridional del Pirineo Central; implicaciones paleogeográficas y tectónicas posthercínicas. Proceedings MAGIBER IV- IV Paleomagnetismo en España y Portugal (Vigo), 47-50 (2006)

Gleizes, G., Leblanc, D., & Bouchez, J. L. (1997). Variscan granites of the Pyrenees revisited: their role as syntectonic markers of the orogen. *Terra Nova*, *9*(1), 38-41.

Gleizes, G., Leblanc, D., Santana, V., Olivier, P., & Bouchez, J. L. (1998). Sigmoidal structures featuring dextral shear during emplacement of the Hercynian granite complex of Cauterets–Panticosa (Pyrenees). Journal of Structural Geology, 20(9-10), 1229-1245.

Gong, Z., Dekkers, M.J., Heslop, D. & Mullender, T.A.T.T. (2009) End-member modelling of isothermal remanent magnetization (IRM) acquisition curves: a novel approach to diagnose remagnetization. *Geophysical Journal International*, **178**, 693–701. doi:10.1111/j.1365-246X.2009.04220.x

Gong, Z., Langereis, C.G. & Mullender, T.A.T. (2008) The rotation of Iberia during the Aptian and the opening of the Bay of Biscay. *Earth and Planetary Science Letters*, **273**, 80–93.

Gutiérrez-Alonso, Gabriel, Collins, A.S., Fernández-Suárez, J., Pastor-Galán, D., González-Clavijo, E., Jourdan, F., Weil, A.B., *et al.* (2015) Dating of lithospheric buckling:40Ar/39Ar ages of syn-orocline strike-slip shear zones in northwestern Iberia. *Tectonophysics*, **643**, 44–54, Elsevier B.V. doi:10.1016/j.tecto.2014.12.009

Gutiérrez-Alonso, G., López-Carmona, A., Núñez-Guerrero, E., García, A.M., Fernández-Suárez, J., Pastor-Galán, D., Gutiérrez-Marco, J.C., *et al.* (2020) Neoproterozoic-Palaeozoic detrital sources in the Variscan foreland of northern Iberia: primary vs. recycled sediments. *Geological Society, London, Special Publications*, **503**, Geological Society of London. doi:10.1144/SP503-2020-21

Heslop, D., Dekkers, M.J., Kruiver, P.P. & Van Oorschot, I.H.M. (2002) Analysis of isothermal remanent magnetization acquisition curves using the expectation-maximization algorithm. *Geophysical Journal International*, **148**, 58–64. doi:10.1046/j.0956-540x.2001.01558.x

Heslop, D. & Dillon, M. (2007) Unmixing magnetic remanence curves without a priori knowledge. *Geophysical Journal International*, **170**, 556–566, Oxford University Press. doi:10.1111/j.1365-246X.2007.03432.x

Heslop, D., McIntosh, G. & Dekkers, M.J. (2004) Using time- and temperature-dependent Preisach models to investigate the limitations of modelling isothermal remanent magnetization acquisition curves with cumulative log Gaussian functions. *Geophysical Journal International*, **157**, 55–63, Oxford University Press. doi:10.1111/j.1365-246X.2004.02155.x

Hoareau, G., Crognier, N., Lacroix, B., Aubourg, C., Roberts, N. M., Niemi, N., ... & Ruiz, I. S. (2021). Combination of Δ47 and U-Pb dating in tectonic calcite veins unravel the last pulses related to the Pyrenean Shortening (Spain). Earth and Planetary Science Letters, 553, 116636.

Huang, W., Dupont-Nivet, G., Lippert, P.C., Hinsbergen, D.J.J. van, Dekkers, M.J., Guo, Z., Waldrip, R., *et al.* (2015) Can a primary remanence be retrieved from partially remagnetized Eocence volcanic rocks in the Nanmulin Basin (southern Tibet) to date the India-Asia collision? *Journal of Geophysical Research: Solid Earth*, **120**, 42–66. doi:10.1002/2014JB011599

Huang, W., Lippert, P.C., Zhang, Y., Jackson, M.J., Dekkers, M.J., Li, J., Hu, X., *et al.* (2017) Remagnetization of carbonate rocks in southern Tibet: Perspectives from rock magnetic and petrographic investigations. *Journal of Geophysical Research: Solid Earth*, **122**, 2434–2456. doi:10.1002/2017JB013987

Huyghe, D., Mouthereau, F., Castelltort, S., Filleaudeau, P. Y., & Emmanuel, L. (2009). Paleogene propagation of the southern Pyrenean thrust wedge revealed by finite strain analysis in frontal thrust sheets: Implications for mountain building. Earth and Planetary Science Letters, 288(3-4), 421-433.

Izquierdo-Llavall, E., Aldega, L., Cantarelli, V., Corrado, S., Gil-Peña, I., Invernizzi, C., & Casas, A. M. (2013). On the origin of cleavage in the Central Pyrenees: structural and paleo-thermal study. Tectonophysics, 608, 303-318.

Izquierdo-Llavall, E., Casas-Sainz, A., Oliva-Urcia, B., & Scholger, R. (2014). Palaeomagnetism and magnetic fabrics of the Late Palaeozoic volcanism in the Castejón-Laspaúles basin (Central Pyrenees). Implications for palaeoflow directions and basin configuration. Geological Magazine, 151(5), 777-797.

Izquierdo-Llavall, E., Sainz, A. C., Oliva-Urcia, B., Burmester, R., Pueyo, E. L., & Housen, B. (2015). Multi-episodic remagnetization related to deformation in the Pyrenean Internal Sierras. *Geophysical Journal International*, *201*(2), 891-914.

Izquierdo-Llavall, E., Casas-Sainz, A. M., Oliva-Urcia, B., Villalaín, J. J., Pueyo, E., & Scholger, R. (2018). Rotational kinematics of basement antiformal stacks: Paleomagnetic study of the western Nogueras Zone (Central Pyrenees). *Tectonics*, *37*(10), 3456-3478.

Izquierdo-Llavall, E., Menant, A., Aubourg, C., Callot, J. P., Hoareau, G., Camps, P., ... & Lahfid, A. (2020) Pre-orogenic folds and syn-orogenic basement tilts in an inverted hyperextended margin: the northern Pyrenees case study. *Tectonics*, e2019TC005719.

Jackson, M., Rochette, P., Fillion, G., Banerjee, S. & Marvin, J. (1993) Rock magnetism of remagnetized Paleozoic carbonates: Low-temperature behavior and susceptibility characteristics. *Journal of Geophysical Research: Solid Earth*, **98**, 6217–6225. doi:https://doi.org/10.1029/92JB01319

Jolivet, M., Labaume, P., Monié, P., Brunel, M., Arnaud, N., & Campani, M. (2007). Thermochronology constraints for the propagation sequence of the south Pyrenean basement thrust system (France-Spain). Tectonics, 26(5).

Juárez, M. T., Lowrie, W., Osete, M. L., & Meléndez, G. (1998). Evidence of widespread Cretaceous remagnetisation in the Iberian Range and its relation with the rotation of Iberia. Earth and Planetary Science Letters, 160(3-4), 729-743.

Kirschvink, J.L. (1980) The least-squares line and plane and the analysis of palaeomagnetic data. *Geophysical Journal International*, **62**, 699–718. doi:10.1111/j.1365-246X.1980.tb02601.x

Kleinsmiede, W.F.J. (1960) Geology of the Valle de Arán (Central Pyrenees). *Leidse Geologische Mededelingen*, **25**, 129–245.

Koymans, M.R., Hinsbergen, D.J.J. van, Pastor-Galán, D., Vaes, B. & Langereis, C.G. (2020) Towards FAIR Paleomagnetic Data Management Through Paleomagnetism.org 2.0. *Geochemistry, Geophysics, Geosystems*, **21**, e2019GC008838. doi:10.1029/2019GC008838

Koymans, M.R.R., Langereis, C.G.G., Pastor-Galán, D. & Hinsbergen, D.J.J.J.J.D.J.J. van. (2016) Paleomagnetism.org: An online multi-platform open source environment for paleomagnetic data analysis. *Computers and Geosciences*, **93**, 127–137, Elsevier. doi:10.1016/j.cageo.2016.05.007

Kruiver, P.P., Dekkers, M.J. & Heslop, D. (2001) Quantification of magnetic coercivity components by the analysis of acquisition curves of isothermal remanent magnetisation. *Earth and Planetary Science Letters*, **189**, 269–276. doi:10.1016/S0012-821X(01)00367-3

Kuiper, K.F., Deino, A., Hilgen, F.J., Krijgsman, W., Renne, P.R. & Wijbrans, J.R. (2008) Synchronizing Rock Clocks of Earth History. *Science*, **320**, 500–504, American Association for the Advancement of Science. doi:10.1126/science.1154339

Keller, P., Lowrie, W., & Gehring, A. U. (1994). Palaeomagnetic evidence for post-thrusting tectonic rotation in the Southeast Pyrenees, Spain. *Tectonophysics*, *239*(1-4), 29-42.

Labaume, P., & Teixell, A. (2018). 3D structure of subsurface thrusts in the eastern Jaca Basin, southern Pyrenees. *Geologica Acta*, *16*(4), 477-498.

Lagabrielle, Y., Labaume, P. and de Saint Blanquat, M., 2010. Mantle exhumation, crustal denudation, and gravity tectonics during Cretaceous rifting in the Pyrenean realm (SW Europe): Insights from the geological setting of the lherzolite bodies. Tectonics, 29(4).

Lanaja, J. M., 1987. Contribución de la exploración petrolífera al conocimiento de la Geología de España. http://info.igme.es/geologiasubsuelo/GeologiaSubsuelo/Documents.aspx. Instituto Geológico y Minero de España Ed., .465 pp., 17 mapas.

Leite Mendes, B.D., Pastor-Galán, D., Dekkers, M.J. & Krijgsman, W. (2021) Avalonia, get bent! – Paleomagnetism from SW Iberia confirms the Greater Cantabrian Orocline. *Geoscience Frontiers*, **12**, 805–825. doi:10.1016/j.gsf.2020.07.013

Martinez-Peña, M., & Casas-Sainz, A. (2003). Cretaceous–tertiary tectonic inversion of the Cotiella Basin (southern Pyrenees, Spain). International Journal of Earth Sciences, 92(1), 99-113.

Maxbauer, D.P., Feinberg, J.M., Fox, D.L. (2016). MAX UnMix: A web application for unmixing magnetic coercivity distributions. Comp. Geosci., 95, 140-145. doi:10.1016/j.cageo.2016.07.009

McCabe, C., Van der Voo, R., Peacor, D. R., Scotese, C. R., & Freeman, R. (1983). Diagenetic magnetite carries ancient yet secondary remanence in some Paleozoic sedimentary carbonates. Geology, 11(4), 221-223.

McCabe, C., & Elmore, R. D. (1989). The occurrence and origin of late Paleozoic remagnetization in the sedimentary rocks of North America. *Reviews of Geophysics*, *27*(4), 471-494.

McClelland, E. A., & McCaig, A. M. (1988). Palaeomagnetic estimates of total rotation in basement thrust sheets, Axial Zone, Southern Pyrenees. *Cuadernos de Geología Ibérica*, *12*, 181-193.

McClelland, E., & McCaig, A. M. (1989). Palaeomagnetic estimates of rotations in compressional regimes and potential discrimination between thin-skinned and deep crustal deformation. In: Paleomagnetic rotations and continental deformation (Eds: Kissel, C.; Laj, C.) NATO ASI Series C, 254, 365-379. Springer, Dordrecht.

McFadden, P.L.L. & McElhinny, M.W. (1988) The combined analysis of remagnetization circles and direct observations in palaeomagnetism. *Earth and Planetary Science Letters*, **87**, 161–172. doi:10.1016/0012-821X(88)90072-6

Millán-Garrido, H.; Oliva-Urcia, B., & Pocoví-Juan, A. (2006). La transversal de Gavarnie-Guara; estructura y edad de los mantos de Gavarnie, Guara-Gedre y Guarga (Pirineo centro-occidental). Geogaceta, 40, 35-38.

Mochales, T., Casas, A. M., Pueyo, E. L., & Barnolas, A. (2012). Rotational velocity for oblique structures (Boltaña anticline, Southern Pyrenees). *Journal of Structural Geology*, *35*, 2-16.

Mochales, T., Pueyo, E. L., Casas, A. M., & Barnolas, A. (2016). Restoring paleomagnetic data in complex superposed folding settings: the Boltaña anticline (Southern Pyrenees). *Tectonophysics*, *671*, 281-298.

Mujal, E., Fortuny, J., Pérez-Cano, J., Dinarès-Turell, J., Ibáñez-Insa, J., Oms, O., . . . Anadón, P. (2017). Integrated multi-stratigraphic study of the Coll de Terrers late Permian–Early Triassic continental succession from the Catalan Pyrenees (NE Iberian Peninsula): A geologic reference record for equatorial Pangaea. Global and Planetary Change, 159, 46-60. doi:https://doi.org/10.1016/j.gloplacha.2017.10.004

Mullender, T. A. T., T. Frederichs, C. Hilgenfeldt, L. V. de Groot, K. Fabian, and M. J. Dekkers (2016). Automated paleomagnetic and rock magnetic data acquisition with an in-line horizontal "2G" system. Geochem. Geophys. Geosyst., 17, 3546–3559. doi:10.1002/2016GC006436.

Müller, R.D., Zahirovic, S., Williams, S.E., Cannon, J., Seton, M., Bower, D.J., Tetley, M.G., *et al.* (2019) A Global Plate Model Including Lithospheric Deformation Along Major Rifts and Orogens Since the Triassic. *Tectonics*, **38**, 1884–1907, Blackwell Publishing Ltd. doi:10.1029/2018TC005462

Muñoz, J. A., Beamud, E., Fernández, O., Arbués, P., Dinarès-Turell, J., & Poblet, J. (2013). The Ainsa Fold and thrust oblique zone of the central Pyrenees: Kinematics of a curved contractional system from paleomagnetic and structural data. *Tectonics*, *32*(5), 1142-1175.

Muñoz, J. A. (1992). Evolution of a continental collision belt: ECORS-Pyrenees crustal balanced cross-section. In *Thrust tectonics* (pp. 235-246). Springer, Dordrecht.

Muñoz, J. A. (2019). Alpine Orogeny: Deformation and Structure in the Northern Iberian Margin (Pyrenees sl). In *The Geology of Iberia: A Geodynamic Approach* (pp. 433-451). Springer, Cham.

Muñoz, J. A., Martínez, A., & Vergés, J. (1986). Thrust sequences in the eastern Spanish Pyrenees. Journal of Structural Geology, 8(3-4), 399-405.

Nance, R.D., Gutiérrez-Alonso, G., Keppie, J.D., Linnemann, U., Murphy, J.B., Quesada, C., Strachan, R.A., *et al.* (2010) Evolution of the Rheic Ocean. *Gondwana Research*, **17**, 194–222. doi:10.1016/j.gr.2009.08.001

Neres, M., Miranda, J.M. & Font, E. (2013) Testing Iberian kinematics at Jurassic-Cretaceous times. *Tectonics*, **32**, 1312–1319. doi:10.1002/tect.20074

Oliva-Urcia, B., & Pueyo, E. L. (2007a). Gradient of shortening and vertical-axis rotations in the Southern Pyrenees (Spain), insights from a synthesis of paleomagnetic data. *Revista de la Sociedad Geológica de España*, *20*(1-2), 105-118.

Oliva-Urcia, B., & Pueyo, E. L. (2007b). Rotational basement kinematics deduced from remagnetized cover rocks (Internal Sierras, southwestern Pyrenees). *Tectonics*, *26*(4).

Oliva-Urcia, B., & Pueyo, E. L. (2019). Paleomagnetism in structural geology and tectonics. In *Teaching methodologies in structural geology and tectonics* (pp. 55-121). Springer, Singapore.

Oliva-Urcia, B., Pueyo, E. L., & Larrasoaña, J. C. (2008). Magnetic reorientation induced by pressure solution: a potential mechanism for orogenic-scale remagnetizations. *Earth and Planetary Science Letters*, *265*(3-4), 525-534.

Oliva-Urcia, B., Casas, A. M., Pueyo, E. L., Román-Berdiel, T., & Geissman, J. W. (2010). Paleomagnetic evidence for dextral strike-slip motion in the Pyrenees during alpine convergence (Mauléon basin, France). Tectonophysics, 494(3-4), 165-179.

Oliva-Urcia, B., Pueyo, E. L., Larrasoaña, J. C., Casas, A. M., Román-Berdiel, T., Van der Voo, R., & Scholger, R. (2012). New and revisited paleomagnetic data from Permian–Triassic red beds: Two kinematic domains in the west-central Pyrenees. *Tectonophysics*, *522*, 158-175.

Oliveira, J.T., Quesada, C., Pereira, Z., Matos, J.X., Solá, A.R., Rosa, D., Albardeiro, L., *et al.* (2019) South Portuguese Terrane: A Continental Affinity Exotic Unit. in *The Geology of Iberia: A Geodynamic Approach* Regional Geology Reviews eds. Quesada, C. & Oliveira, J.T., pp. 173–206, Cham: Springer International Publishing. doi:10.1007/978-3-030-10519-8_6

Pastor-Galan, D., Groenewegen, T., Brouwer, D., Krijgsman, W. & Dekkers, M.J. (2015) One or two oroclines in the Variscan orogen of Iberia? Implications for Pangea amalgamation. *Geology*, **43**, 527–530. doi:10.1130/G36701.1

Pastor-Galán, Daniel, Nance, R.D., Murphy, J.B. & Spencer, C.J. (2019) Supercontinents: myths, mysteries, and milestones. *Geological Society, London, Special Publications*, **470**, 39–64, Geological Society of London. doi:10.1144/SP470.16

Pastor-Galán, D, Ursem, B., Meere, P.A. & Langereis, C. (2015) Extending the Cantabrian Orocline to two continents (from Gondwana to Laurussia). Paleomagnetism from South Ireland. *Earth and Planetary Science Letters*, **432**. doi:10.1016/j.epsl.2015.10.019

Pastor-Galán, Daniel, Dekkers, M.J.M.J.M.J., Gutiérrez-Alonso, G., Brouwer, D., Groenewegen, T., Krijgsman, W., Fernández-Lozano, J., *et al.* (2016) Paleomagnetism of the Central Iberian curve's putative hinge: Too many oroclines in the Iberian Variscides. *Gondwana Research*, **39**, 96–113, International Association for Gondwana Research. doi:10.1016/j.gr.2016.06.016

Pastor-Galán, Daniel, Gutiérrez-Alonso, G., Dekkers, M.J.M.J. & Langereis, C.G.C.G.C.G. (2017) Paleomagnetism in Extremadura (Central Iberian zone, Spain) Paleozoic rocks: extensive remagnetizations and further constraints on the extent of the Cantabrian orocline. *Journal of Iberian Geology*, **43**, 583–600, Springer International Publishing. doi:10.1007/s41513-017-0039-x

Pastor-Galán, Daniel, Gutiérrez-Alonso, G., Murphy, J.B.B., Fernández-Suárez, J., Hofmann, M. & Linnemann, U. (2013) Provenance analysis of the Paleozoic sequences of the northern Gondwana margin in NW Iberia: Passive margin to Variscan collision and orocline development. *Gondwana Research*, **23**, 1089–1103, International Association for Gondwana Research. doi:10.1016/j.gr.2012.06.015

Pastor-Galán, Daniel, Gutiérrez-Alonso, G. & Weil, A.B. (2011) Orocline timing through joint analysis: Insights from the Ibero-Armorican Arc. *Tectonophysics*, **507**, 31–46. doi:10.1016/j.tecto.2011.05.005

Pastor-Galán, Daniel, Gutiérrez-Alonso, G. & Weil, A.B. (2020) The enigmatic curvature of Central Iberia and its puzzling kinematics. *Solid Earth*, **11**, 1247–1273, Copernicus GmbH. doi:https://doi.org/10.5194/se-11-1247-2020

Pastor-Galán, Daniel, Pueyo, E.L., Diederen, M., García-Lasanta, C. & Langereis, C.G. (2018) Late Paleozoic Iberian Orocline(s) and the Missing Shortening in the Core of Pangea. Paleomagnetism From the Iberian Range. *Tectonics*, **37**, 3877–3892, John Wiley & Sons, Ltd. doi:10.1029/2018TC004978

Pereira, M.F., Castro, A., Chichorro, M., Fernández, C., Díaz-Alvarado, J., Martí, J. & Rodríguez, C. (2014) Chronological link between deep-seated processes in magma chambers and eruptions: Permo-Carboniferous magmatism in the core of Pangaea (Southern Pyrenees). *Gondwana Research*, **25**, 290–308, Elsevier. doi:10.1016/J.GR.2013.03.009

Pérez-Cáceres, I., Martínez Poyatos, D., Simancas, J.F. & Azor, A. (2017) Testing the Avalonian affinity of the South Portuguese Zone and the Neoproterozoic evolution of SW Iberia through detrital zircon populations. *Gondwana Research*, **42**, 177–192. doi:10.1016/j.gr.2016.10.010

Porquet, M., Pueyo, E. L., Román-Berdiel, T., Olivier, P., Longares, L. A., Cuevas, J., ... & Auréjac, J. B. (2017). Anisotropy of magnetic susceptibility of the Pyrenean granites. *Journal of Maps*, *13*(2), 438-448.

Pueyo, E. L. (2000). Rotaciones paleomagnéticas en sistemas de pliegues y cabalgamientos. Tipos, causas, significado y aplicaciones (ejemplos del Pirineo Aragonés). *Unpublished PhD thesis, Universidad de Zaragoza*, *296*.

Pueyo, E. L., Sussman, A. J., Oliva-Urcia, B., & Cifelli, F. (2016a). Palaeomagnetism in fold and thrust belts: use with caution. *Geological Society, London, Special Publications*, *425*(1), 259-276.

Pueyo, E. L., Beamud, E., Muñoz, J. A., Rodríguez-Pintó, A., & San Miguel, G. (2016b). Remagnetización alpina en la Serra del Cadí (Pirineo Oriental). Geo-Temas, 16 (1) 869-872.

Pueyo, E. L., García-Lasanta, C., López, M. A., Oliván, C., San Miguel, G., Gil-Garbi, H et al. the GeoKin3DPyr working group (2017). Metodología para el desarrollo de la BBDD paleomagnética de Iberia (EPOS-DDSS Iberian Paleomagnetism). In MAGIBER X. (pp. 94–99). Instituto de Investigación en Ciencias Ambientales (IUCA). Universidad de Zaragoza. ISBN: 978-84-16723-40-9

Pueyo, E. L., Oliva-Urcia, B., Sánchez-Moreno, E.M., Arenas, C., Silva-Casal, R., Calvín, P., Santolaria, P., García-Lasanta, C., Oliván, C., Gil-Imaz, A., Compaired, F., Casas, A.M., Pocoví, A. (2021a). The geometry and kinematics of the Southwestern termination of the Pyrenees; A field guide to the Santo Domingo anticline. In Structural Geology and Tectonics Field Guidebook - Mukherjee, S. (Editor). Chapter 3, 52pp. Springer. ISBN 978-3-030-60142-3

Pueyo, E.L.; Rodríguez-Pintó, A.; Serra-Kiel, J.; Barnolas, A. (2021b in press). The chronology and rotational kinematics in the Eastern Jaca Basin (Southern Pyrenees): Las Bellostas section. Geologica Acta.

Puigdefàbregas, C., Muñoz, J. A., & Vergés, J. (1992). Thrusting and foreland basin evolution in the southern Pyrenees. In Thrust tectonics (pp. 247-254). Springer, Dordrecht.

Ramón, M. J., Pueyo, E. L., Oliva-Urcia, B., Scholger, R., Román-Berdiel, M. T., & Casas, A. M. (2016). Squeezing paleomagnetic information using virtual directions; an example from the Bielsa granite (Axial Pyrenees). Geotemas, 16(1), 873-876.

Ramón, M. J., Pueyo, E. L., Oliva-Urcia, B., & Larrasoaña, J. C. (2017). Virtual directions in paleomagnetism: A global and rapid approach to evaluate the NRM components. *Frontiers in Earth Science*, *5*, 8.

Ribeiro, M.L., Reche, J., López-Carmona, A., Aguilar, C., Bento dos Santos, T., Chichorro, M., Dias da Silva, Í., *et al.* (2019) Variscan Metamorphism. in *The Geology of Iberia: A Geodynamic Approach* Regional Geology Reviews eds. Quesada, C. & Oliveira, J.T., pp. 431–495, Cham: Springer International Publishing. doi:10.1007/978-3-030-10519-8_12

Robardet, M. (2003) The Armorica 'microplate': fact or fiction? Critical review of the concept and contradictory palaeobiogeographical data. *Palaeogeography, Palaeoclimatology, Palaeoecology*, **195**, 125–148. doi:10.1016/S0031-0182(03)00305-5

Rodríguez-Pintó, A., Pueyo, E. L., Calvín, P., Sánchez, E., Ramajo, J., Casas, A. M., ... & Román, T. (2016). Rotational kinematics of a curved fold: The Balzes anticline (Southern Pyrenees). *Tectonophysics*, *677*, 171-189.

Rouvier, H., Henry, B., & Le Goff, M. (2012). Mise en évidence par le paléomagnétisme de rotations régionales dans la virgation des Corbières (France). Bulletin de la Société géologique de France, 183(5), 409-424.

Santolaria, P., Ayala, C., Pueyo, E. L., Rubio, F. M., Soto, R., Calvín, P., ... & Casas-Sainz, A. M. (2020). Structural and geophysical characterization of the western termination of the South Pyrenean triangle zone. Tectonics, 39(8), e2019TC005891.

Scheepers, P. J. J., & Zijderveld, J. D. A. (1992). Stacking in Paleomagnetism: application to marine sediments with weak NRM. *Geophysical Research Letters*, *19*(14), 1519-1522.

Schmidt, P. W. (1982). Linearity spectrum analysis of multi-component magnetizations and its application to some igneous rocks from south-eastern Australia. *Geophysical Journal International*, *70*(3), 647-665.

Schwarz, E. J. (1963). A paleomagnetic investigation of Permo-Triassic red beds and andesites from the Spanish Pyrenees. Journal of Geophysical Research, 68(10), 3265-3271.

Schwarz, E.J. (1974) Magnetic Fabric in Massive Sulfide Deposits. *Canadian Journal of Earth Sciences*, **11**, 1669–1675, NRC Research Press Ottawa, Canada. doi:10.1139/e74-165

Schwarz, E.J. & Vaughan, D.J. (1972) Magnetic Phase Relations of Pyrrhotite. *Journal of geomagnetism and geoelectricity*, **24**, 441–458. doi:10.5636/jgg.24.441

Shaw, J., Johnston, S.T. & Gutiérrez-Alonso, G. (2015) Orocline formation at the core of Pangea: A structural study of the Cantabrian orocline, NW Iberian Massif. *Lithosphere*, **7**, 653–661, GeoScienceWorld. doi:10.1130/L461.1

Sitter, L.U. de & Zwart, H.J. (1957) Geological map of the Paleozoic of the Central Pyrenees. *Leidse Geologische Mededelingen*, **22**, 351–418.

Stampfli, G.M., Hochard, C., Vérard, C., Wilhem, C. & VonRaumer, J. (2013) The Formation of Pangea. *Tectonophysics*, **593**, 1–19. doi:10.1016/j.tecto.2013.02.037

Sussman, A. J., Butler, R. F., Dinarès-Turell, J., & Vergés, J. (2004). Vertical-axis rotation of a foreland fold and implications for orogenic curvature: an example from the Southern Pyrenees, Spain. *Earth and Planetary Science Letters*, *218*(3-4), 435-449.

Tait, J. (1999) New Early Devonian paleomagnetic data from NW France: Paleogeography and implications for the Armorican microplate hypothesis. *Journal of Geophysical Research*, **104**, PP. 2831--2839. doi:10.1029/98JB02787

Tait, J., Bachtadse, V. & Soffel, H. (1994) New palaeomagnetic constraints on the position of central Bohemia during Early Ordovician times. *Geophysical Journal International*, **116**, 131–140. doi:10.1111/j.1365-246X.1994.tb02132.x

Tait, J. A., Bachtadse, V., & Dinarès-Turell, J. (2000). Paleomagnetism of Siluro-Devonian sequences, NE Spain. Journal of Geophysical Research: Solid Earth, 105(B10), 23595-23603.

Teixell, A. (1996). The Ansó transect of the southern Pyrenees: basement and cover thrust geometries. Journal of the Geological Society, 153(2), 301-310.

Torsvik, T.H., Voo, R.V.D., Preeden, U., Mac, C., Steinberger, B., Doubrovine, P.V., Hinsbergen, D.J.J.V., *et al.* (2012) Phanerozoic polar wander, palaeogeography and dynamics. *Earth-Science Reviews*, **114**, 325–368, Elsevier B.V. doi:10.1016/j.earscirev.2012.06.007

Van Dongen, P. G. (1967). The rotation of Spain: palaeomagnetic evidence from the eastern Pyrenees. Palaeogeography, Palaeoclimatology, Palaeoecology, 3, 417-432.

van der Lingen, G. J. (1960). Geology of the Spanish Pyrenees, north of Canfranc, Huesca province (Doctoral dissertation, Instituto di investigaciones geologicas). Estudios Geológicos XVI, 206-242

Van der Voo, R. (1969). Paleomagnetic evidence for the rotation of the Iberian Peninsula. *Tectonophysics*, *7*(1), 5-56.

Van der Voo, R. (1993). *Paleomagnetism of the Atlantic, Tethys and Iapetus oceans*. Cambridge University Press.

Van der Voo, R., & Torsvik, T. H. (2012). The history of remagnetization of sedimentary rocks: deceptions, developments and discoveries. Geological Society, London, Special Publications, 371(1), 23-53.

van Velzen, A.J. & Zijderveld, J.D.A. (1995) Effects of weathering on single-domain magnetite in Early Pliocene marine marls. *Geophysical Journal International*, **121**, 267–278. doi:10.1111/j.1365-246X.1995.tb03526.x

Villalaín, J. J., Casas-Sainz, A. M., & Soto, R. (2016). Reconstruction of inverted sedimentary basins from syn-tectonic remagnetizations. A methodological proposal. Geological Society, London, Special Publications, 425(1), 233-246.

Vine, F.J. & Matthews, D.H. (1963) Magnetic Anomalies Over Oceanic Ridges. *Nature*, **199**, 947–949, Nature Publishing Group. doi:10.1038/199947a0

Vissers, R.L.M. & Meijer, P.Th. (2012) Mesozoic rotation of Iberia: Subduction in the Pyrenees? *Earth-Science Reviews*, **110**, 93–110. doi:10.1016/j.earscirev.2011.11.001

Waldner, M (2019). Cinématique et thermicité du prisme orogénique des Pyrénées : nouvelles données géo-thermochronologiques de la Zone Axiale. Sciences de la Terre. Sorbonne Université, 2019.

Weil, A. B, Gutiérrez-Alonso, G. & Conan, J. (2010) New time constraints on lithospheric-scale oroclinal bending of the Ibero-Armorican Arc: a palaeomagnetic study of earliest Permian rocks from Iberia. *Journal of the Geological Society*, **167**, 127–143. doi:10.1144/0016-76492009-002

Weil, A. B, Voo, R. van der & Pluijm, B.A. van der. (2001) Oroclinal bending and evidence against the Pangea megashear: The Cantabria-Asturias arc (northern Spain). *Geology*, **29**, 991–994.

Weil, Arlo B, Van der Voo, R. & Voo, R.V.D. (2002) Insights into the mechanism for orogen-related carbonate remagnetization from growth of authigenic Fe-oxide: A scanning electron microscopy and rock magnetic study of Devonian carbonates from northern Spain. *Journal of Geophysical Research-Solid Earth*, **107**, 14–14.

Weil, Arlo Brandon, Gutiérrez-Alonso, G. & Wicks, D. (2013) Investigating the kinematics of local thrust sheet rotation in the limb of an orocline: a paleomagnetic and structural analysis of the Esla tectonic unit, Cantabrian–Asturian Arc, NW Iberia. *Int J Earth Sci (Geol Rundsch)*, **102**, 43–60. doi:10.1007/s00531-012-0790-3

Weltje, G.J. (1997) End-member modeling of compositional data: Numerical-statistical algorithms for solving the explicit mixing problem. *Mathematical Geology*, **29**, 503–549. doi:10.1007/BF02775085

Zijderveld, J. D. A. (1967). AC demagnetization of rocks: analysis of results. In Methods in Paleomagnetism, Eds D.W. Collinson, K.M. Creen and S.K. Runcorn, Elsevier, Amsterdam.

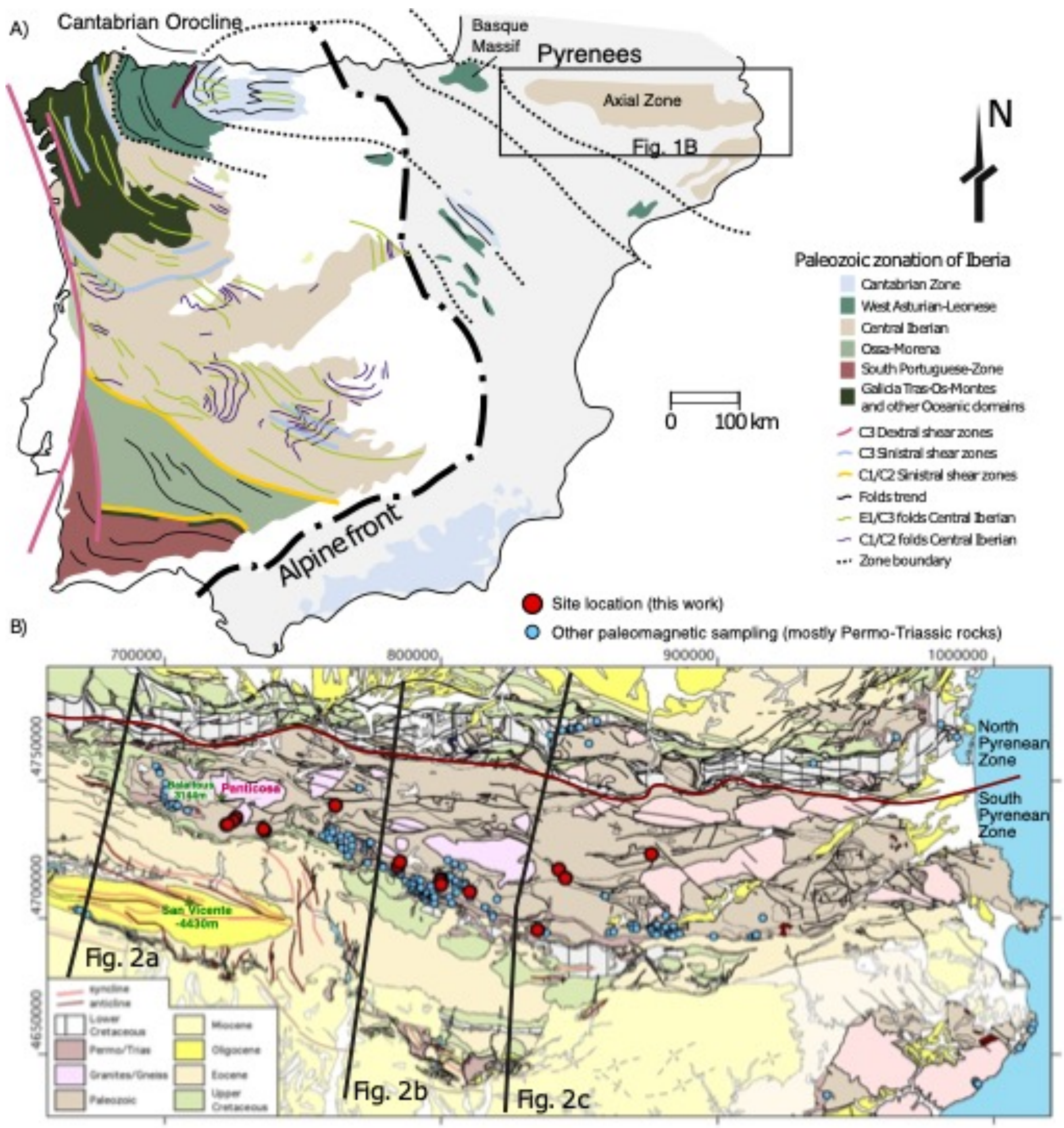

Figure 1: A) Simplified map of the Iberian Peninsula showing the main Paleozoic outcrops and the areas affected by the Alpine orogeny (after Pastor-Galán et al., 2020). B) Geological map of the Pyrenees (modified from Barnolas et al., 2008 according to Choukroune and Seguret, 1973) showing our sampling locations (red dots) and the extensive paleomagnetic studies in the Pyrenees focused mainly on Permo-Triassic rocks (blue dots). Lines show the trend of the cross sections in figure 2.

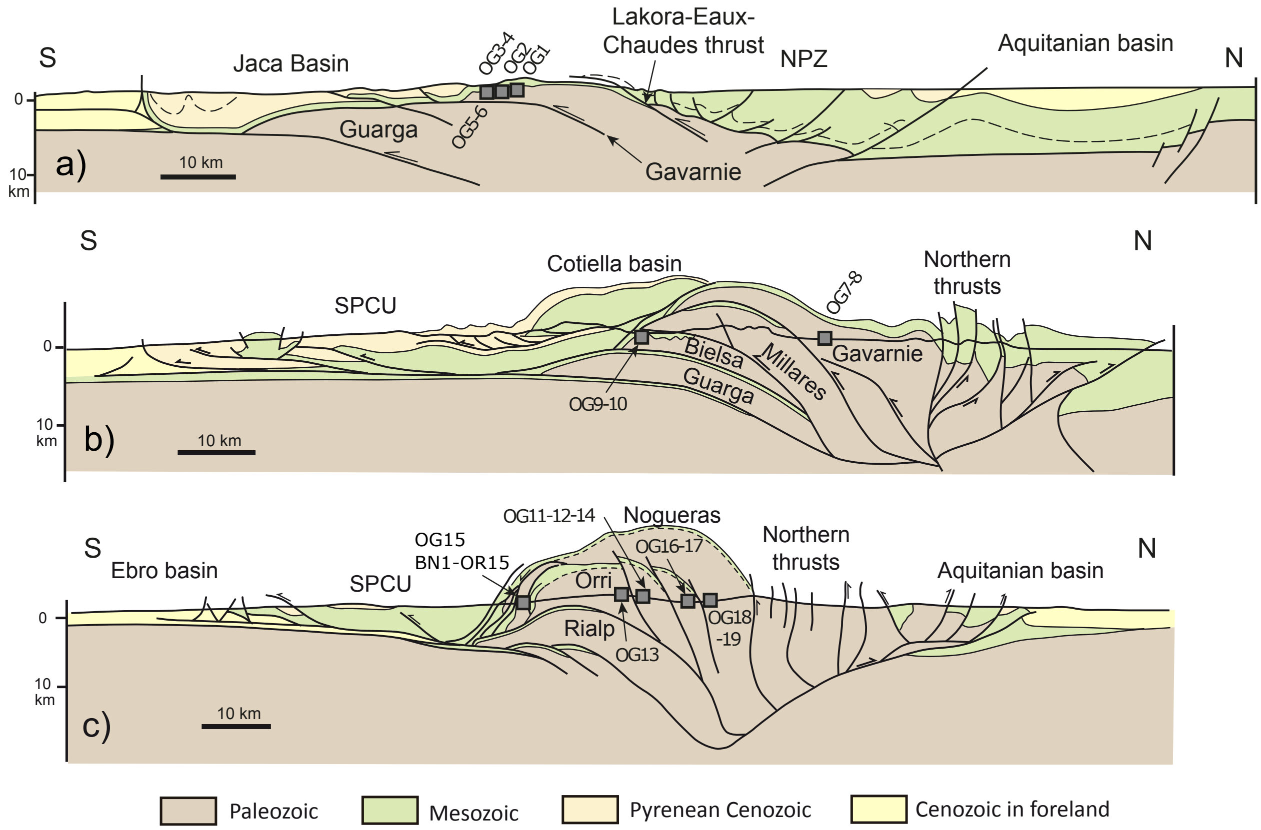

Figure 2: Cross sections through the Pyrenees with projected positions of our sampling sites.

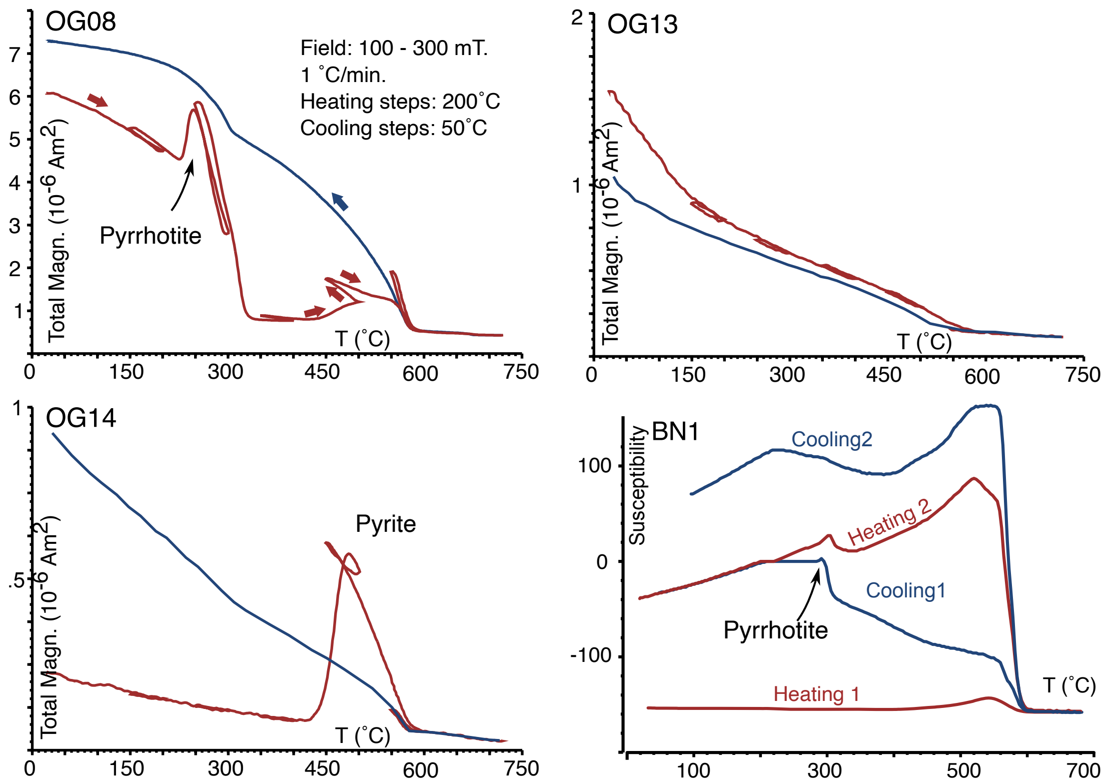

Figure 3: Selected magnetization vs. temperature curves (OG8, OG13, OG14) and susceptibility vs. temperature (BN1). Note that magnetic and non magnetic sulfides are common. All measurements performed are available in supplementary file SF1.

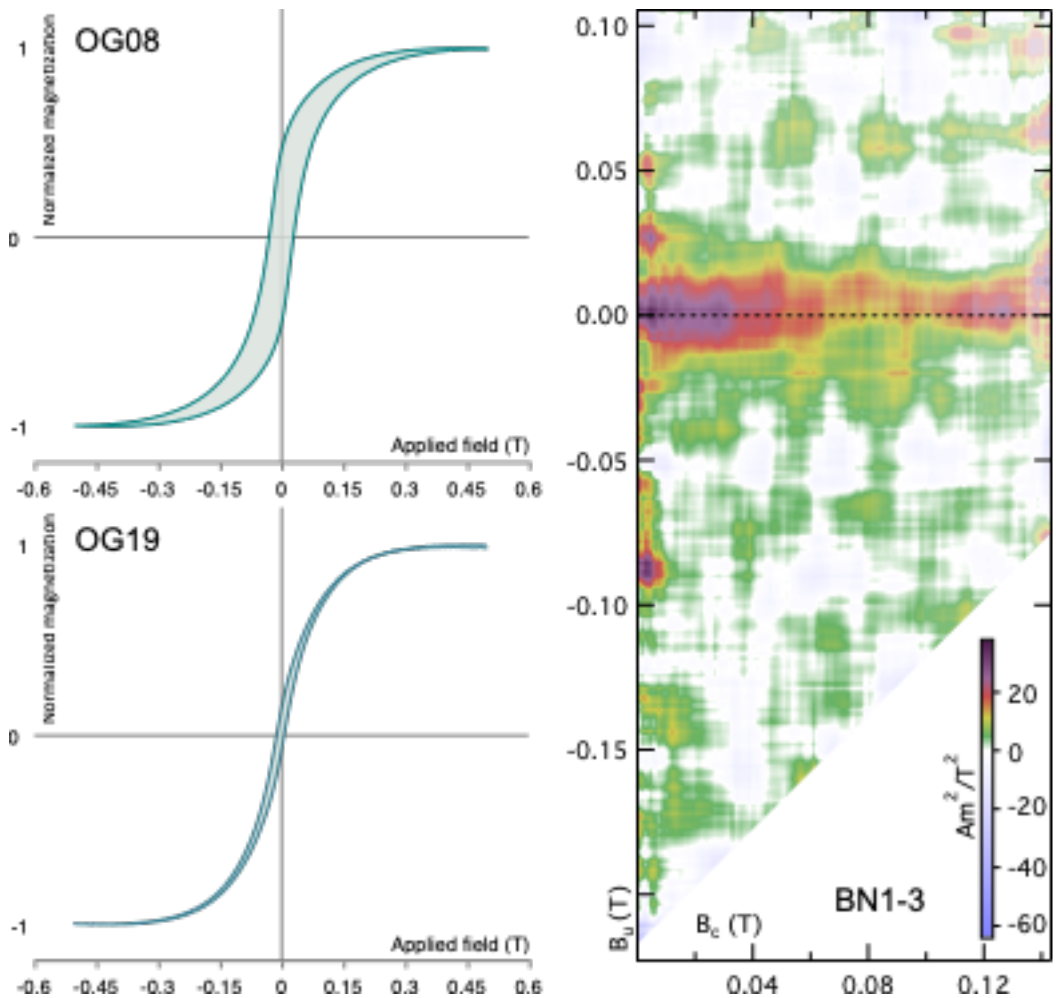

Figure 4: Selected slope corrected hysteresis loops and FORC diagram (plotted with FORCINEL (Harrison and Feinberg, 2008, smoothing factor 13). All measurements performed are available in supplementary file SF2.

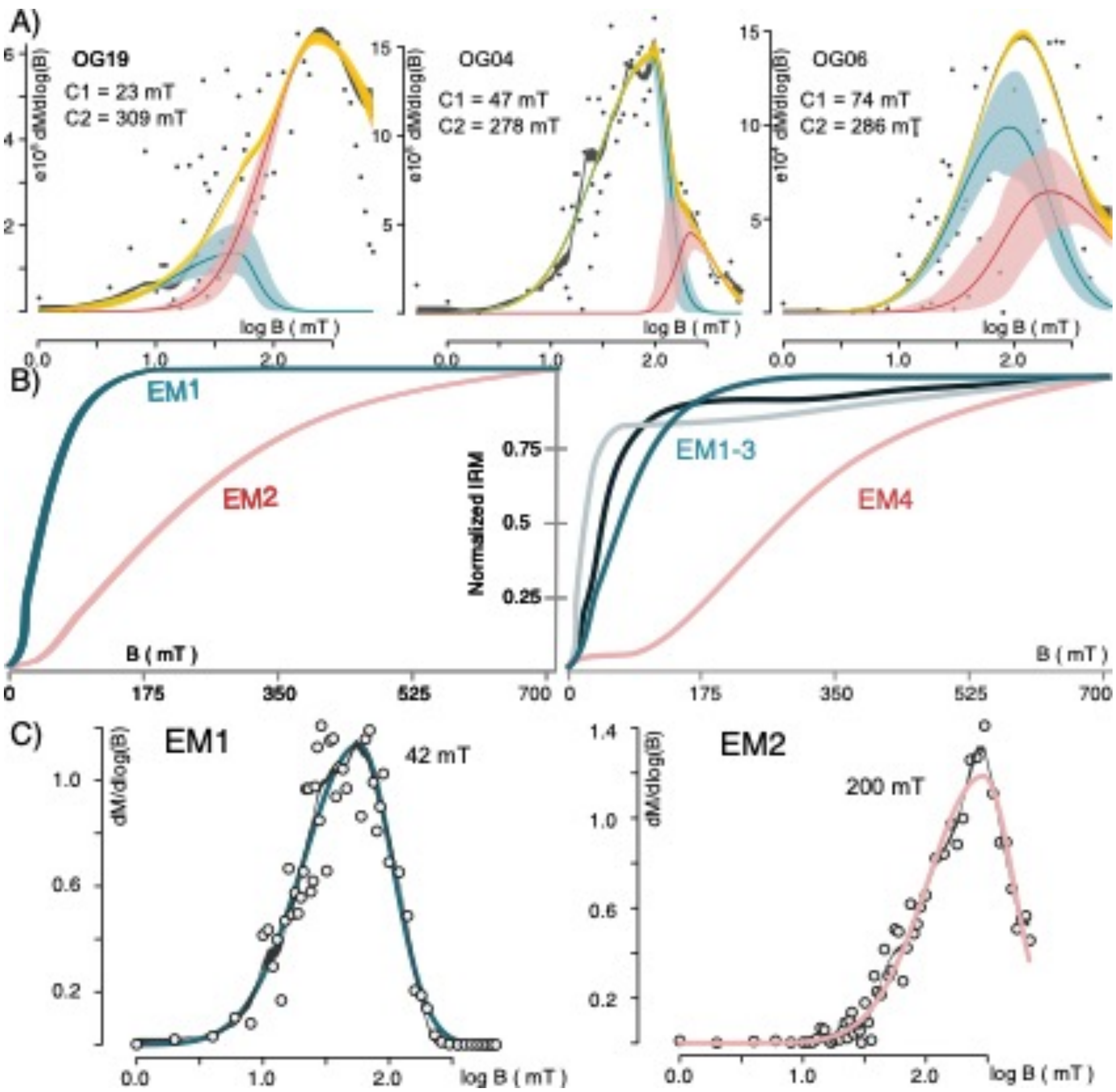

Figure 5: A) Unmixing of IRM acquisition curve for three samples showing different proportions of a 'soft' mineral that saturates below 75 mT (magnetite) and a 'harder' one that saturates over 200 mT (pyrrhotite). B) Results from the endmember modeling showing our preferred two end-member solution (left) and the four end-member solution (right). C) Unmixing of the IRM synthetic acquisition curve from the two end members showing the same two magnetic mineralogies as in the forward modeling of different samples: magnetite to the left and pyrrhotite to the right.

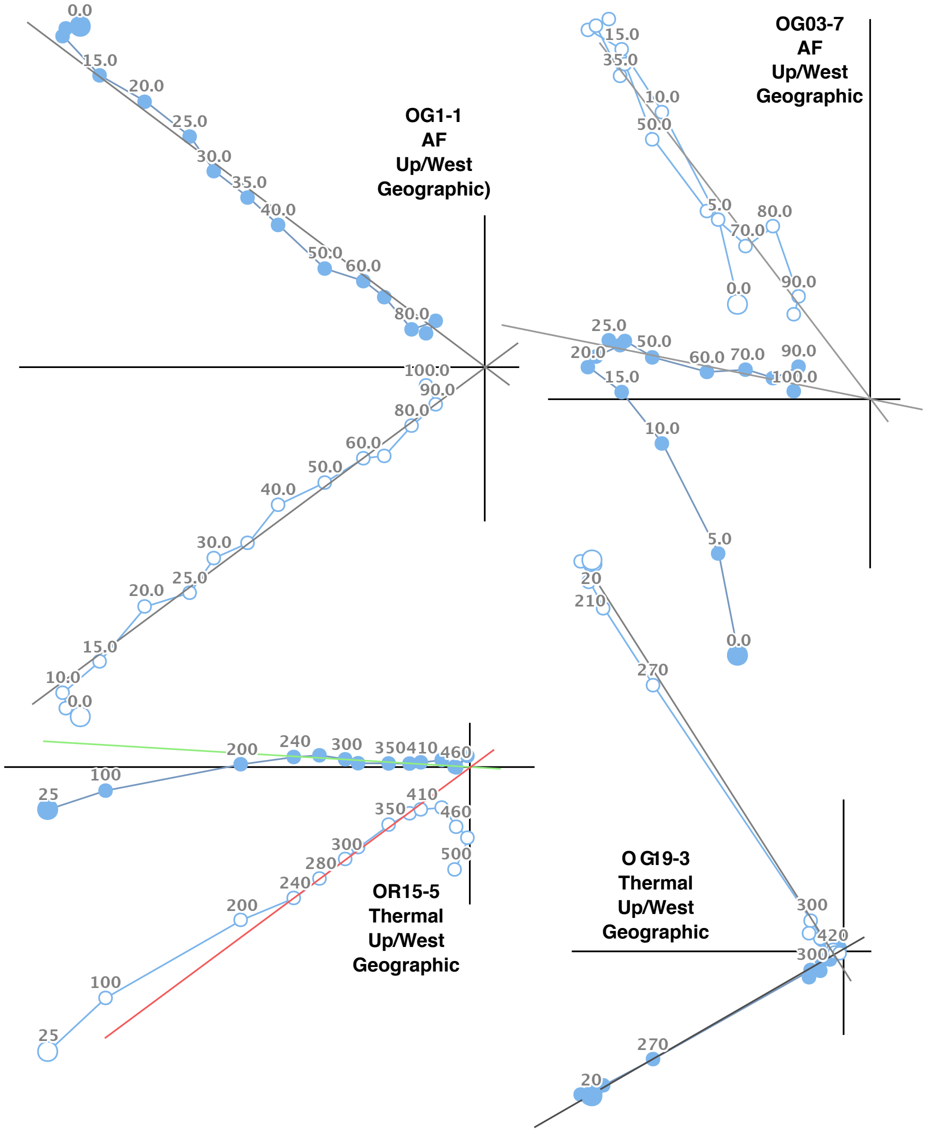

Figure 6: Examples of 'Zijderveld' (Zijderveld, 1967) vector-end point plots for selected samples. All samples plotted in geographic coordinates. Close-open circles represent declination and inclination projections respectively. Complete analyses are available in paleomagnetism.org through the Persistent identifyer PID given in the acknowledgements.

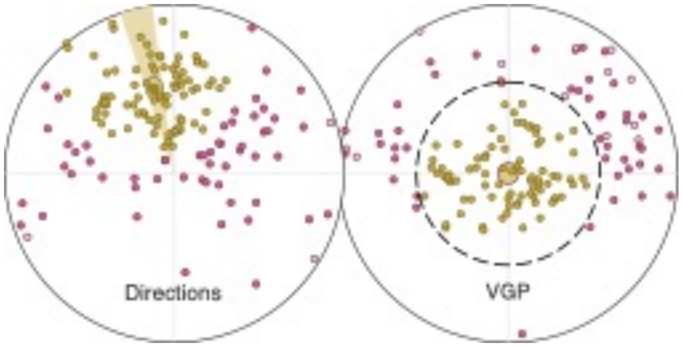

Figure 7: Viscous remanent magnetization (VRM) from all samples is compatible with the present-day field (geographic coordinates). Red dots are those that fall outside of the 45° cut-off. Uncertainty envelope is in both cases VGP A95. The rather large scattering is likely due to the small number of demagnetization levels containing the VRM (3-4) and the possible migration of the VRM during transport, storage and analysis.

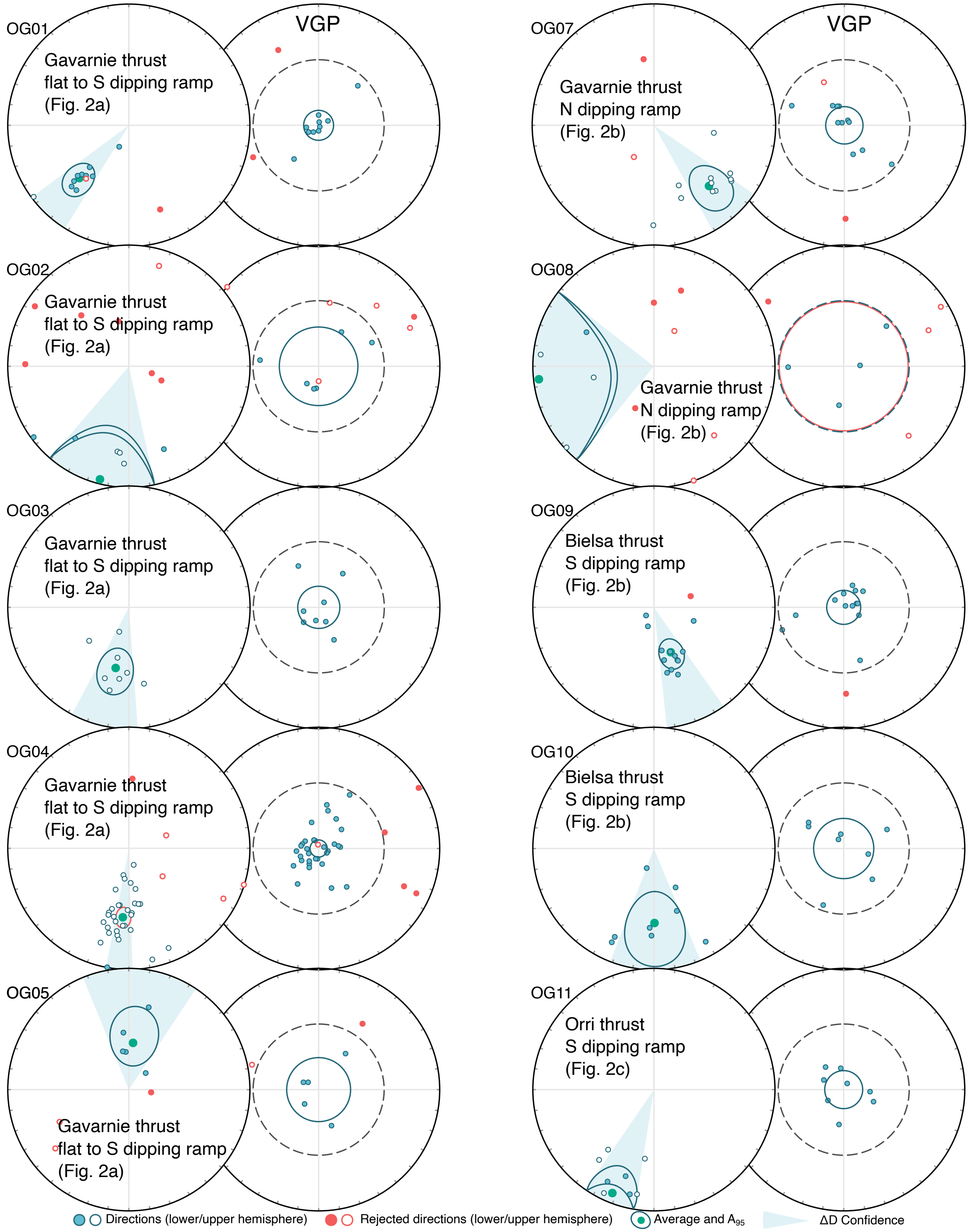
OG01
Gavarnie thrust
flat to S dipping ramp
(Fig. 2a)
VGP
OG02
Gavarnie thrust
flat to S dipping ramp
(Fig. 2a)
OG03
Gavarnie thrust
flat to S dipping ramp
(Fig. 2a)
OG04
Gavarnie thrust
flat to S dipping ramp
(Fig. 2a)
OG05
Gavarnie thrust
flat to S dipping ramp
(Fig. 2a)
OG07
Gavarnie thrust
N dipping ramp
(Fig. 2b)
VGP
OG08
Gavarnie thrust
N dipping ramp
(Fig. 2b)
OG09
Bielsa thrust
S dipping ramp
(Fig. 2b)
OG10
Bielsa thrust
S dipping ramp
(Fig. 2b)
OG11
Orri thrust
S dipping ramp
(Fig. 2c)
Directions (lower/upper hemisphere)
Rejected directions (lower/upper hemisphere)
Average and A95
ΔD Confidence

1241

Figure 8: Directional and VGP results in geographic coordinates of sites OG01 to OG11. Uncertainty envelope is in both cases VGP A95. Red dots are those that fall outside of the 45° cut-off. Sites OG02, 05 and 08 did not provide statistically meaningful results and were not interpreted.

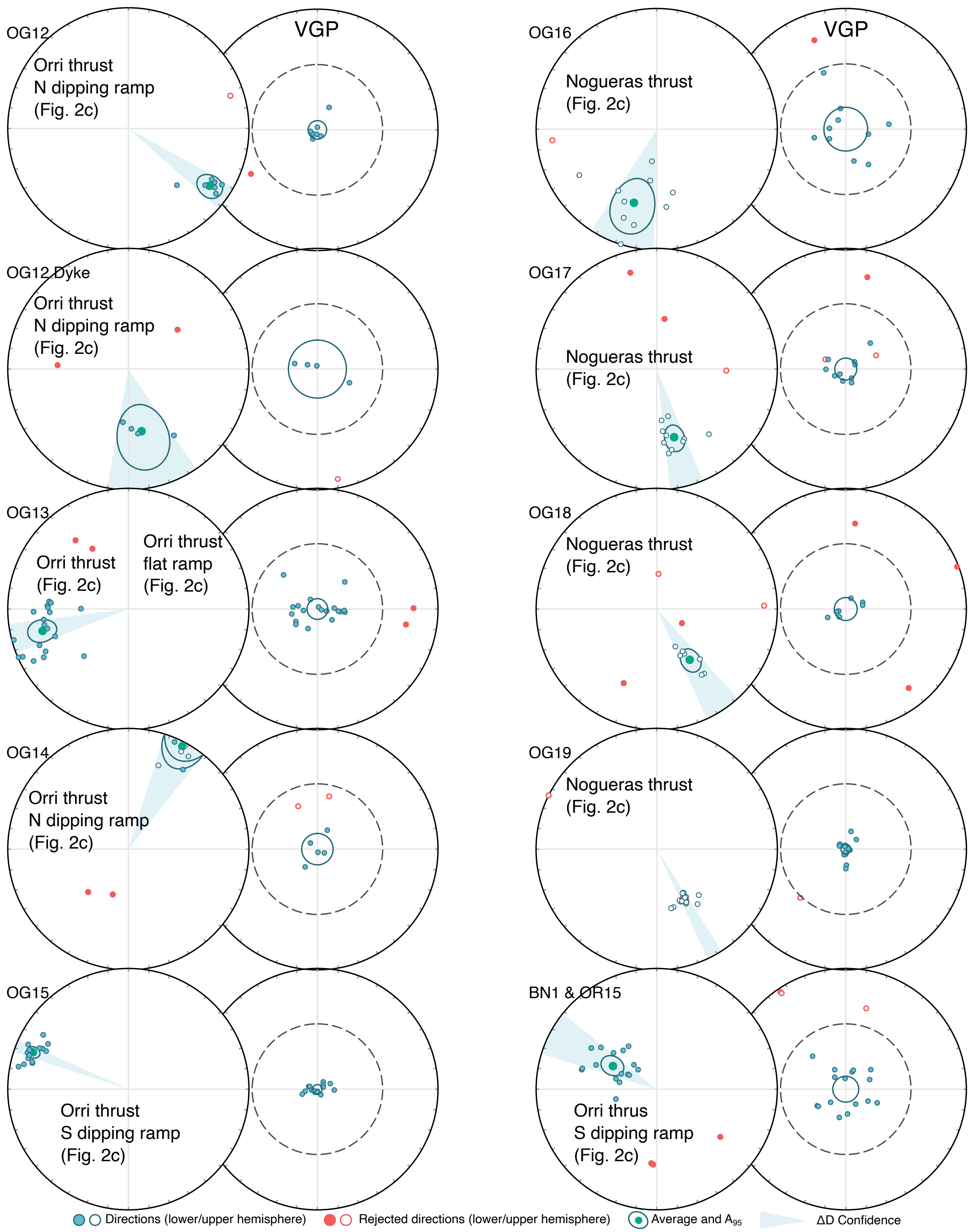
OG12
Orri thrust
N dipping ramp
(Fig. 2c)
VGP
OG16
Nogueras thrust
(Fig. 2c)
VGP
OG12 Dyke
Orri thrust
N dipping ramp
(Fig. 2c)
OG17
Nogueras thrust
(Fig. 2c)
OG13
Orri thrust
(Fig. 2c)
Orri thrust
flat ramp
(Fig. 2c)
OG18
Nogueras thrust
(Fig. 2c)
OG14
Orri thrust
N dipping ramp
(Fig. 2c)
OG19
Nogueras thrust
(Fig. 2c)
OG15
Orri thrust
S dipping ramp
(Fig. 2c)
BN1 & OR15
Orri thrus
S dipping ramp
(Fig. 2c)
Directions (lower/upper hemisphere)
Rejected directions (lower/upper hemisphere)
Average and A_{95}
ΔD Confidence

1247

Figure 9: Directional and VGP results in geographic coordinates of sites OG12 to OG19 and BN1-OR15. Uncertainty envelope is in both cases VGP A95. Red dots are those that fall outside of the 45° cut-off. Sites OG02, 05 and 08 did not provide statistically meaningful results and were not interpreted.

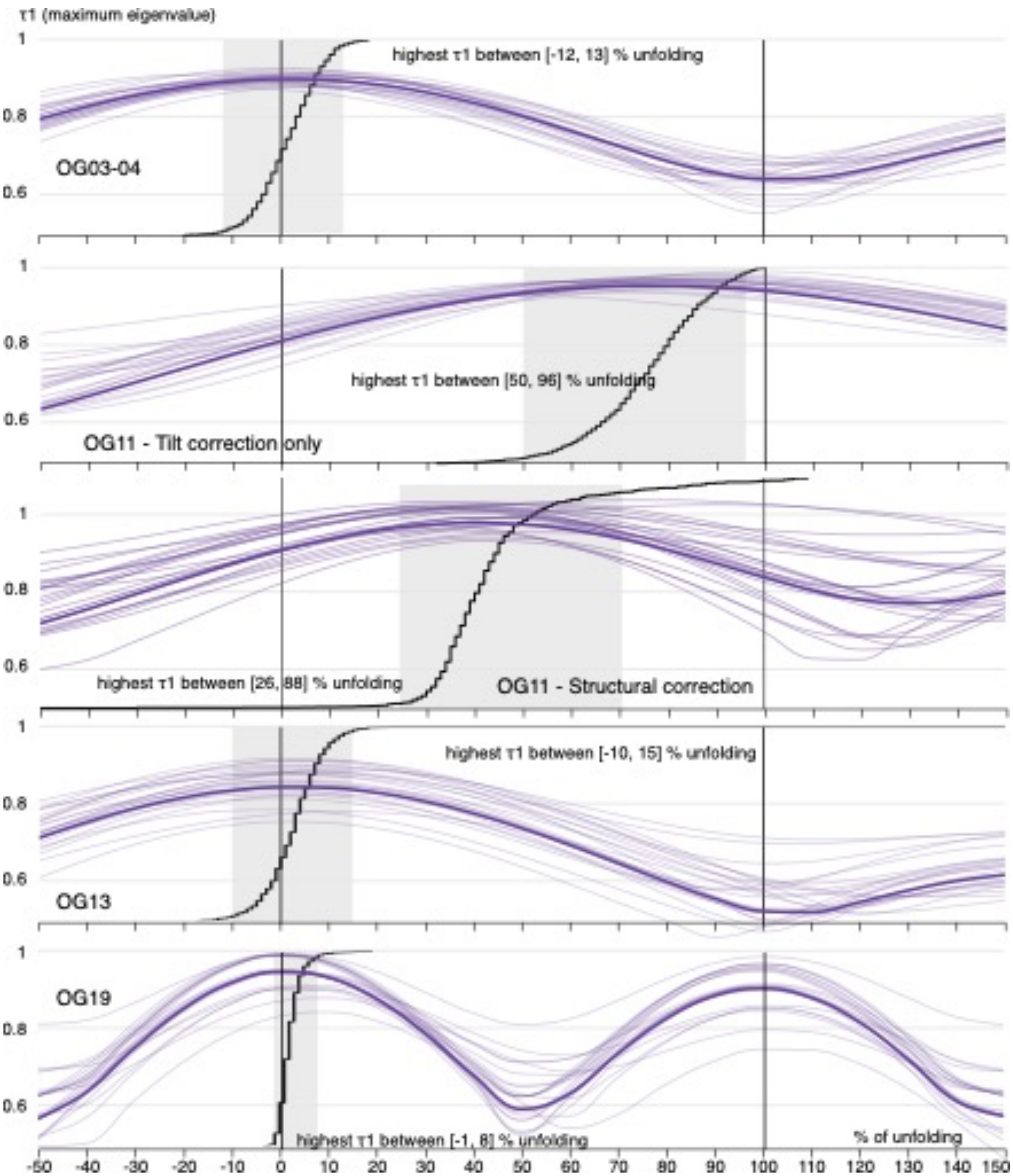

Figure 10: Within-site fold tests. All are negative but OG11, which is inconclusive.

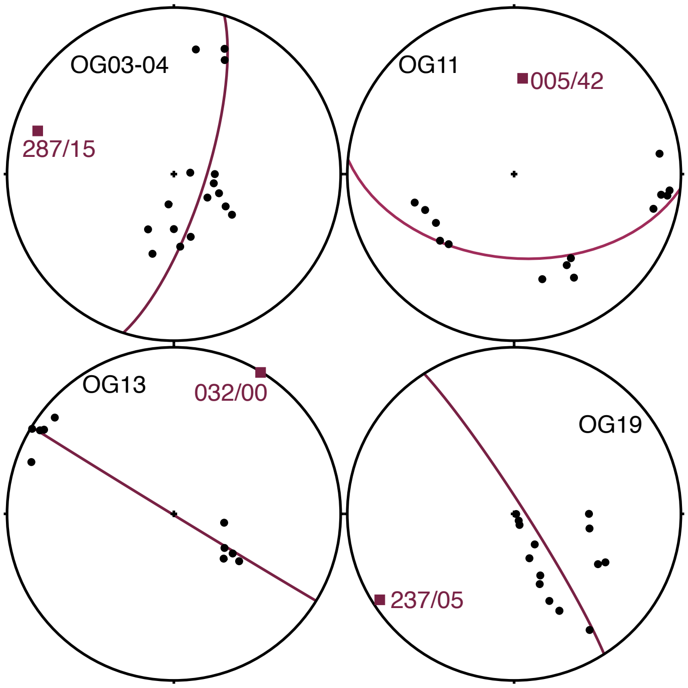

Figure 11: Pi diagrams for the studied folds. Only OG11 shows a steeply plunging axis.

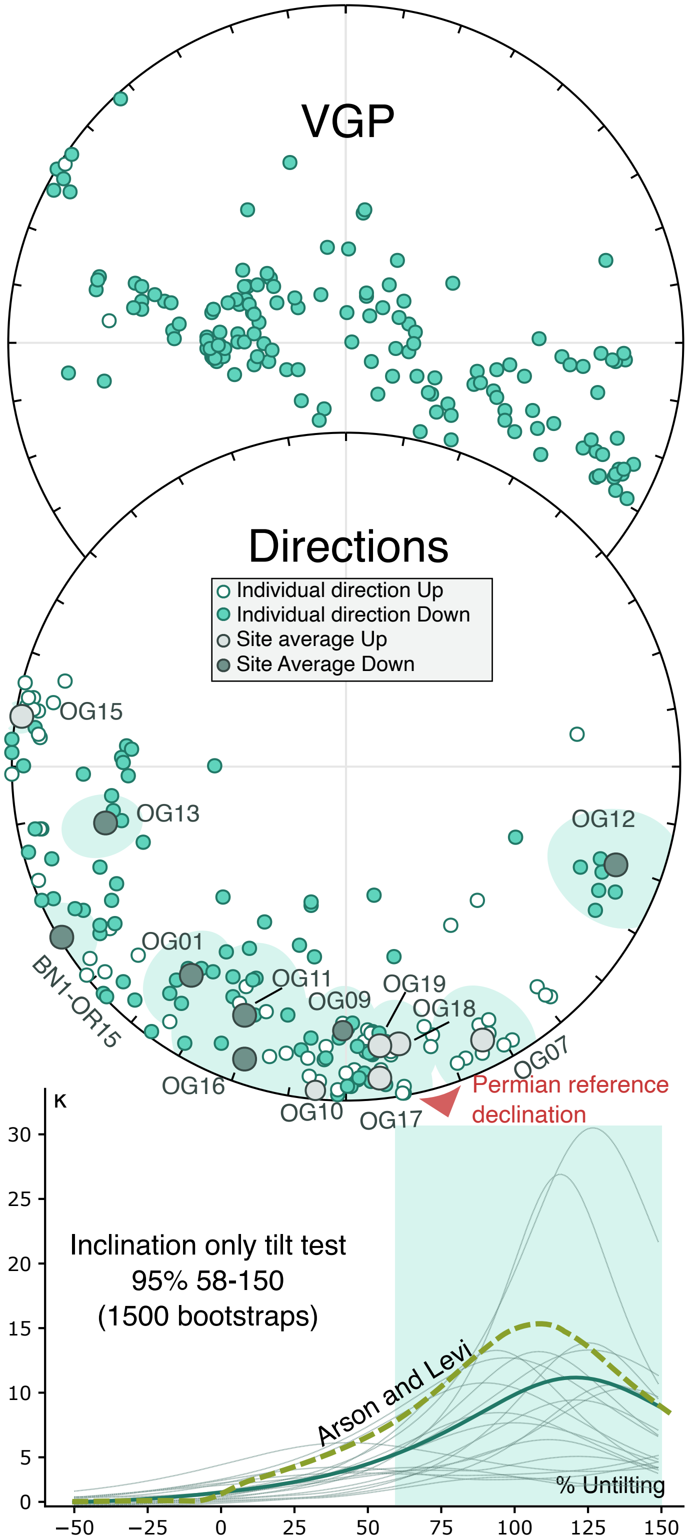

Figure 12: Results after the inferred Alpine tilt correction. Permian reference declination for Iberia is after Weil et al. (2010). The results show a positive inclination only tilt test following

the methodology of Enkin and Watson (1996) (selected bootstraps in thin gray lines) and Arson and Levi (2010) approach (dashed line).

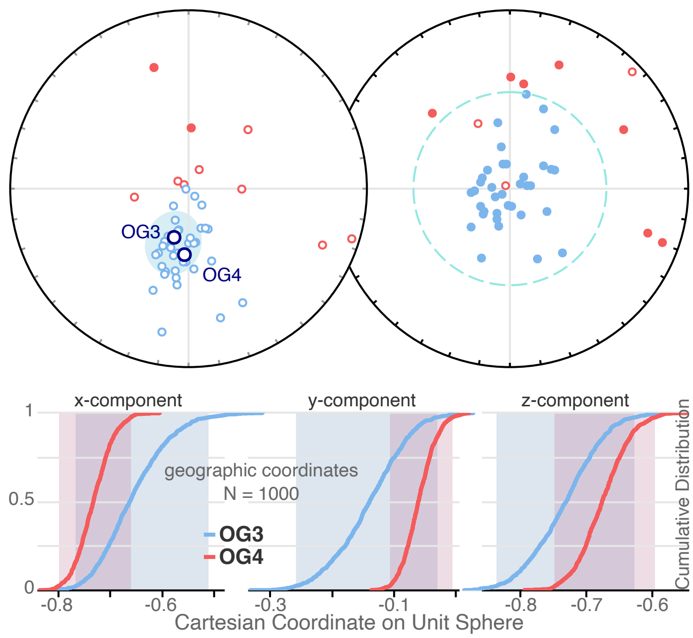

Figure 13: OG03 and OG04 show a common true mean bootstrapped direction (after Tauxe, 2010) in geographic (and Alpine tilt corrected) coordinates.

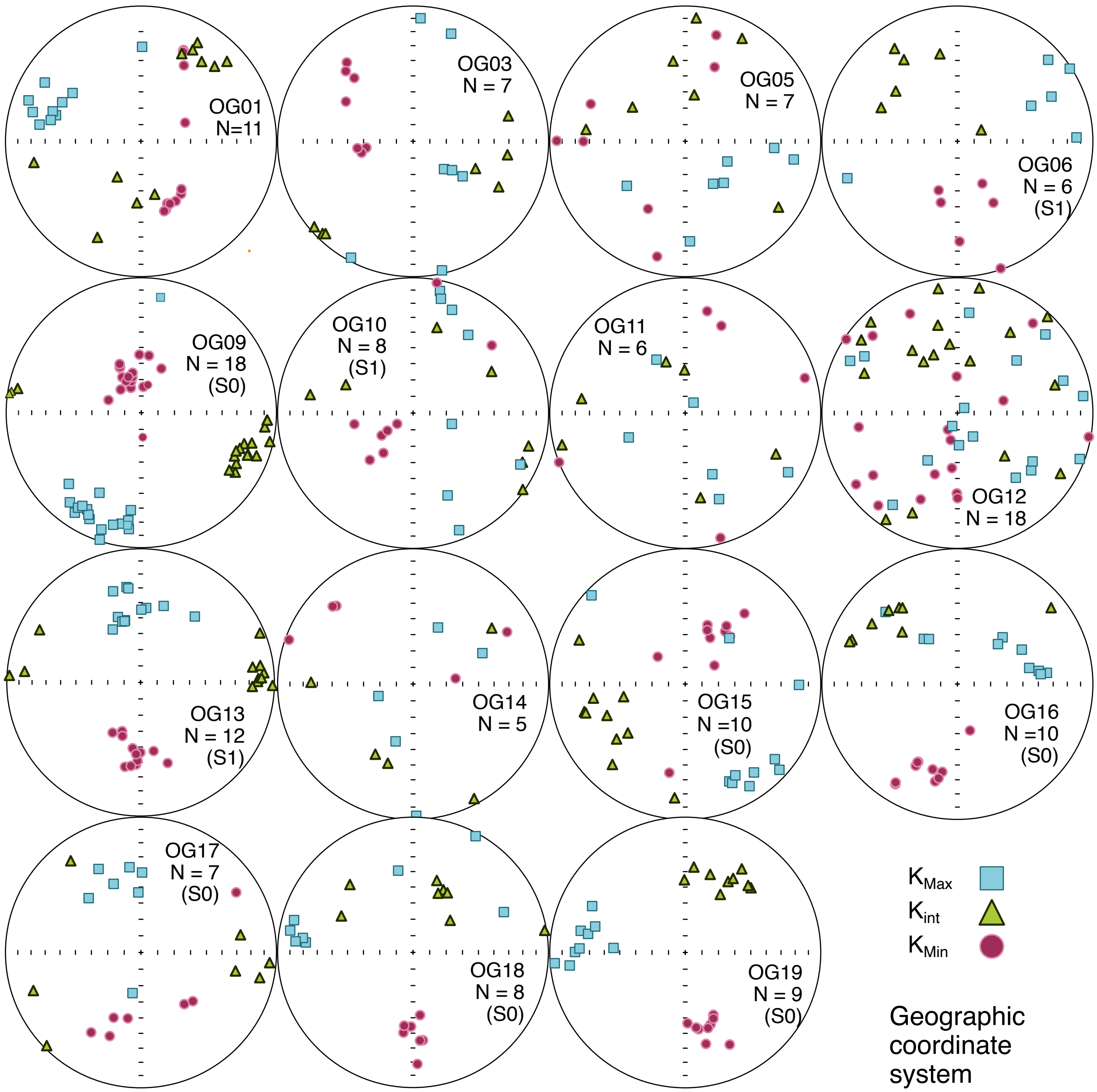

Figure 14: Results from the anisotropy of the magnetic susceptibility analyses. Magnetic fabrics represent bedding or S1 cleavage. Magnetic fabric directions do not coincide with the paleomagnetic directions, which allows us to discard an internal deformation control of the paleomagnetic remanence.

Table 1: Site Location and key structural data from each site.

Structure	S0 (Bedding)		Fold Axis		S1		Inferred Alpine tilt		Location	
	Dip Direction	Dip	Trend	Plunge	Dip direction	Dip	Dip Direction	Dip	Latitude	Longitude
OG01	-	-	-	-	-	-	185	20	42.7473	-0.24497
OG02*	Fold		191	14	-	-	185	20	42.7361	-0.25841
OG03	199	66	287	15	-	-	185	20	42.7249	-0.28900
OG04	Fold				20	60	185	20	42.7259	-0.28300
OG05*	299	17	-	-	-	-	180	20	42.7023	-0.12022
OG06*	358	62	-	-	256	78	180	20	42.7064	-0.12464
OG07	36	42	-	-	35	55	25	45	42.7771	0.19758
OG08*	10	36	-	-	-	-	25	45	42.7759	0.19858
OG09	89	13	-	-	-	-	205	45	42.5673	0.46444
OG10	17	31	-	-	-	-	205	45	42.5824	0.47447
OG11	Fold		5	42	-	-	25	30	42.5222	0.65244
OG12	40	39	-	-	-	-	25	30	42.5167	0.65100
OG13	Fold		32	0	-	-	25	0	42.5028	0.65228
OG14*	Fold		292	19	-	-	25	30	42.4752	0.77733
OG15	234	48	-	-	-	-	205	90	42.3380	1.06883
OG16	16	51	-	-	-	-	25	45	42.5339	1.17550
OG17	17	50	-	-	-	-	25	45	42.5048	1.20275
OG18	359	51	-	-	254	67	25	45	42.5689	1.59106
OG19	Fold		237	5	250	60	25	45	42.5682	1.58550
BN1 & OR15	185	25	-	-	-	-	205	90	42.3220	1.10466

*Unrealiable paleomagnetic result

Table 2: Paleomagnetic results for all sites in geographic and tilt (bedding) corrected coordinates.

Geographic	N	Ns	Cutoff	S	Dec	Inc	R	k	a95	K	A95	A95min	A95max	ΔDx	ΔIx	λ
OG01	10	12	45	16.71	222.7	40.19	9.48	17.27	11.96	24.19	10.02	4.78	19.22	10.89	13.79	22.9
OG02*	6	13	45	30.38	194.24	-4.41	4.97	4.86	33.88	7.34	26.5	5.86	26.52	26.52	52.76	-2.21
OG03	8	8	45	20.23	191.98	-47.6	7.66	20.67	12.47	16.32	14.13	5.22	22.12	16.16	16.7	-28.7
OG04	32	37	45	18.08	184.57	-42.53	30.18	17.02	6.34	20.49	5.75	3	9.24	6.33	7.56	-24.64
OG05*	5	8	45	22.16	5.71	58.01	4.78	17.93	18.57	13.61	21.51	6.3	29.75	28.01	19.81	38.68
OG06*	2	3	45	24.06	248.92	-20.54	1.88	8.48	100.98	11.42	82.51	9.09	52.99	NaN	149.78	-10.61
OG07	11	13	45	21.77	137.77	-32.97	10.37	15.83	11.84	14.29	12.51	4.6	18.1	13.16	19.46	-17.97
OG08*	4	10	45	35.85	263.68	-5.38	3.11	3.36	59.54	5.28	44.25	6.89	34.24	44.31	87.91	-2.7
OG09	13	14	45	21.87	159.34	57.48	12.55	26.68	8.18	14.19	11.4	4.3	16.29	14.55	10.64	38.1
OG10	8	8	45	28.26	179.3	38.56	7.17	8.42	20.28	8.45	20.23	5.22	22.12	21.86	28.68	21.73
OG11	8	8	45	18.26	201.72	-9.18	7.18	8.58	20.06	19.89	12.73	5.22	22.12	12.77	24.98	-4.62
OG12	7	8	45	8.33	125.38	18.71	6.89	53.04	8.36	95.15	6.22	5.51	24.07	6.31	11.48	9.61
OG12-Dyke	4	6	45	16.99	167.95	46.44	3.9	28.77	17.42	23.01	19.57	6.89	34.24	22.23	23.72	27.73
OG13	19	21	45	16.57	255.81	27.7	18.01	18.2	8.09	24.22	6.96	3.7	12.83	7.2	11.67	14.71
OG14*	5	7	45	11.11	27.96	-4.07	4.79	19.12	17.95	53.41	10.56	6.3	29.75	10.57	21.05	-2.04
OG15	15	15	45	6.56	291.06	16.61	14.87	107.25	3.71	152.91	3.1	4.06	14.89	3.14	5.82	8.48
OG16	10	11	45	23.96	197.11	-36.31	9.14	10.48	15.66	11.72	14.72	4.78	19.22	15.71	21.7	-20.18
OG17	10	13	45	12.28	165.55	-41.26	9.79	41.99	7.54	43.86	7.38	4.78	19.22	8.06	9.94	-23.69
OG18	7	11	45	10.29	146.65	-48.47	6.88	49.71	8.64	62.26	7.71	5.51	24.07	8.86	8.94	-29.45
OG19	15	16	45	6.98	151.24	-50.69	14.93	188.02	2.8	135.26	3.3	4.06	14.89	3.87	3.64	-31.41
BN1 & OR15	16	19	45	18.76	297.88	56.61	15.43	26.13	7.35	18.89	8.71	3.96	14.3	10.96	8.32	37.18
Tilt corrected																
OG01	10	12	45	16.71	222.7	40.19	9.48	17.27	11.96	24.19	10.02	4.78	19.22	10.89	13.79	22.9
OG02*	5	13	45	28.84	290.83	0.19	4.02	4.07	43.34	8.09	28.63	6.3	29.75	28.63	57.26	0.1
OG03	8	8	45	24.81	30.57	-65.75	7.66	20.67	12.47	10.9	17.56	5.22	22.12	26.79	13.23	-47.98
OG04	32	37	45	18.27	179.62	-19.66	29.27	11.35	7.89	19.99	5.83	3	9.24	5.92	10.66	-10.13
OG05*	6	8	45	27.91	19.38	45.79	5.54	10.9	21.23	8.67	24.12	5.86	26.52	27.35	29.65	27.2
OG06*	2	3	45	16.59	230.08	-10.25	1.88	8.48	100.98	23.93	53.52	9.09	52.99	53.83	104.49	-5.17
OG07	11	13	45	16.8	156.89	-16.86	10.37	15.83	11.84	23.56	9.61	4.6	18.1	9.72	18	-8.62
OG08*	3	10	45	26.69	247.31	-2.42	2.63	5.46	58.88	9.34	42.85	7.73	41.04	42.86	85.58	-1.21
OG09	13	14	45	17.61	164.17	45.05	12.55	26.68	8.18	21.64	9.12	4.3	16.29	10.21	11.39	26.6
OG10	6	8	45	30.89	169.06	56.53	5.52	10.48	21.7	7.09	27.03	5.86	26.52	34.74	25.85	37.1
OG11	8	8	45	11.72	200.07	-4.48	7.75	27.93	10.66	48.06	8.07	5.22	22.12	8.08	16.07	-2.24
OG12	8	8	45	16.16	111.8	5.44	7.43	12.25	16.48	25.83	11.11	5.22	22.12	11.12	22.06	2.72
OG12-Dyke	4	6	45	19.2	127.4	56.64	3.85	20.52	20.78	18.07	22.22	6.89	34.24	28.35	21.19	37.21
OG13	11	21	45	19.66	183.15	41.74	10.46	18.38	10.94	17.25	11.31	4.6	18.1	12.4	15.1	24.04
OG14*	5	7	45	21.6	46.47	-55.84	4.79	19.12	17.95	14.34	20.91	6.3	29.75	26.32	20.34	-36.39
OG15	15	15	45	5.25	289.1	-11.31	14.87	107.25	3.71	238.05	2.48	4.06	14.89	2.5	4.82	-5.71
OG16	10	11	45	20.18	15.07	-14.68	9.14	10.48	15.66	16.44	12.28	4.78	19.22	12.38	23.37	-7.46
OG17	11	13	45	16.57	171.02	0.43	10.41	16.87	11.45	24.55	9.4	4.6	18.1	9.4	18.8	0.21
OG18	8	11	45	17.99	159.26	-8.83	7.4	11.66	16.93	20.94	12.39	5.22	22.12	12.43	24.35	-4.44
OG19	9	16	45	4.48	155.85	10.2	8.96	217.22	3.5	327.87	2.85	4.98	20.54	2.86	5.56	5.14
BN1 & OR15	14	19	45	21.46	257.17	56	13.43	22.91	8.49	14.47	10.82	4.18	15.55	13.51	10.49	36.55

* Less than n = 7 was not considered

Table 3: Paleomagnetic results after the Alpine tilt correction (tilt associated to the emplacement of the thrusts).

ALPINE TILT CORRECTION	Dec	Inc
OG01	215.64	23.55
OG03	197.28	-67.34
OG04	184.57	-60.42
OG07	153.46	-8.93
OG09	145.47	21.97
OG10	180.36	-3.3
OG11	185.14	20.77
OG12	110.54	15.53
OG13	255.81	27.7
OG15	278.36	-3.78
OG16	198.58	8.37
OG17	173.76	-6.78
OG18	168.95	-16.46
OG19	172.82	-16.4
BN1 & OR15	238.36	1.58

Table 4: Concentration parameters of inclination only statistics from the mean values of the sites.

Inclination only statistics			
Geographic	k	Inclination	α95
Site means avg.	0	0	90
Bedding corrected			
Site means avg.	2.17	18.25	38.91
Site means avg. but OG03 & 04	3.93	22.67	25.44
Alpine tilt corrected			
Site means avg.	4.19	-3.4	21.25
Site means avg. but OG03 & 04	14.42	5.08	11.3

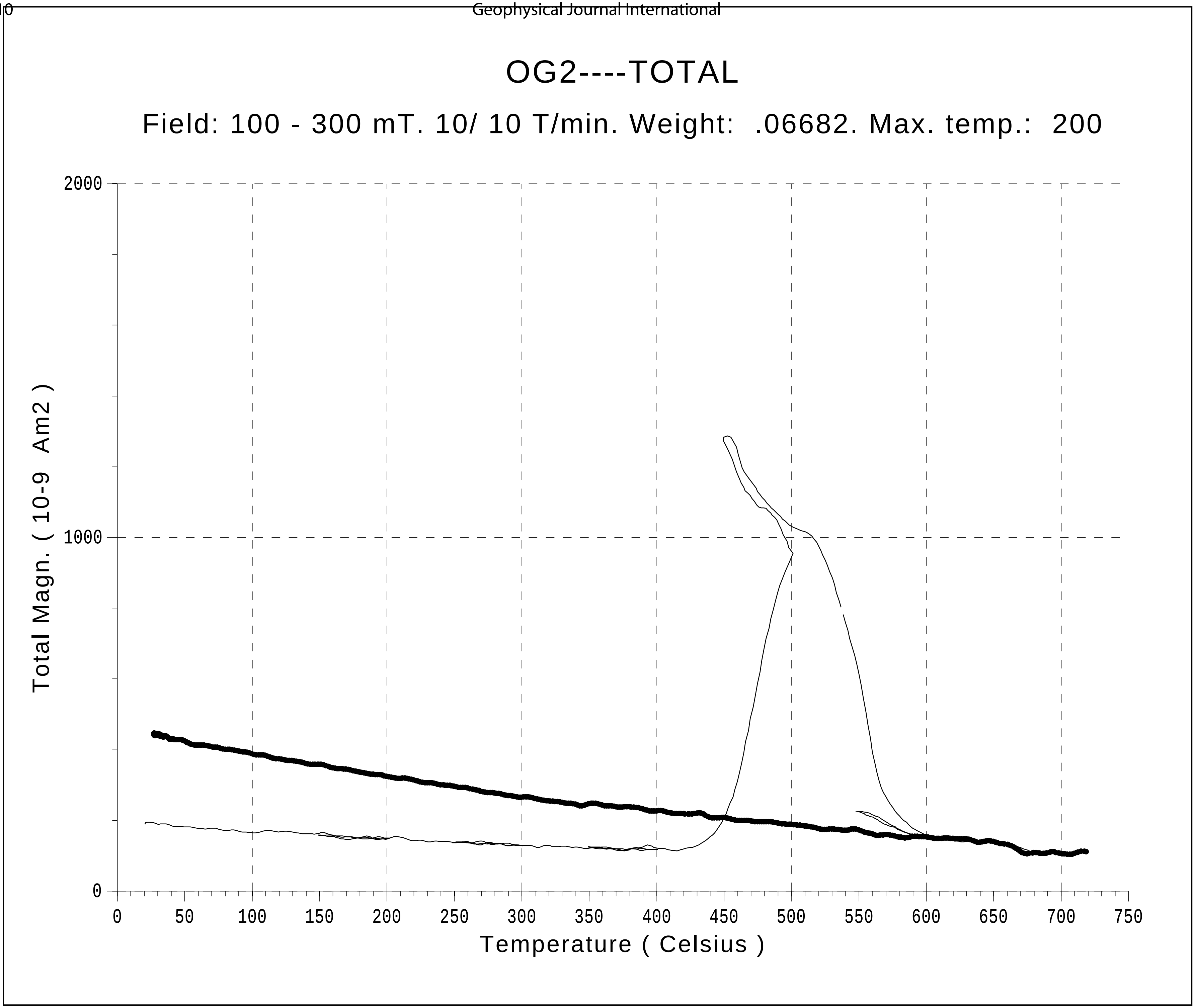
OG2----TOTAL
Field: 100 - 300 mT. 10/ 10 T/min. Weight: .06682. Max. temp.: 200
Total Magn. (10-9 Am2)
2000
1000
0
0
50
100
150
200
250
300
350
400
450
500
550
600
650
700
750
Temperature (Celsius)

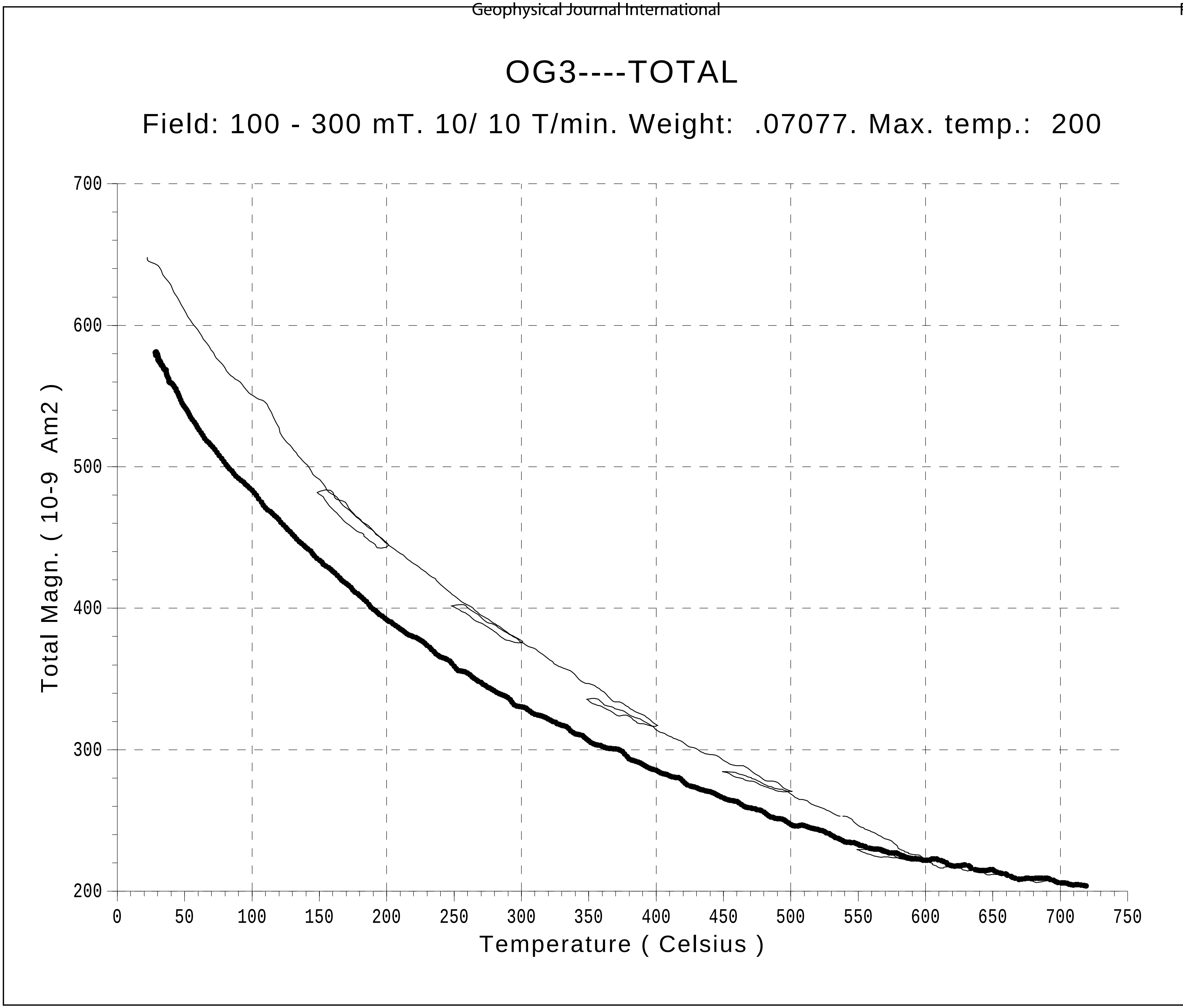

OG3----TOTAL
Field: 100 - 300 mT. 10/ 10 T/min. Weight: .07077. Max. temp.: 200
Total Magn. (10-9 Am2)
700
600
500
400
300
200
0
50
100
150
200
250
300
350
400
450
500
550
600
650
700
750
Temperature (Celsius)

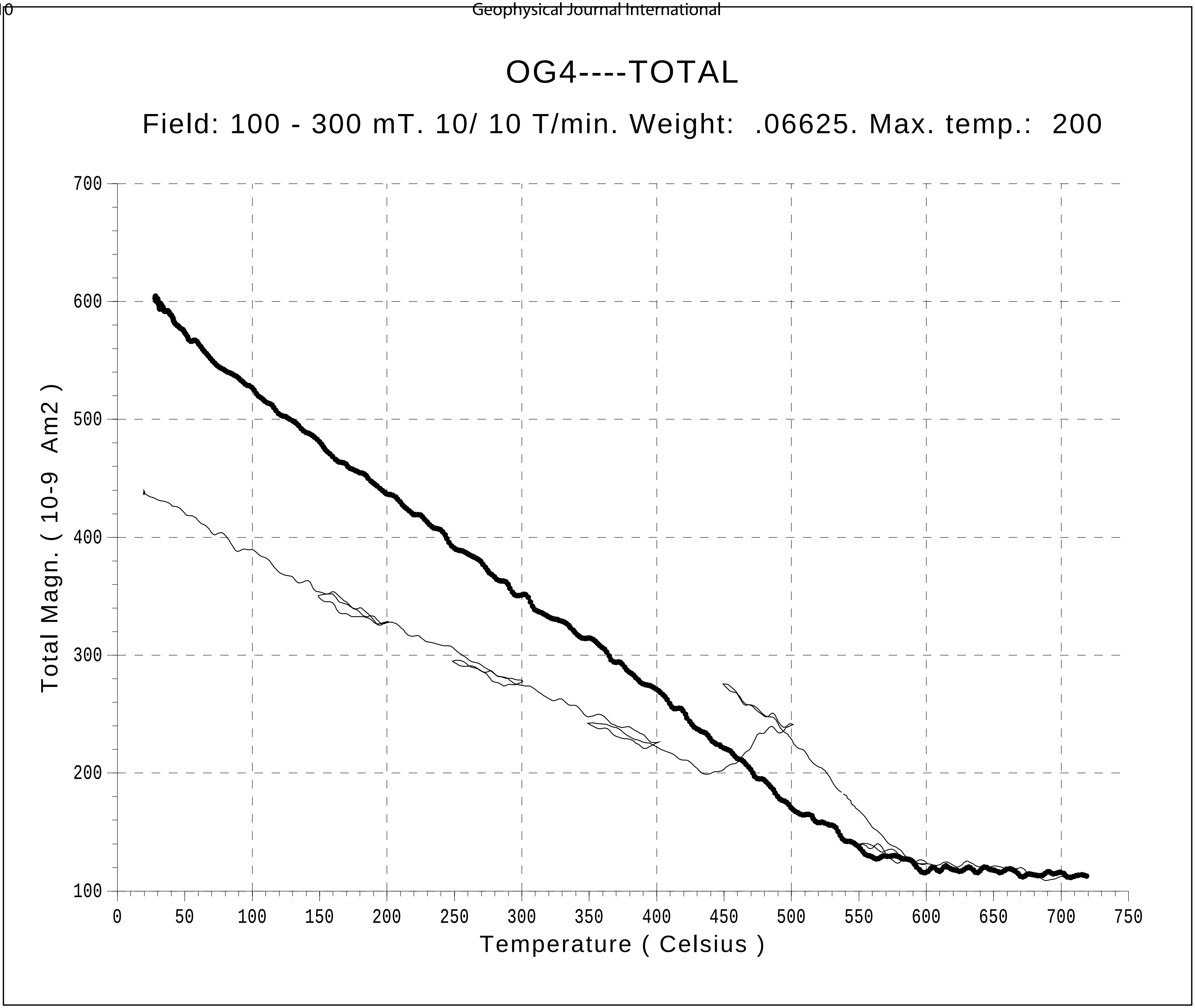
OG4----TOTAL
Field: 100 - 300 mT. 10/ 10 T/min. Weight: .06625. Max. temp.: 200
Total Magn. (10-9 Am2)
Temperature (Celsius)
700
600
500
400
300
200
100
0
50
100
150
200
250
300
350
400
450
500
550
600
650
700
750

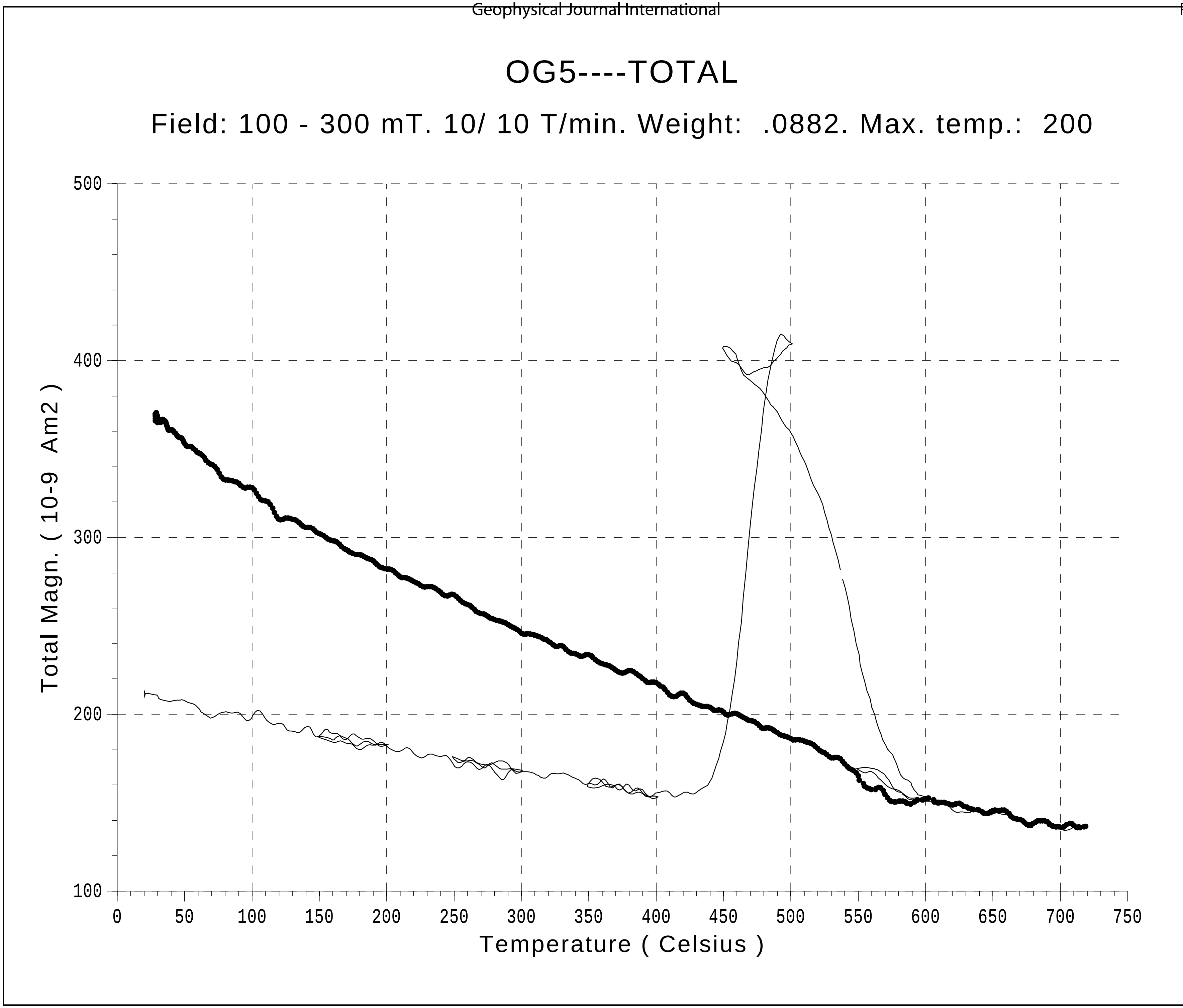
OG5----TOTAL
Field: 100 - 300 mT. 10/ 10 T/min. Weight: .0882. Max. temp.: 200
Total Magn. (10-9 Am2)
500
400
300
200
100
0
50
100
150
200
250
300
350
400
450
500
550
600
650
700
750
Temperature (Celsius)

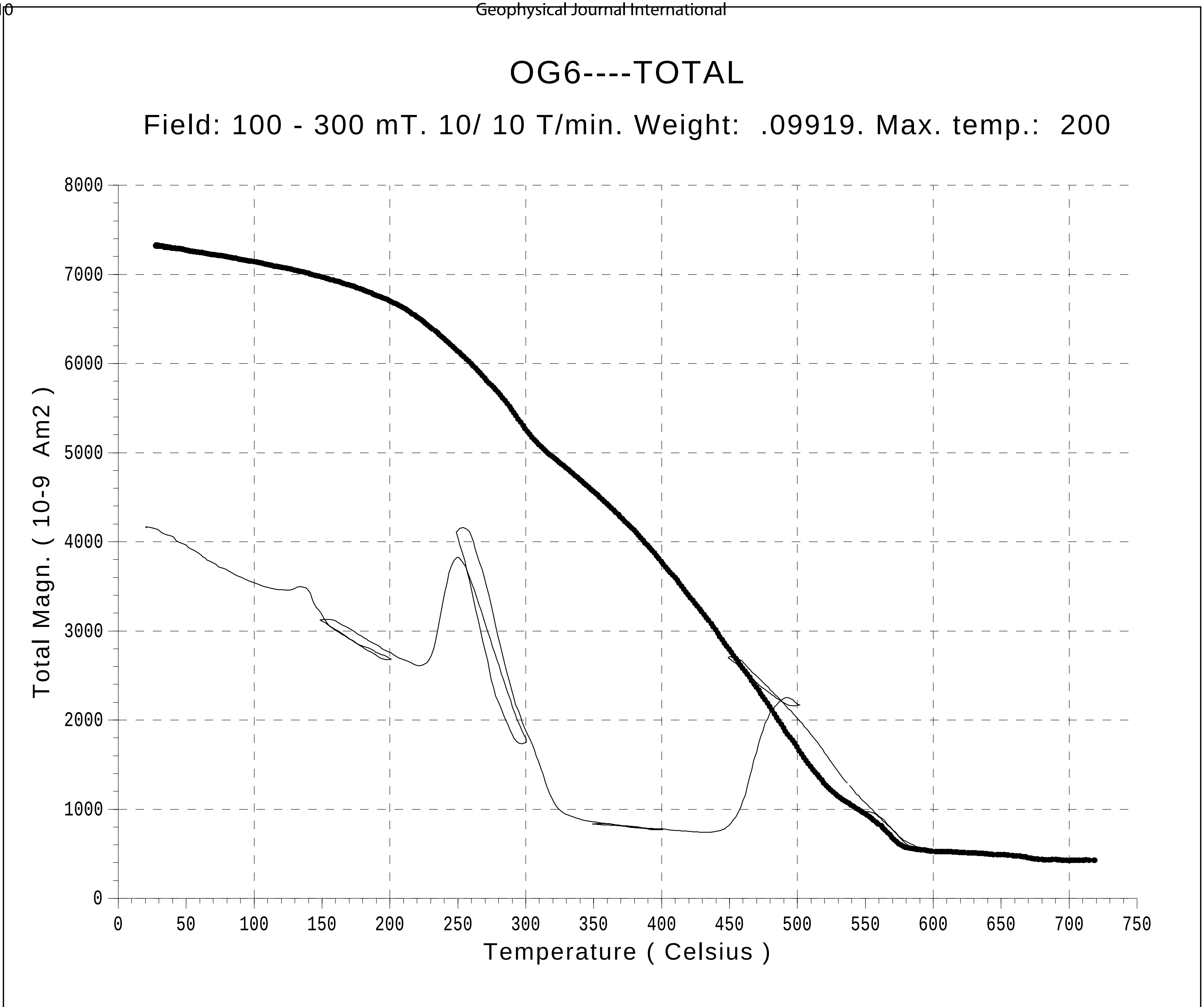
OG6----TOTAL
Field: 100 - 300 mT. 10/ 10 T/min. Weight: .09919. Max. temp.: 200
Total Magn. (10-9 Am2)
8000
7000
6000
5000
4000
3000
2000
1000
0
0
50
100
150
200
250
300
350
400
450
500
550
600
650
700
750
Temperature (Celsius)

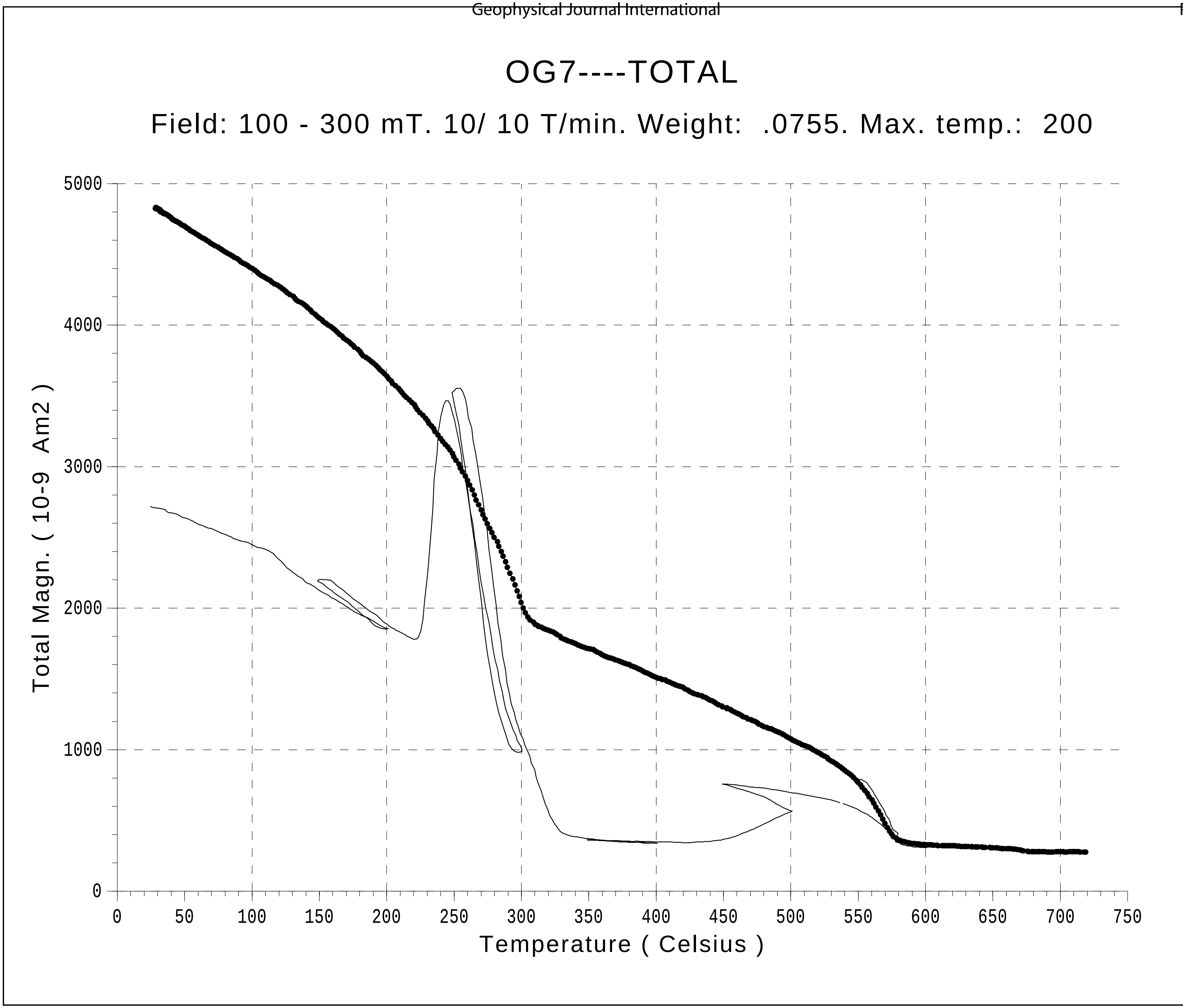
OG7----TOTAL
Field: 100 - 300 mT. 10/ 10 T/min. Weight: .0755. Max. temp.: 200
Total Magn. (10-9 Am2)
5000
4000
3000
2000
1000
0
0
50
100
150
200
250
300
350
400
450
500
550
600
650
700
750
Temperature (Celsius)

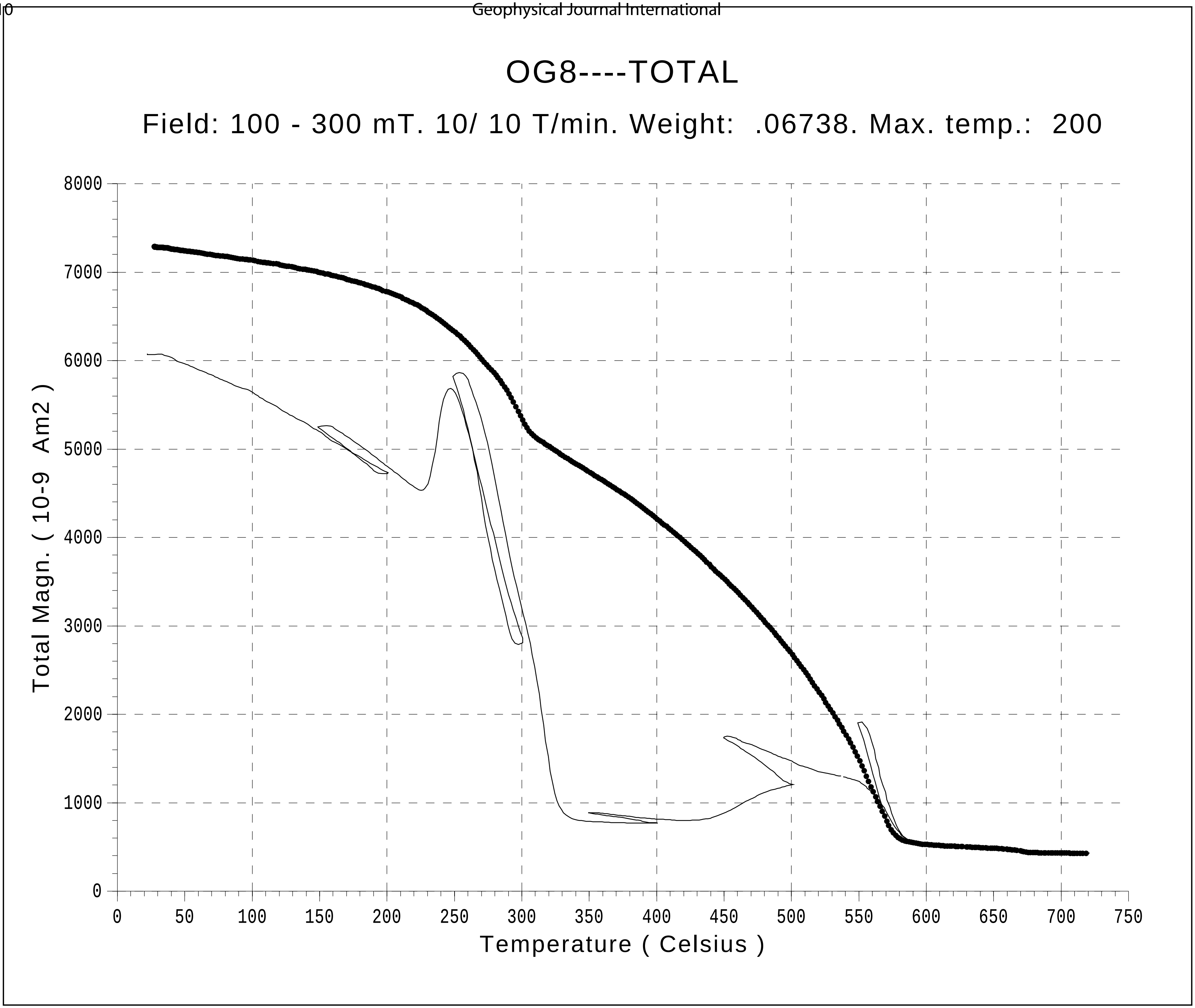
OG8----TOTAL
Field: 100 - 300 mT. 10/ 10 T/min. Weight: .06738. Max. temp.: 200
Total Magn. (10-9 Am2)
8000
7000
6000
5000
4000
3000
2000
1000
0
0
50
100
150
200
250
300
350
400
450
500
550
600
650
700
750
Temperature (Celsius)

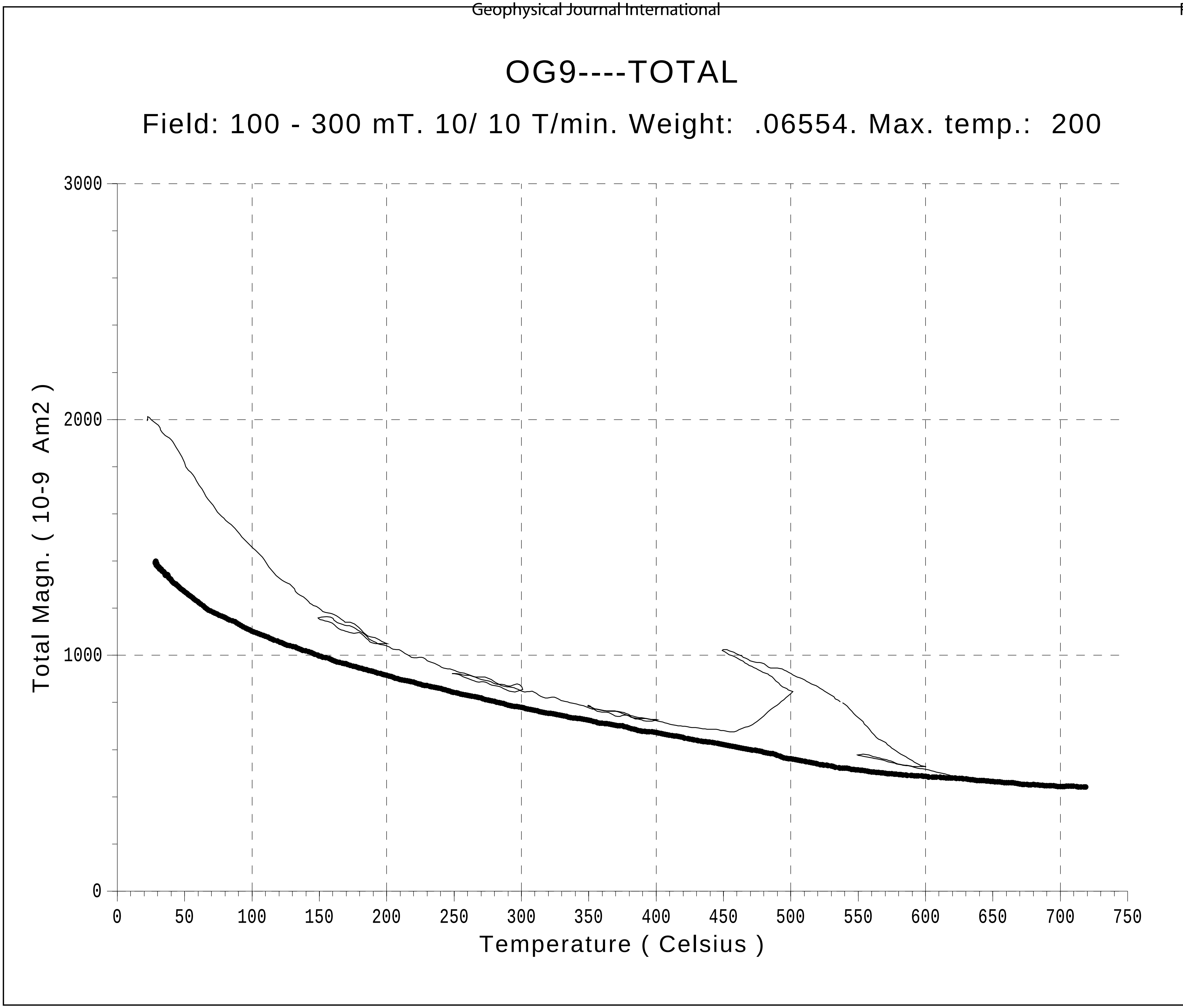
OG9----TOTAL
Field: 100 - 300 mT. 10/ 10 T/min. Weight: .06554. Max. temp.: 200
Total Magn. (10-9 Am2)
3000
2000
1000
0
0
50
100
150
200
250
300
350
400
450
500
550
600
650
700
750
Temperature (Celsius)

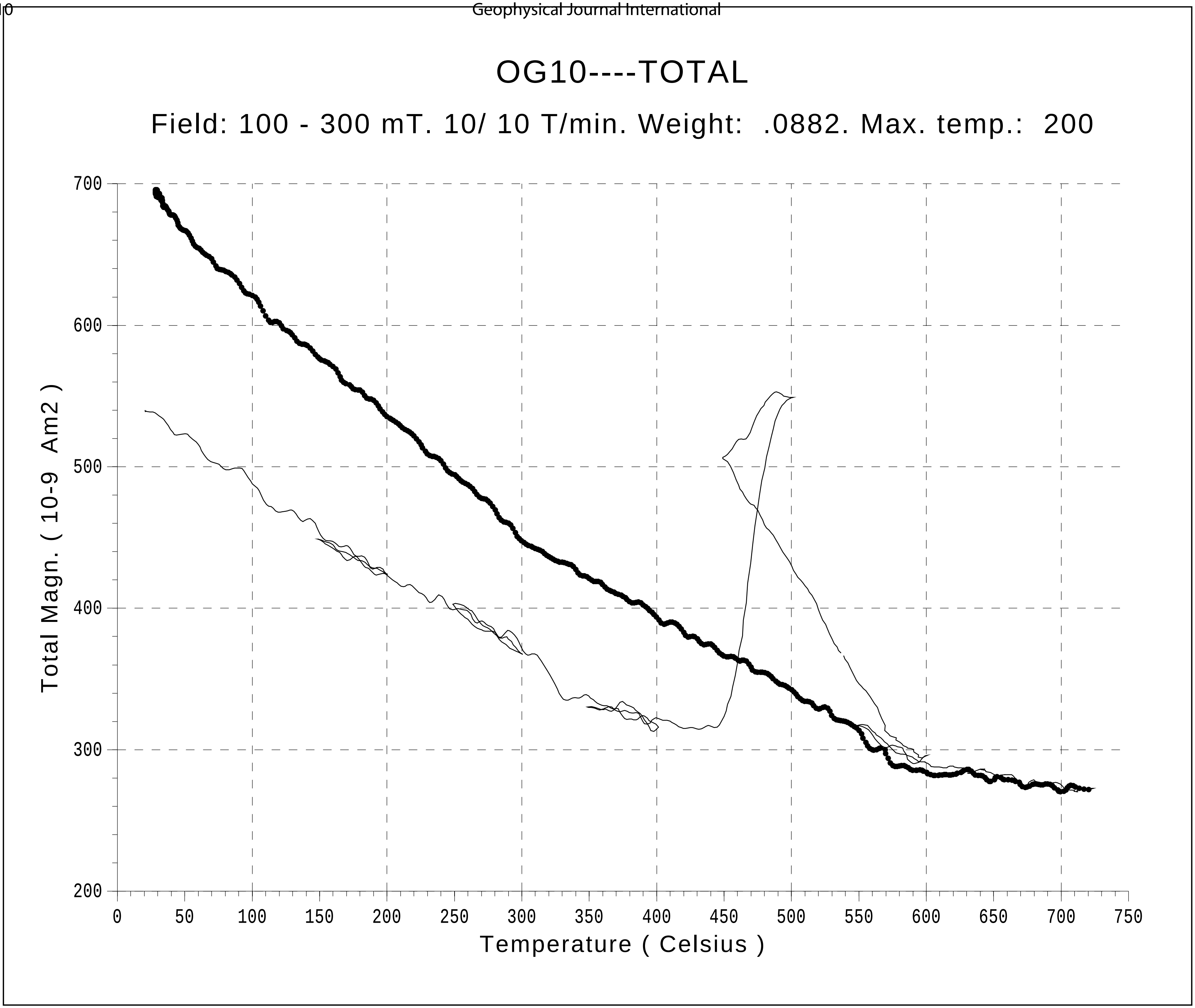
OG10----TOTAL
Field: 100 - 300 mT. 10/ 10 T/min. Weight: .0882. Max. temp.: 200
Total Magn. (10-9 Am2)
700
600
500
400
300
200
0
50
100
150
200
250
300
350
400
450
500
550
600
650
700
750
Temperature (Celsius)

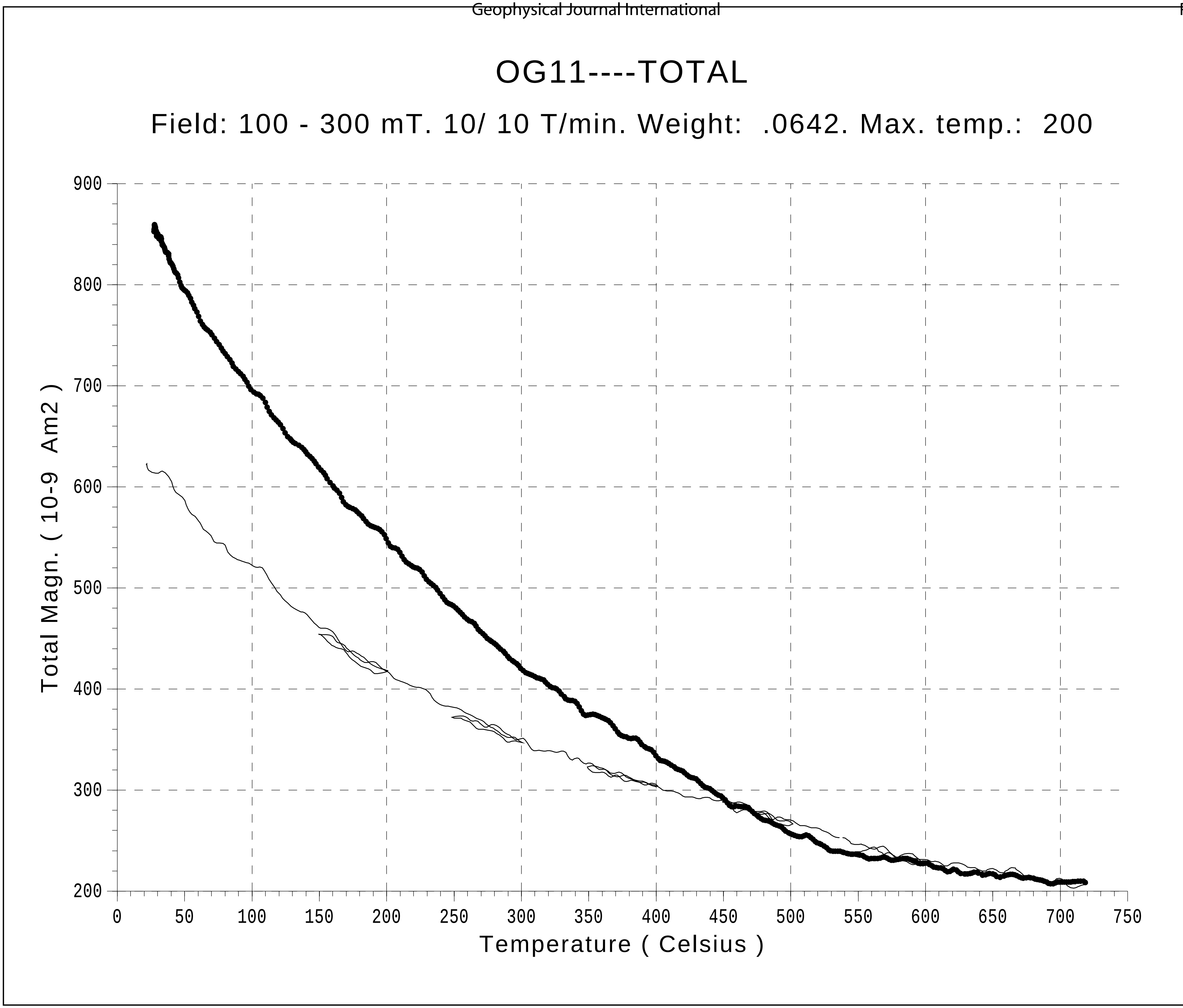
OG11----TOTAL
Field: 100 - 300 mT. 10/ 10 T/min. Weight: .0642. Max. temp.: 200
Total Magn. (10-9 Am2)
900
800
700
600
500
400
300
200
0
50
100
150
200
250
300
350
400
450
500
550
600
650
700
750
Temperature (Celsius)

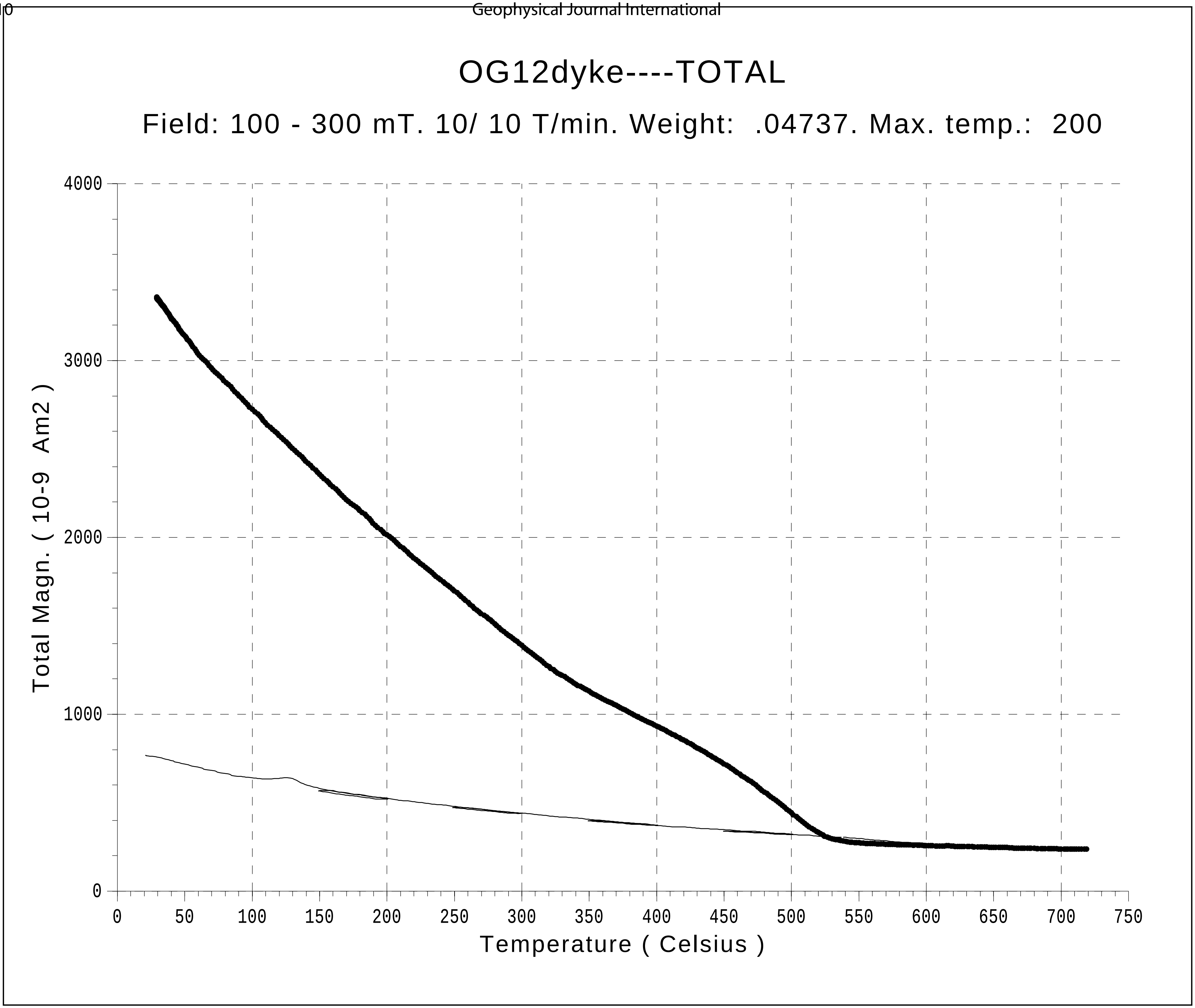
OG12dyke----TOTAL
Field: 100 - 300 mT. 10/ 10 T/min. Weight: .04737. Max. temp.: 200
Total Magn. (10-9 Am2)
4000
3000
2000
1000
0
0
50
100
150
200
250
300
350
400
450
500
550
600
650
700
750
Temperature (Celsius)

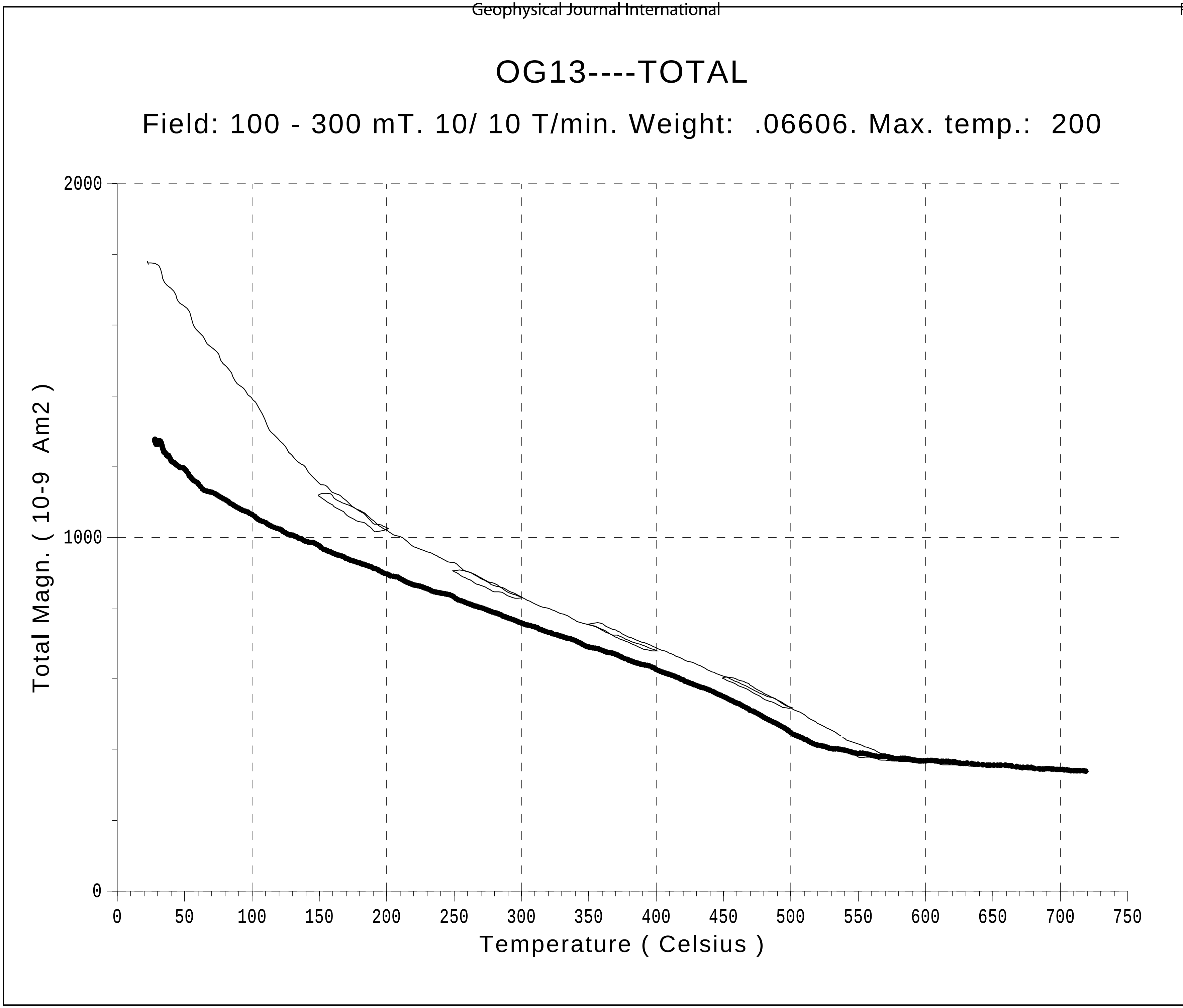
OG13----TOTAL
Field: 100 - 300 mT. 10/ 10 T/min. Weight: .06606. Max. temp.: 200
Total Magn. (10-9 Am2)
2000
1000
0
0 50 100 150 200 250 300 350 400 450 500 550 600 650 700 750
Temperature (Celsius)

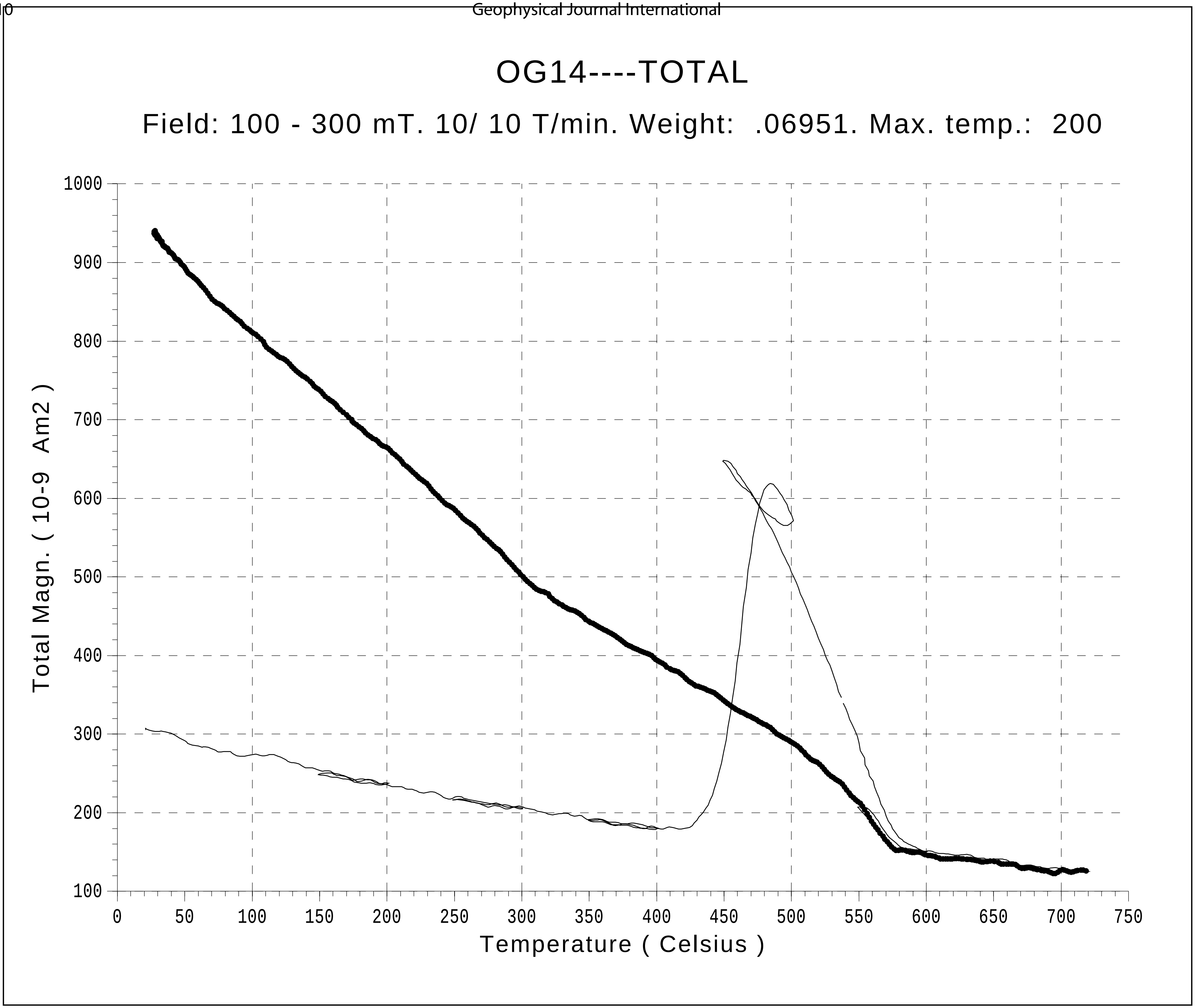
OG14----TOTAL
Field: 100 - 300 mT. 10/ 10 T/min. Weight: .06951. Max. temp.: 200
Total Magn. (10-9 Am2)
1000
900
800
700
600
500
400
300
200
100
0
50
100
150
200
250
300
350
400
450
500
550
600
650
700
750
Temperature (Celsius)

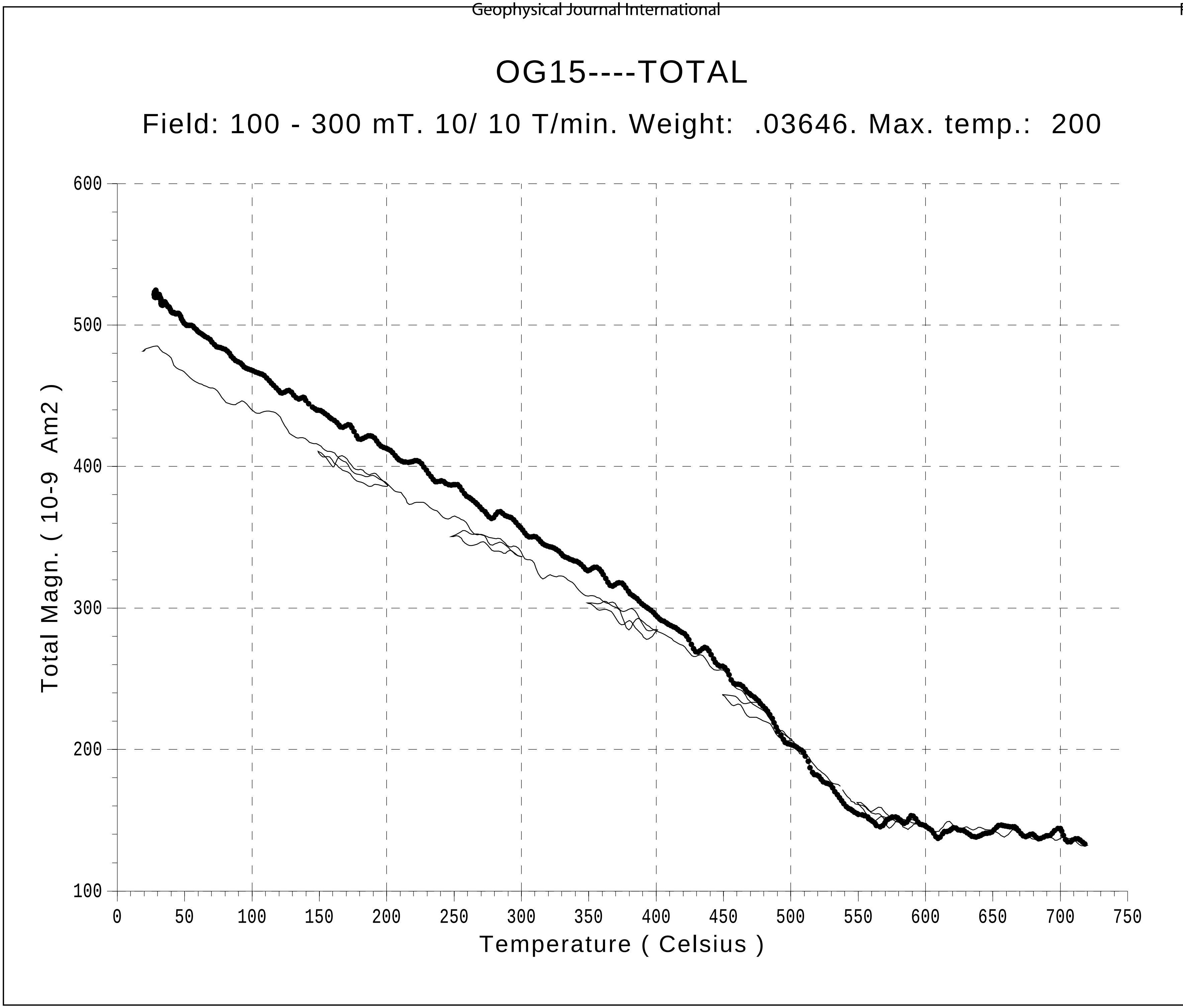
OG15----TOTAL
Field: 100 - 300 mT. 10/ 10 T/min. Weight: .03646. Max. temp.: 200
Total Magn. (10-9 Am2)
600
500
400
300
200
100
0
50
100
150
200
250
300
350
400
450
500
550
600
650
700
750
Temperature (Celsius)

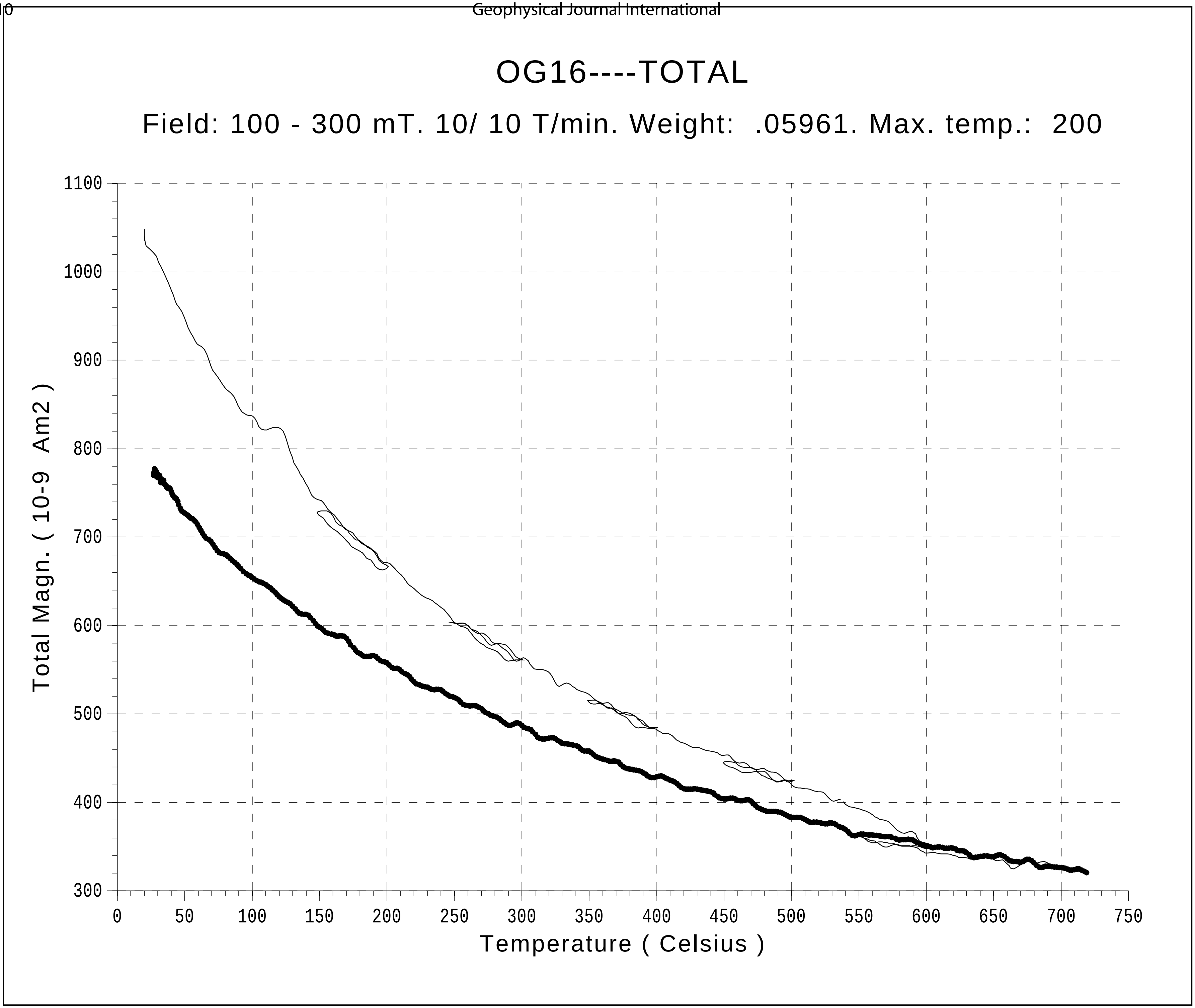
OG16----TOTAL
Field: 100 - 300 mT. 10/ 10 T/min. Weight: .05961. Max. temp.: 200
Total Magn. (10-9 Am2)
1100
1000
900
800
700
600
500
400
300
0
50
100
150
200
250
300
350
400
450
500
550
600
650
700
750
Temperature (Celsius)

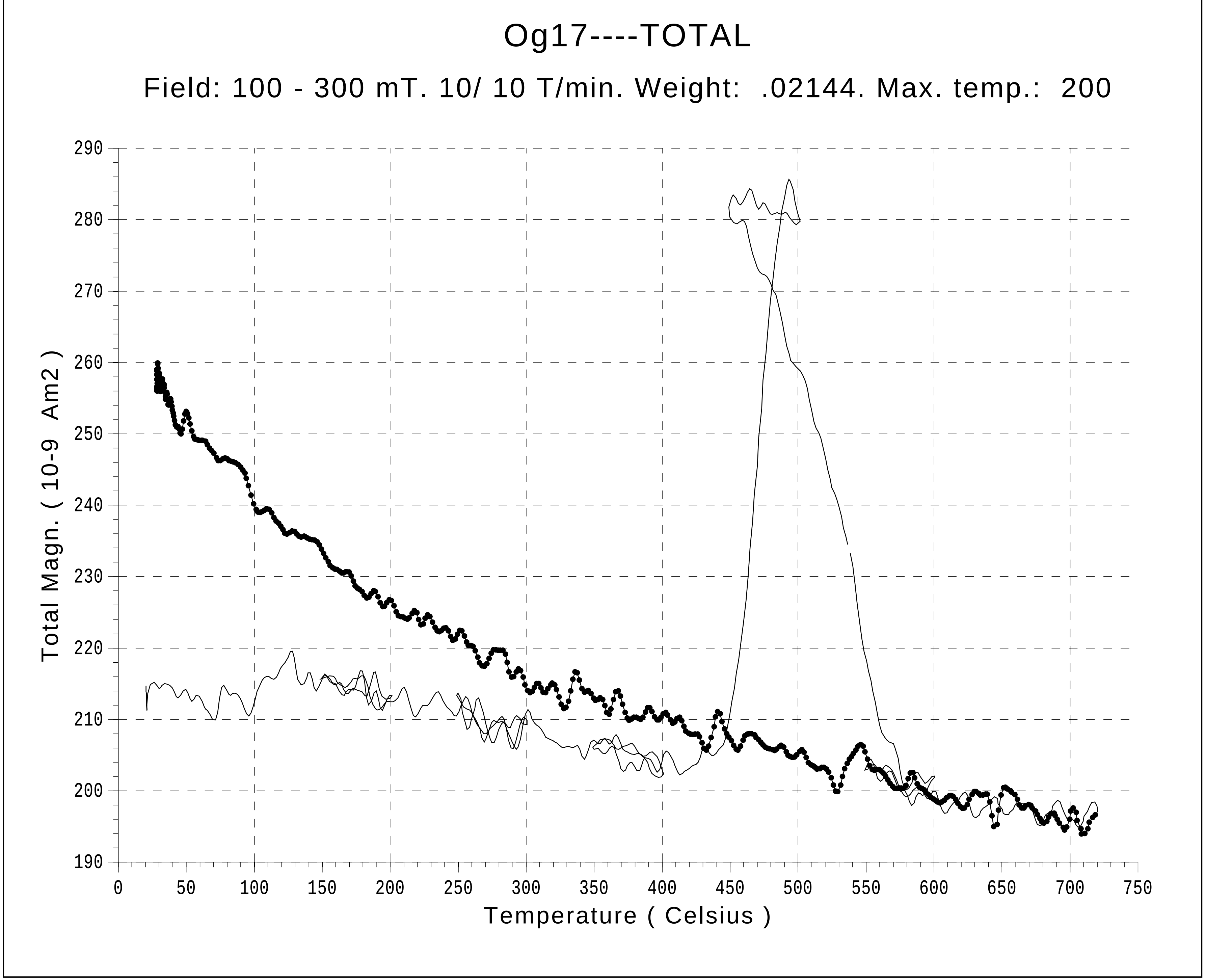
Og17----TOTAL
Field: 100 - 300 mT. 10/ 10 T/min. Weight: .02144. Max. temp.: 200
Total Magn. (10-9 Am2)
290
280
270
260
250
240
230
220
210
200
190
0
50
100
150
200
250
300
350
400
450
500
550
600
650
700
750
Temperature (Celsius)

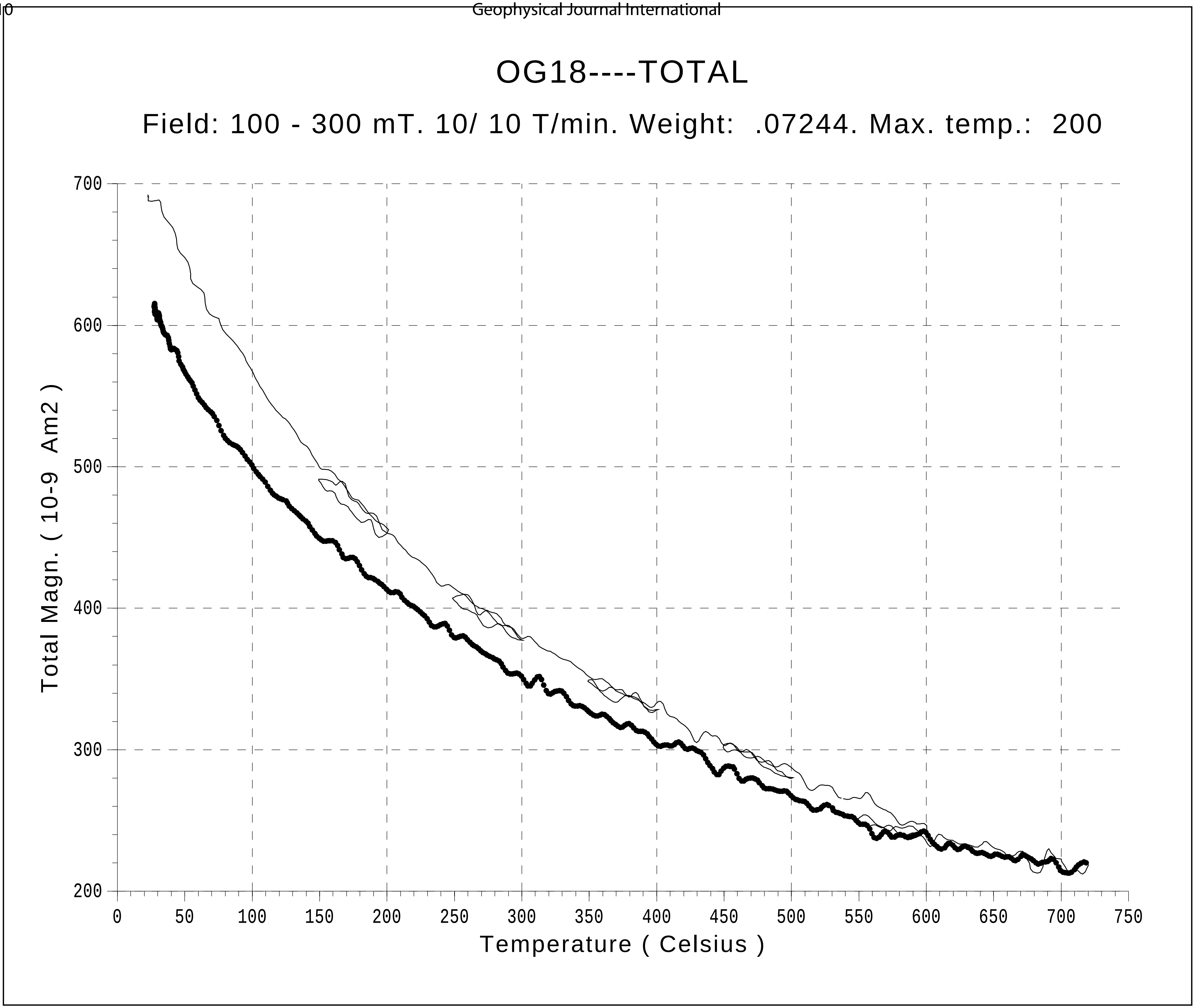
OG18----TOTAL
Field: 100 - 300 mT. 10/ 10 T/min. Weight: .07244. Max. temp.: 200
Total Magn. (10-9 Am2)
700
600
500
400
300
200
0
50
100
150
200
250
300
350
400
450
500
550
600
650
700
750
Temperature (Celsius)

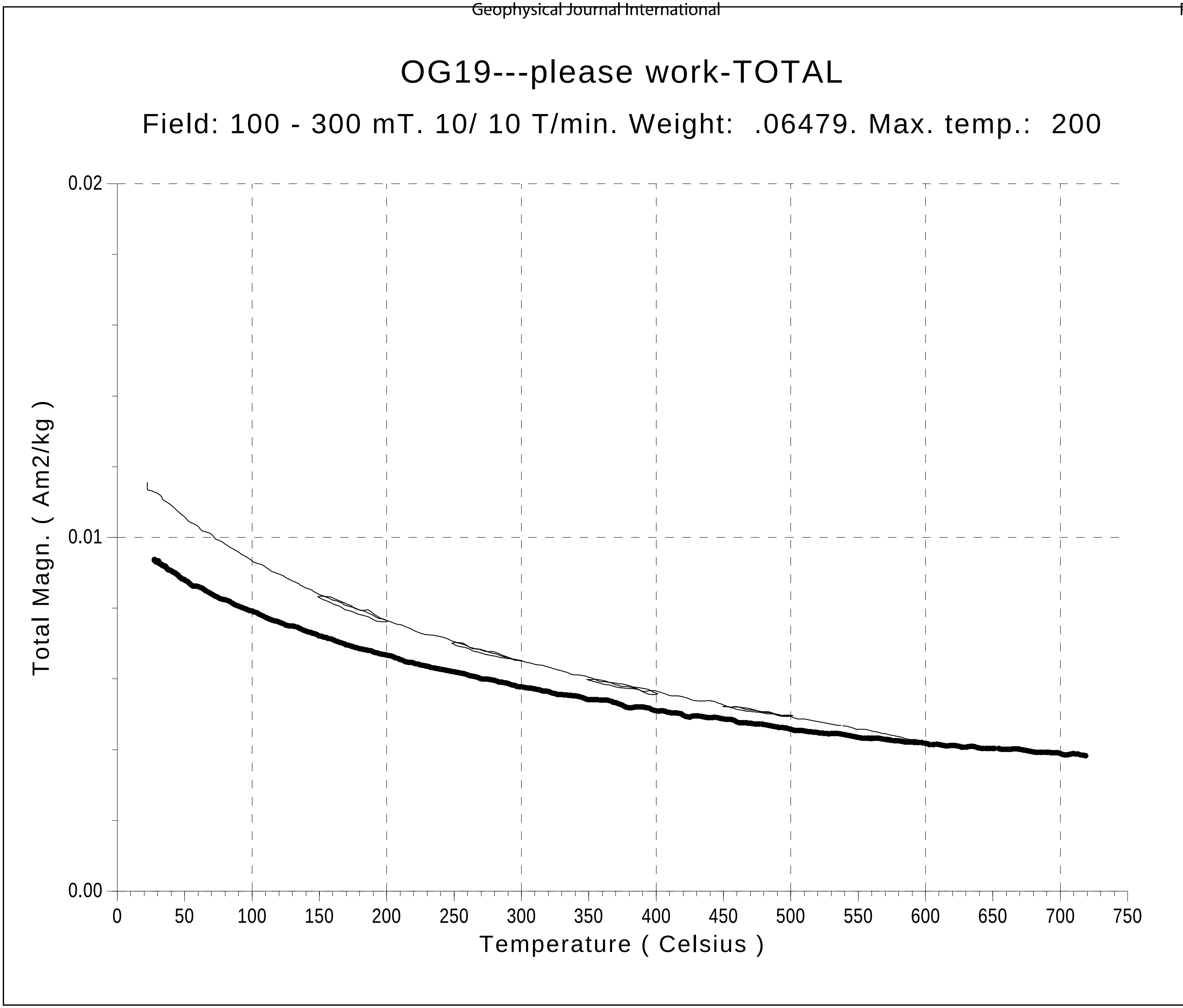
OG19---please work-TOTAL
Field: 100 - 300 mT. 10/ 10 T/min. Weight: .06479. Max. temp.: 200
Total Magn. (Am2/kg)
0.02
0.01
0.00
0
50
100
150
200
250
300
350
400
450
500
550
600
650
700
750
Temperature (Celsius)

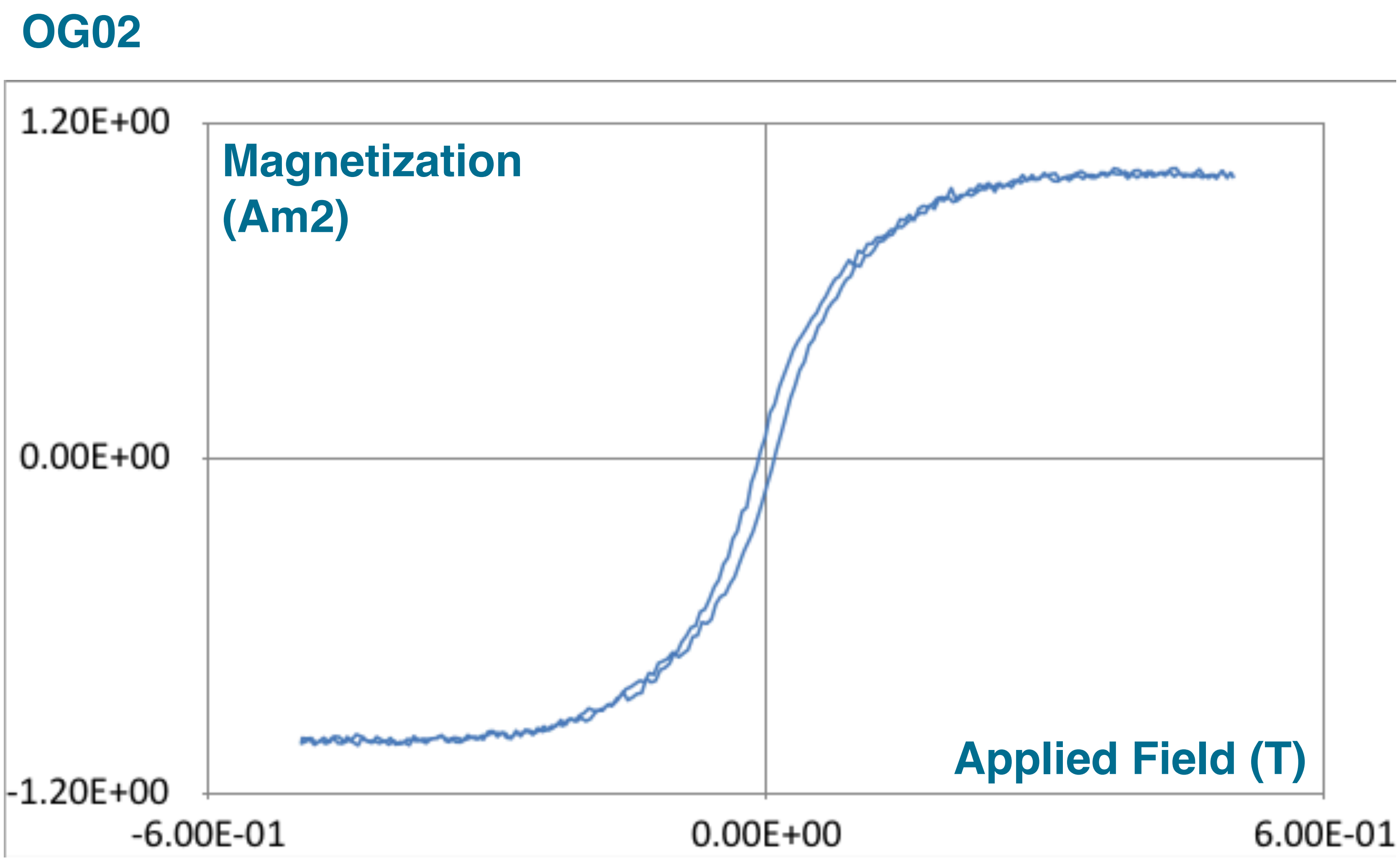
OG02
1.20E+00
Magnetization
(Am2)
0.00E+00
-1.20E+00
Applied Field (T)
-6.00E-01
0.00E+00
6.00E-01

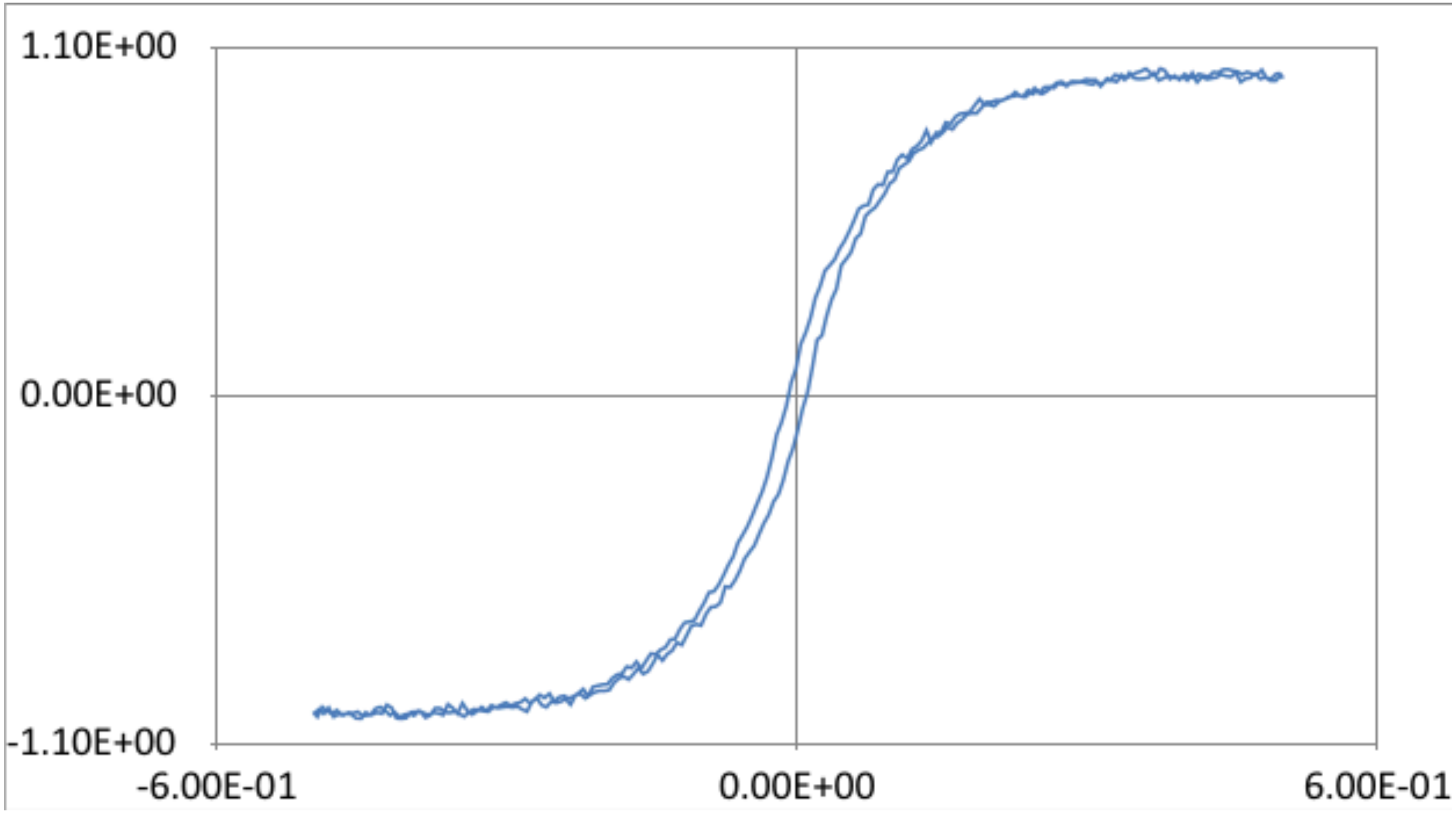
1.10E+00
0.00E+00
-1.10E+00
-6.00E-01
0.00E+00
6.00E-01

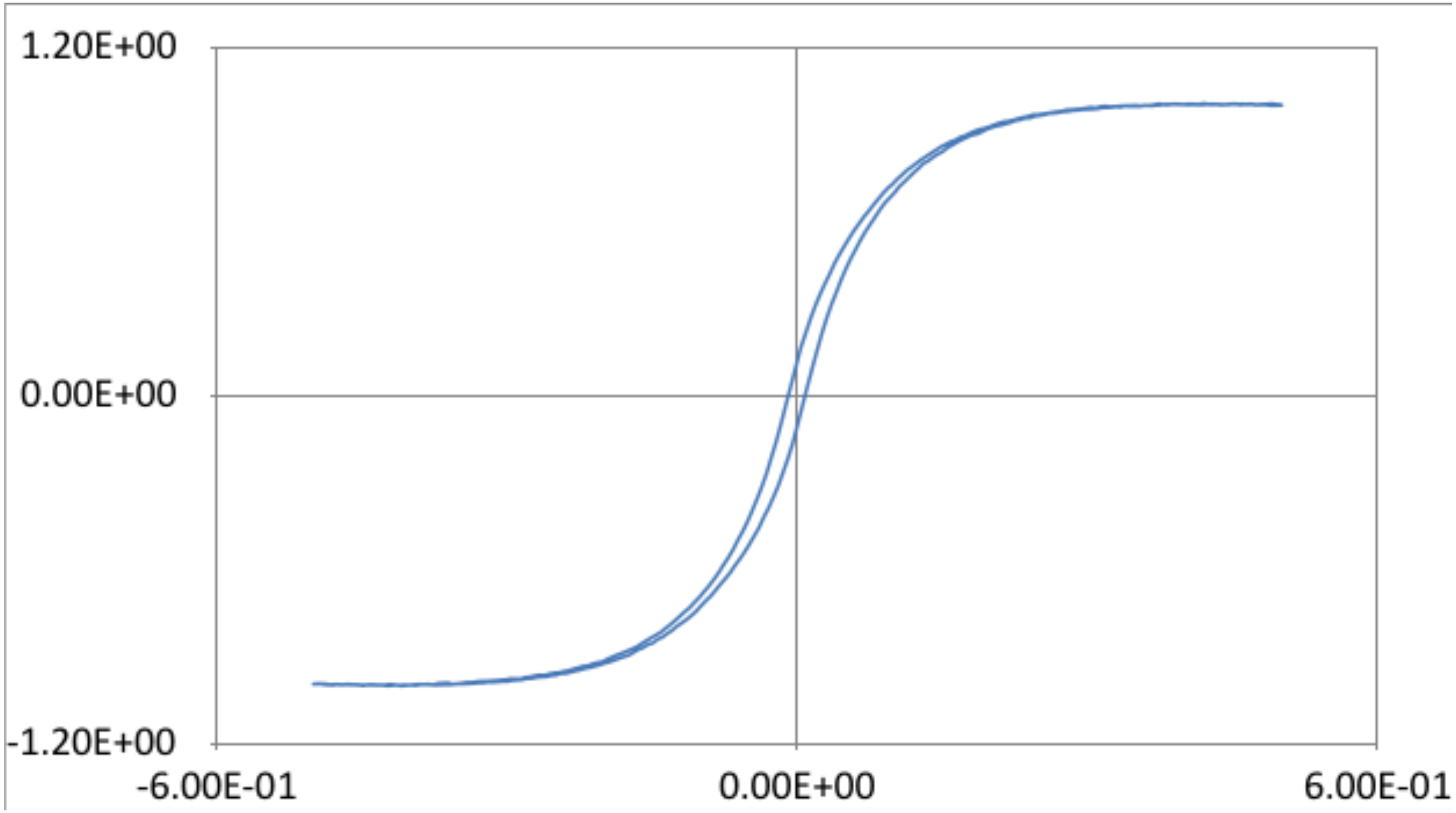
1.20E+00
0.00E+00
-1.20E+00
-6.00E-01
0.00E+00
6.00E-01

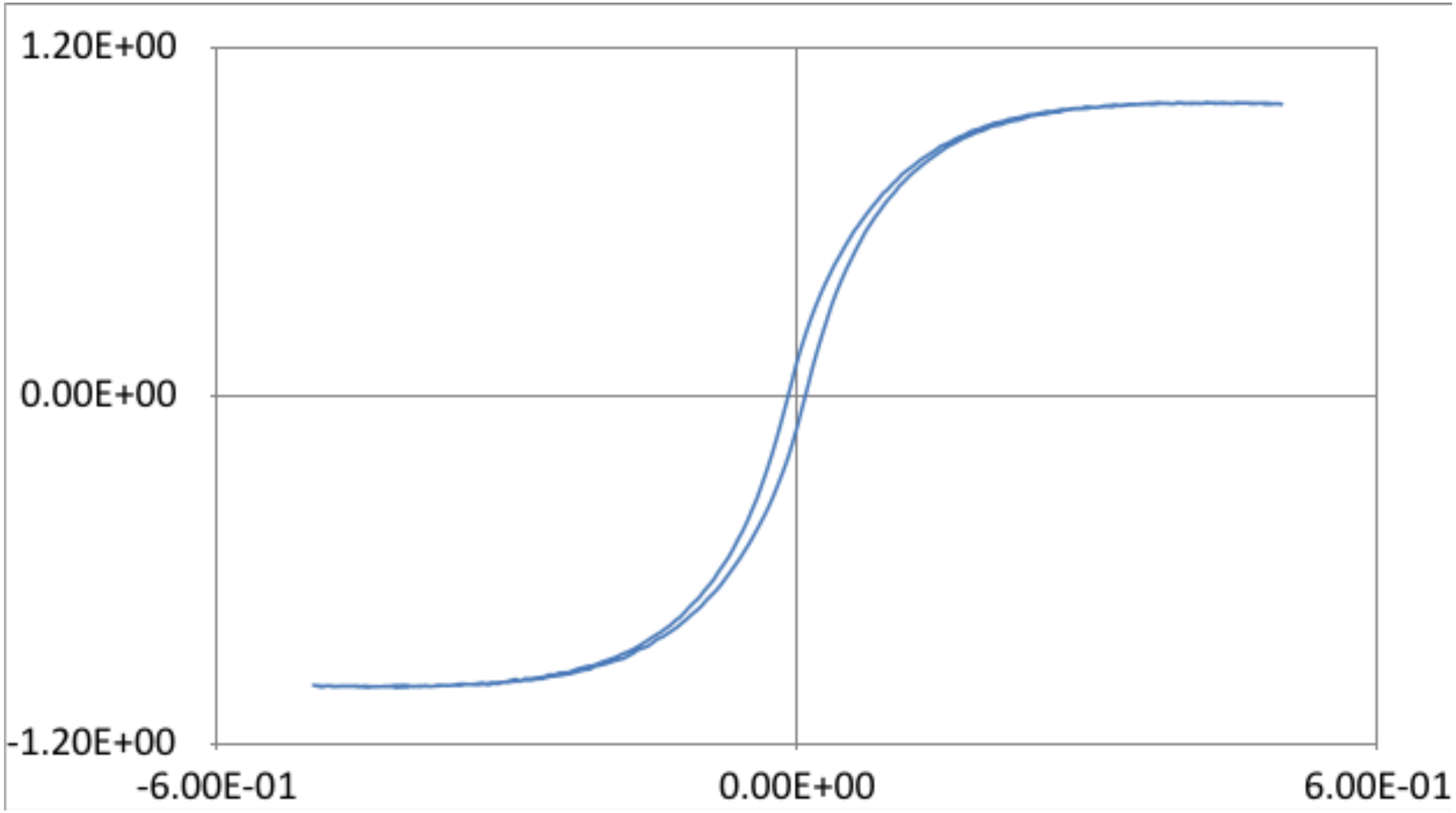
1.20E+00
0.00E+00
-1.20E+00
-6.00E-01
0.00E+00
6.00E-01

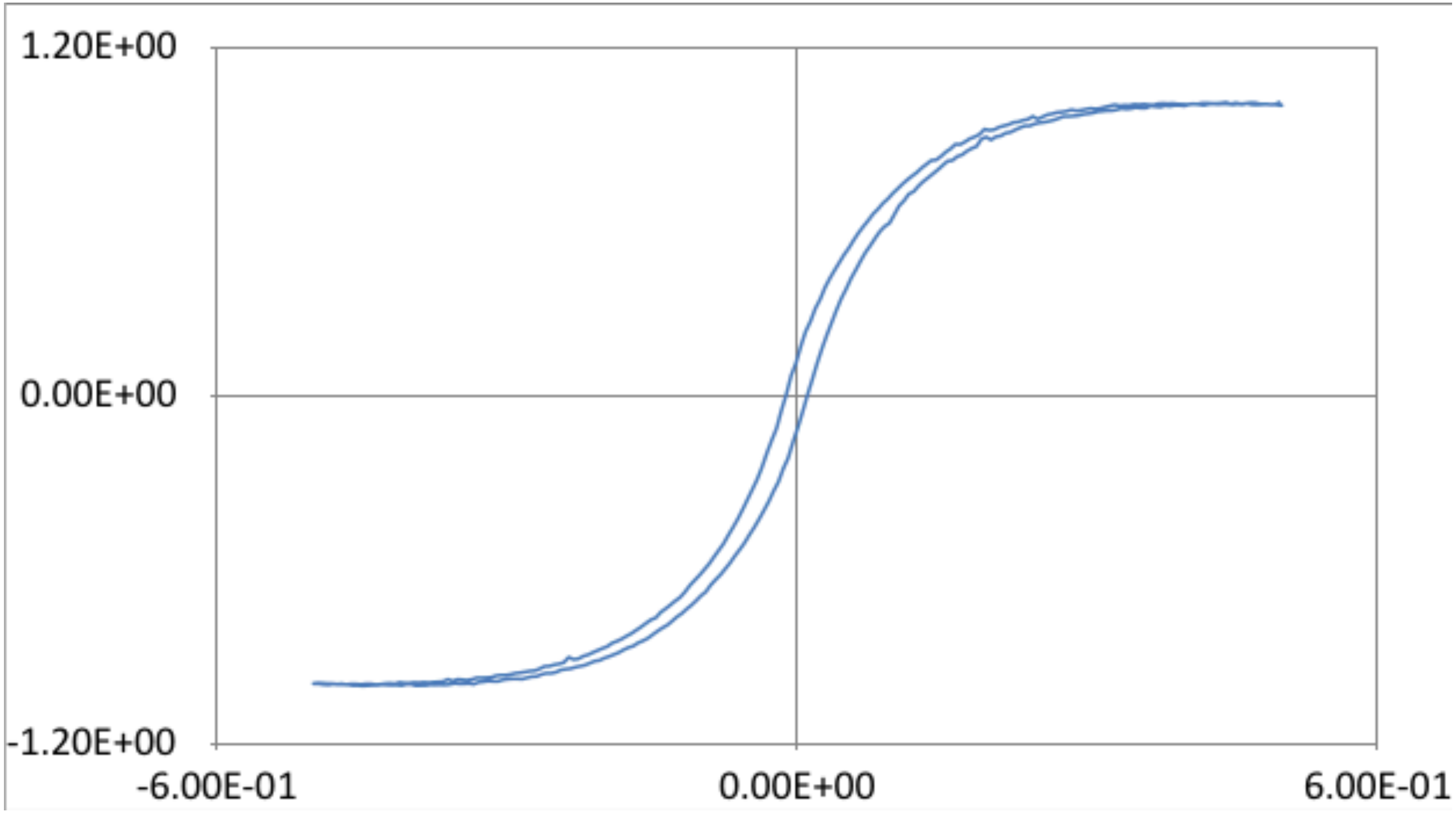
1.20E+00
0.00E+00
-1.20E+00
-6.00E-01
0.00E+00
6.00E-01

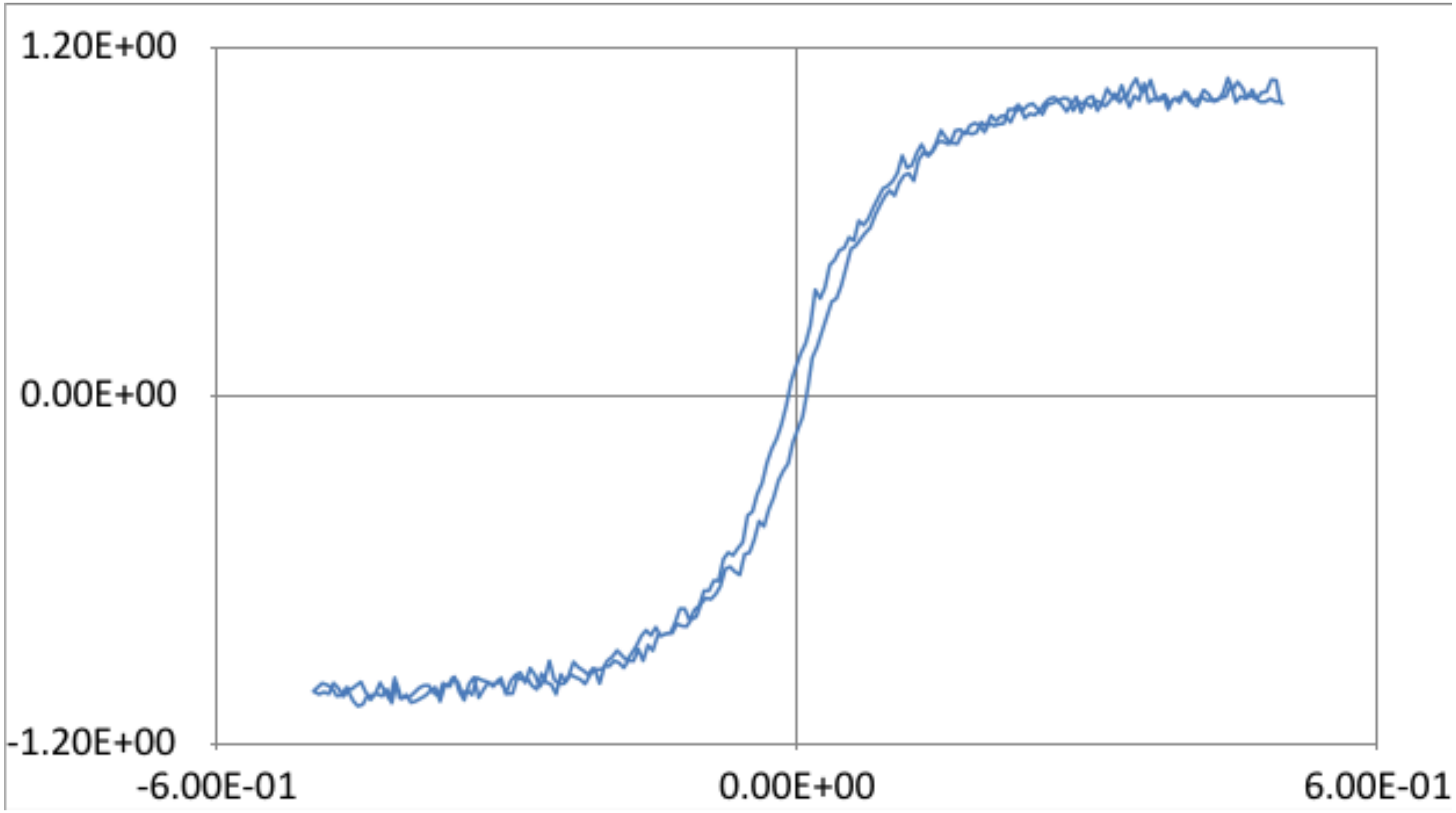
1.20E+00
0.00E+00
-1.20E+00
-6.00E-01
0.00E+00
6.00E-01

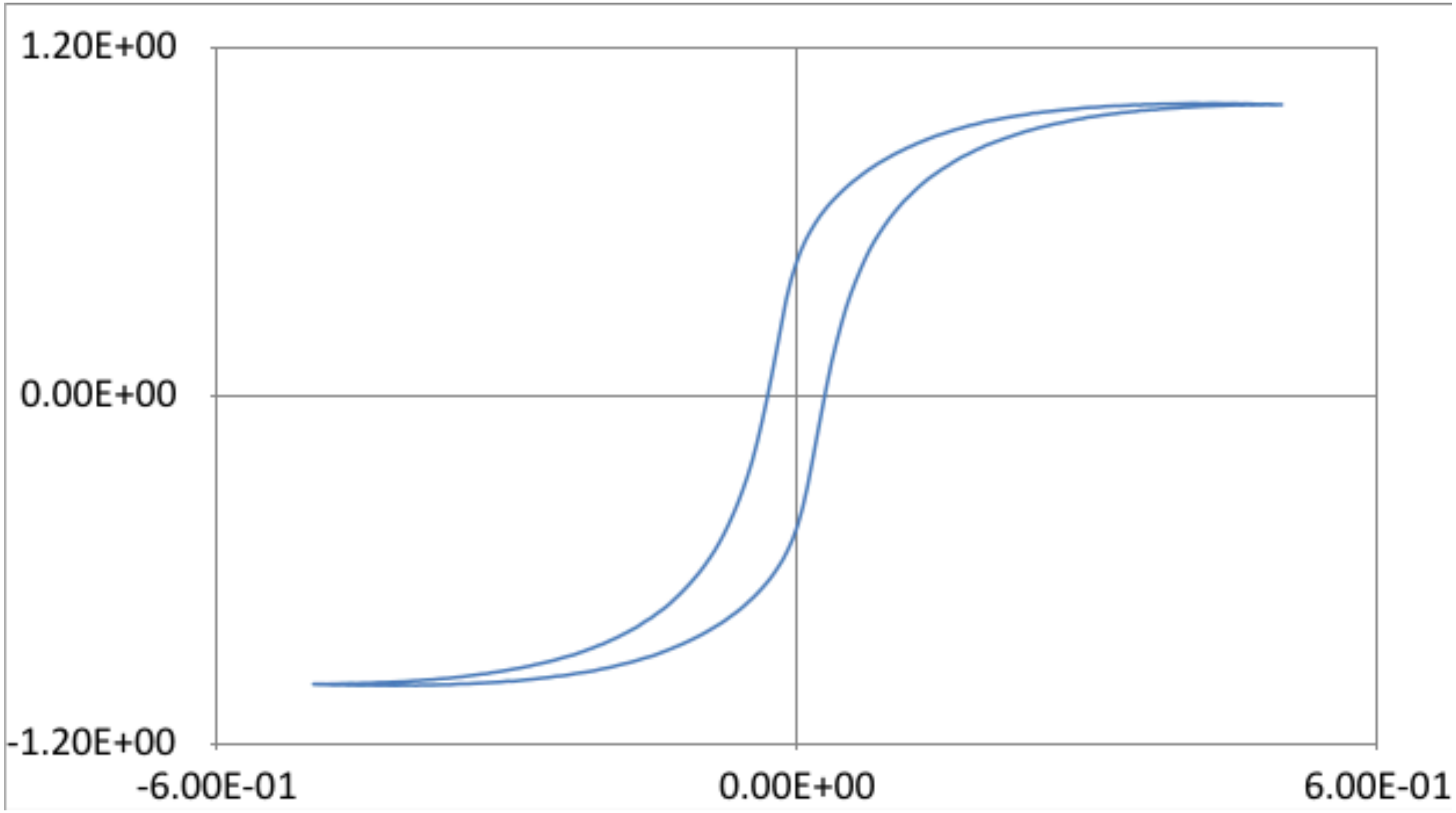
1.20E+00
0.00E+00
-1.20E+00
-6.00E-01
0.00E+00
6.00E-01

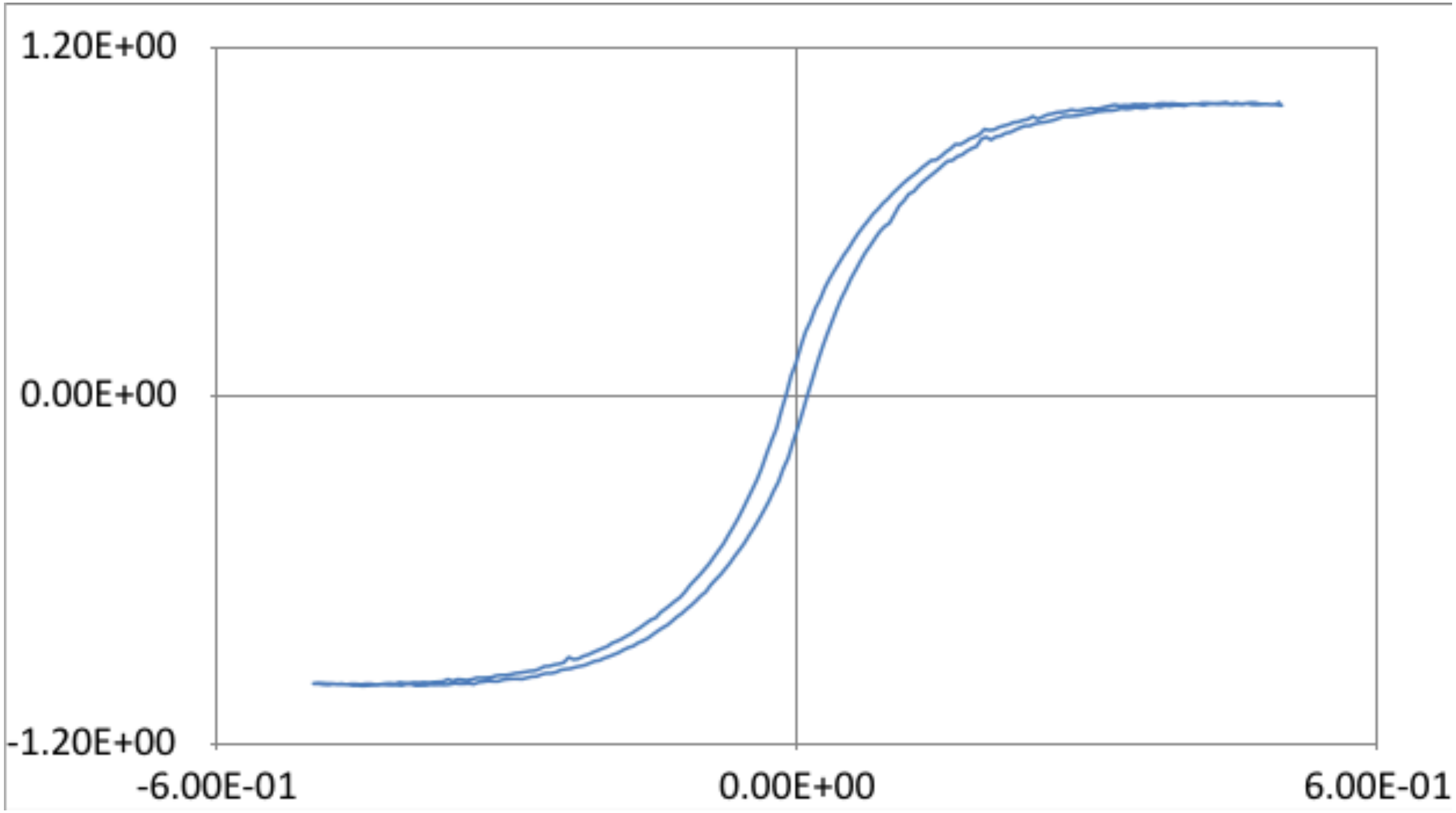
1.20E+00
0.00E+00
-1.20E+00
-6.00E-01
0.00E+00
6.00E-01

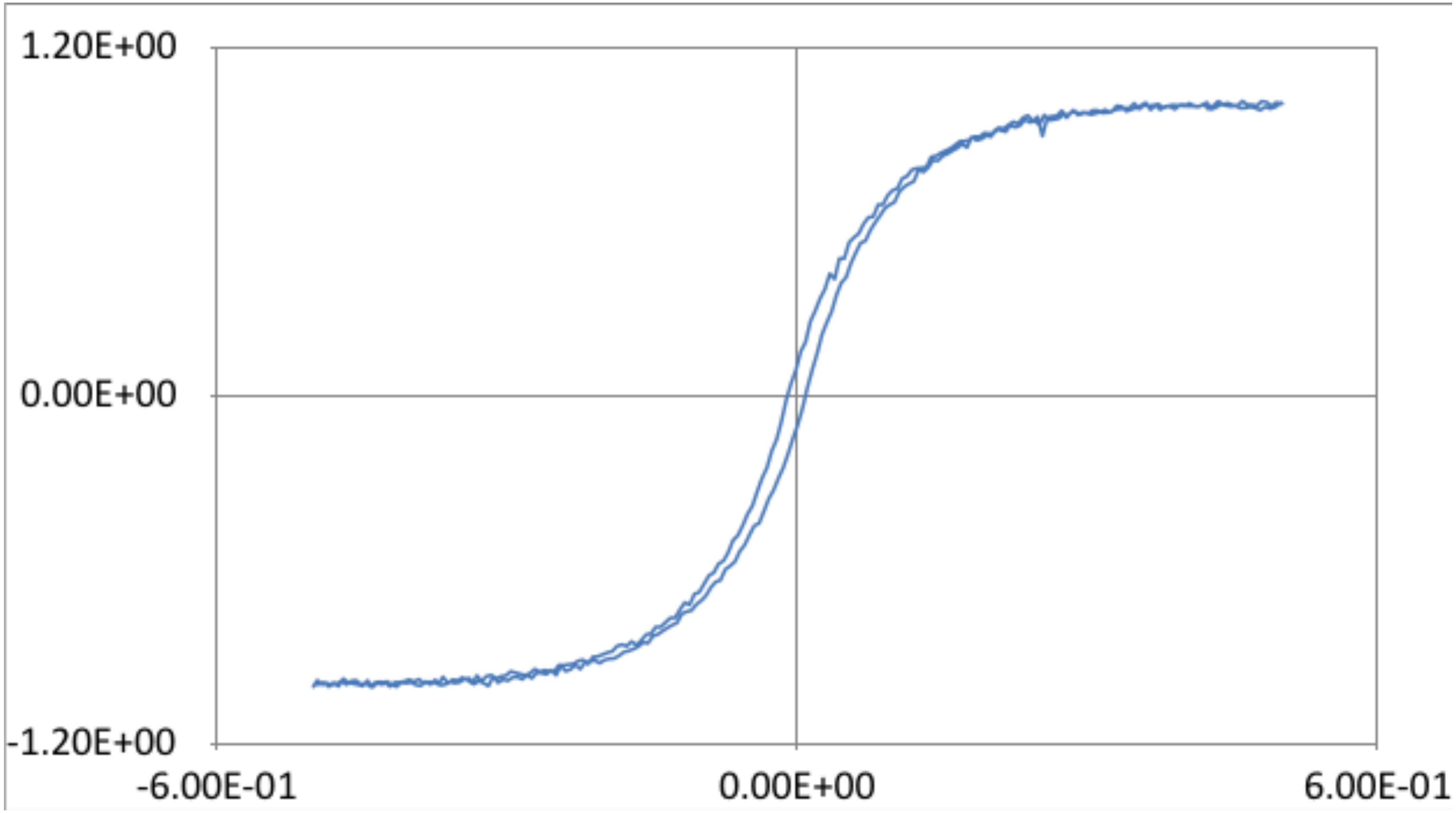
1.20E+00
0.00E+00
-1.20E+00
-6.00E-01
0.00E+00
6.00E-01

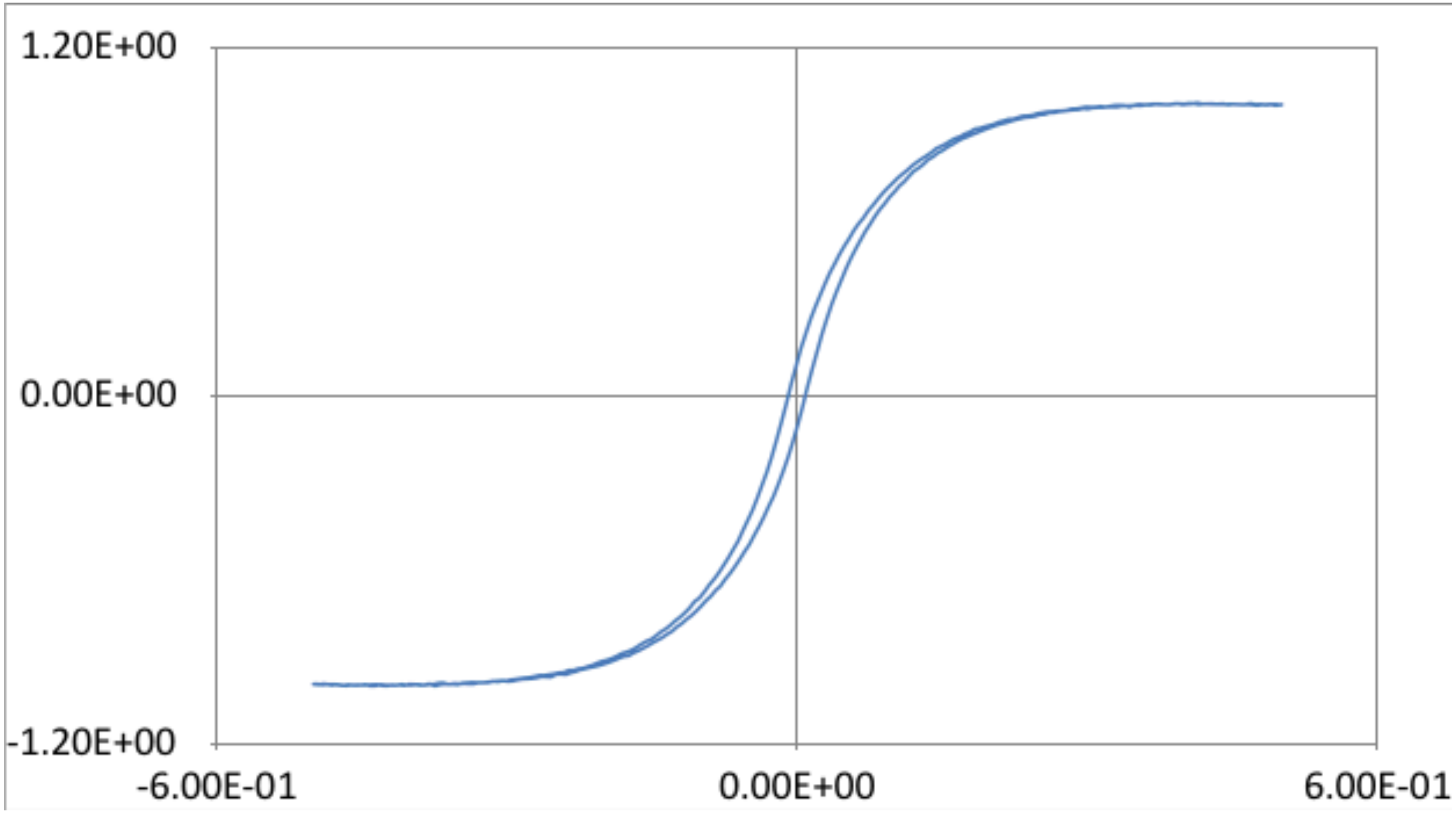
1.20E+00
0.00E+00
-1.20E+00
-6.00E-01
0.00E+00
6.00E-01

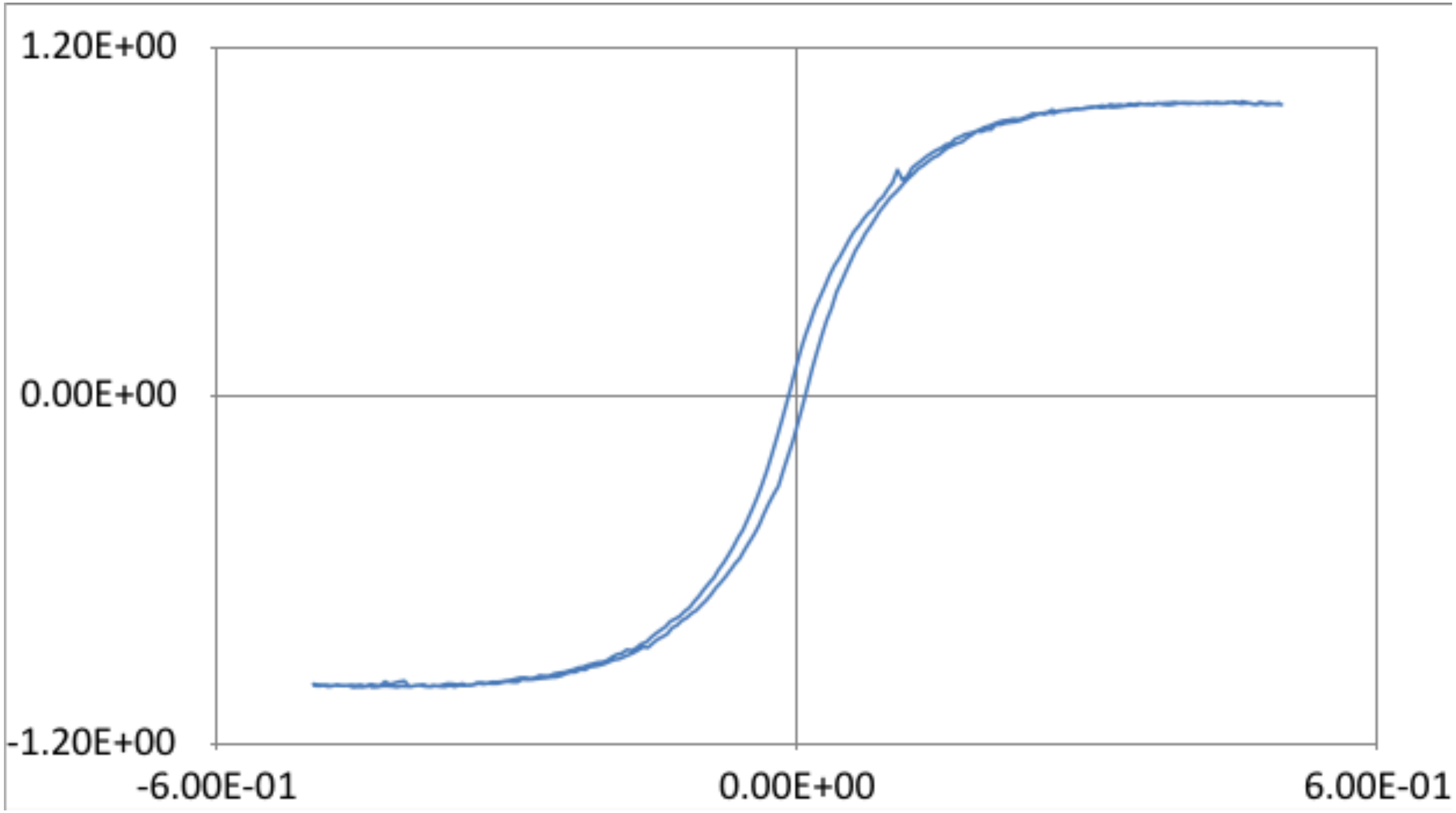
1.20E+00
0.00E+00
-1.20E+00
-6.00E-01
0.00E+00
6.00E-01

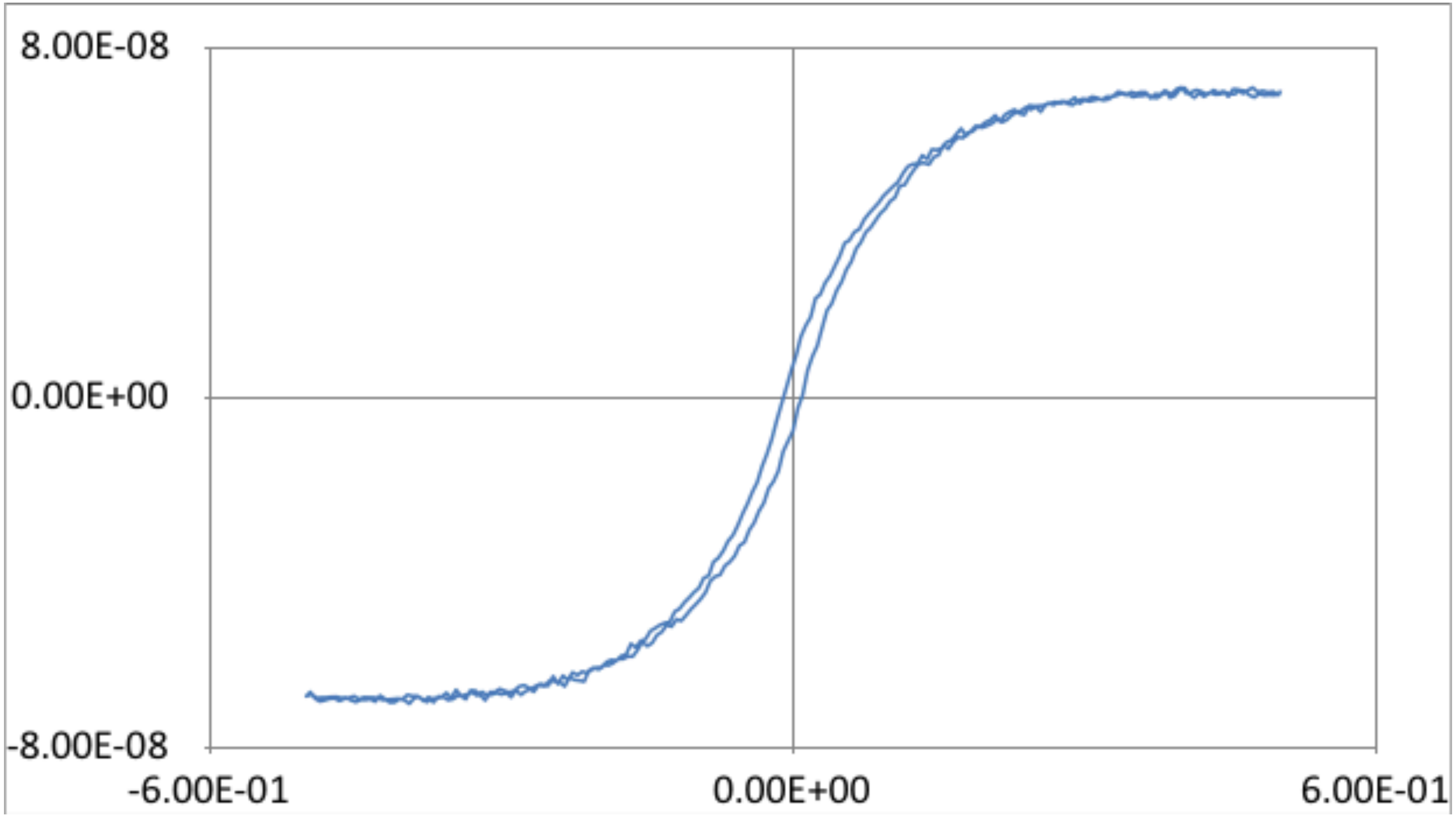
8.00E-08
0.00E+00
-8.00E-08
-6.00E-01
0.00E+00
6.00E-01

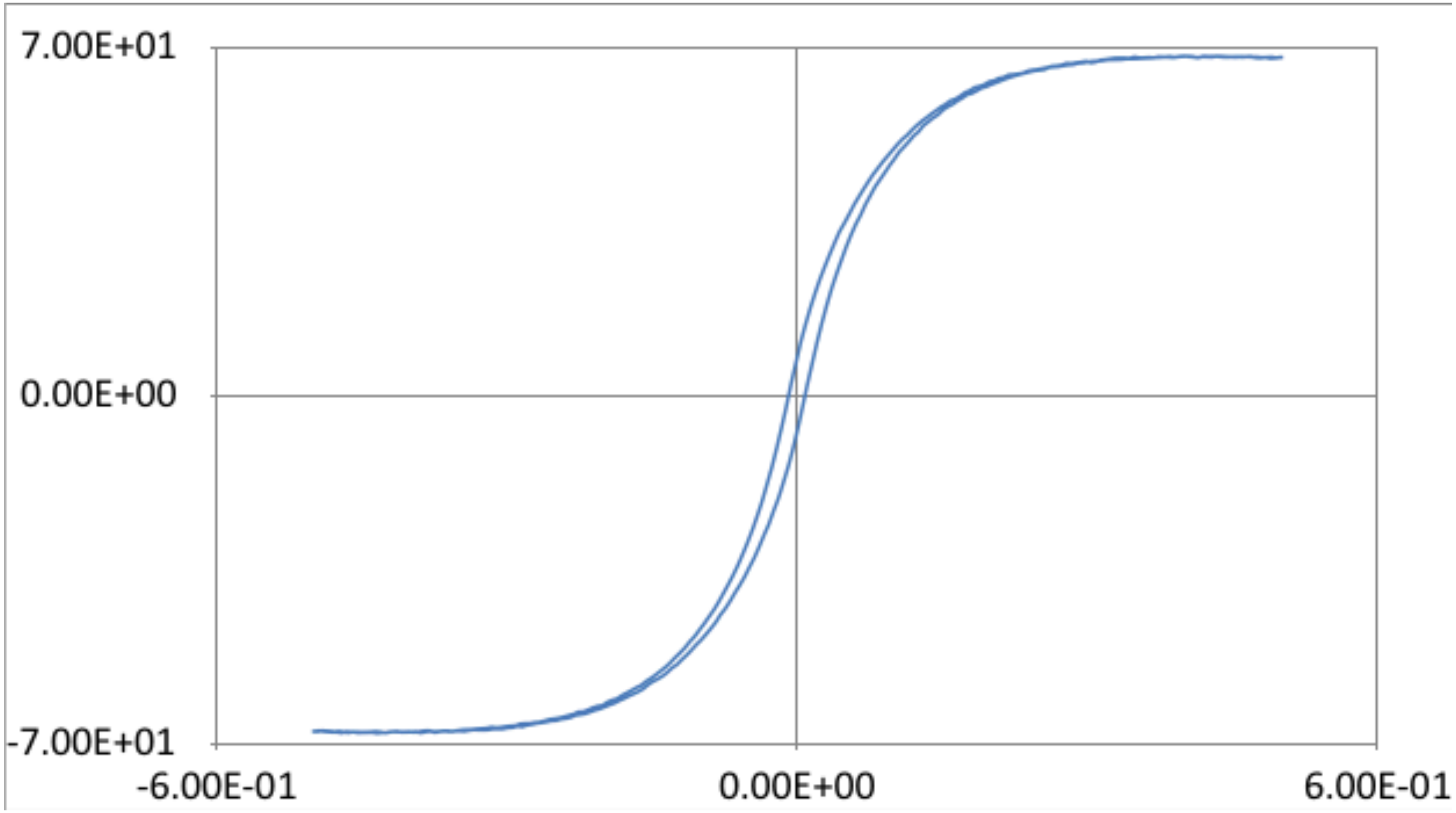
7.00E+01
0.00E+00
-7.00E+01
-6.00E-01
0.00E+00
6.00E-01

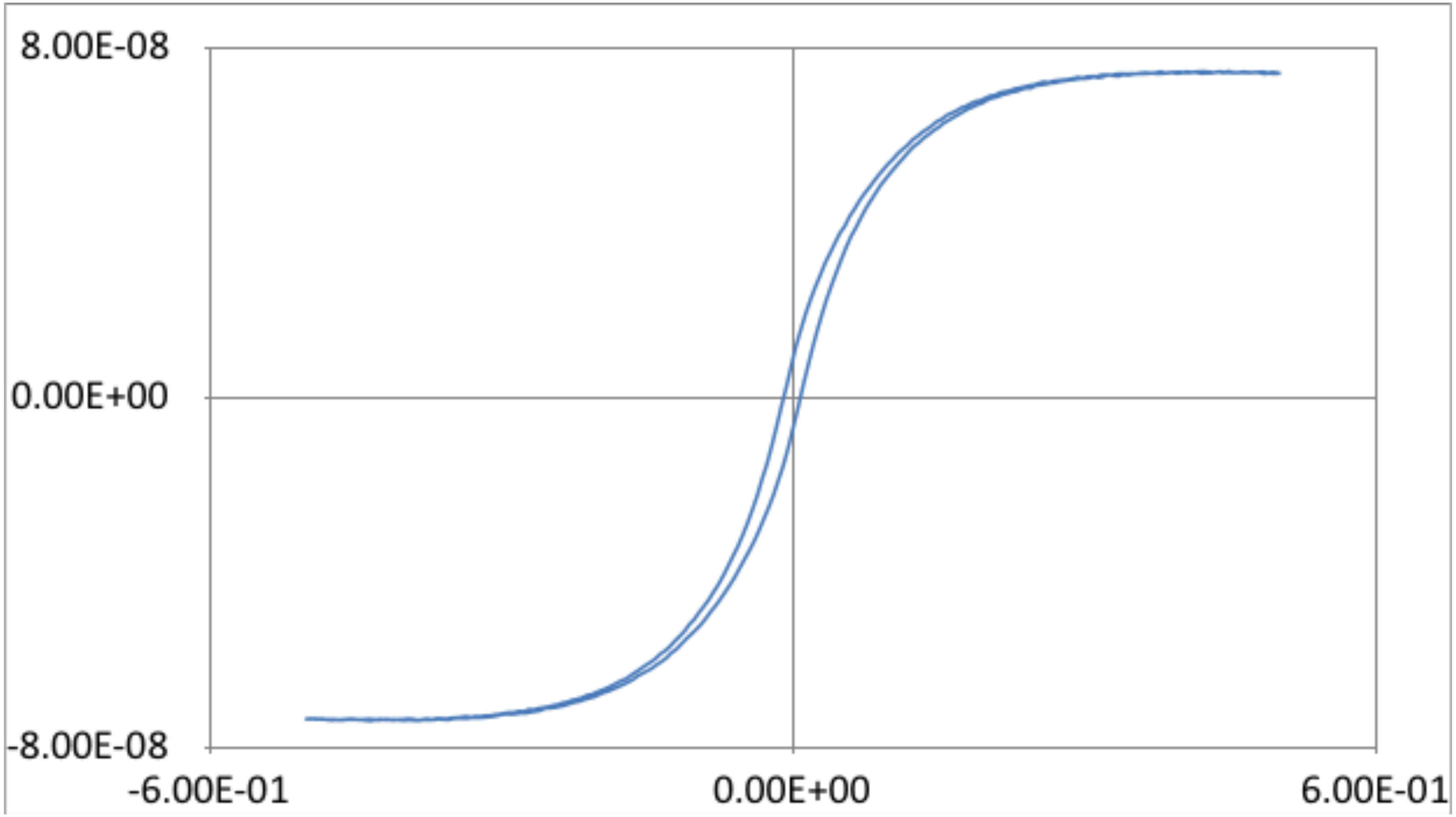
8.00E-08
0.00E+00
-8.00E-08
-6.00E-01
0.00E+00
6.00E-01

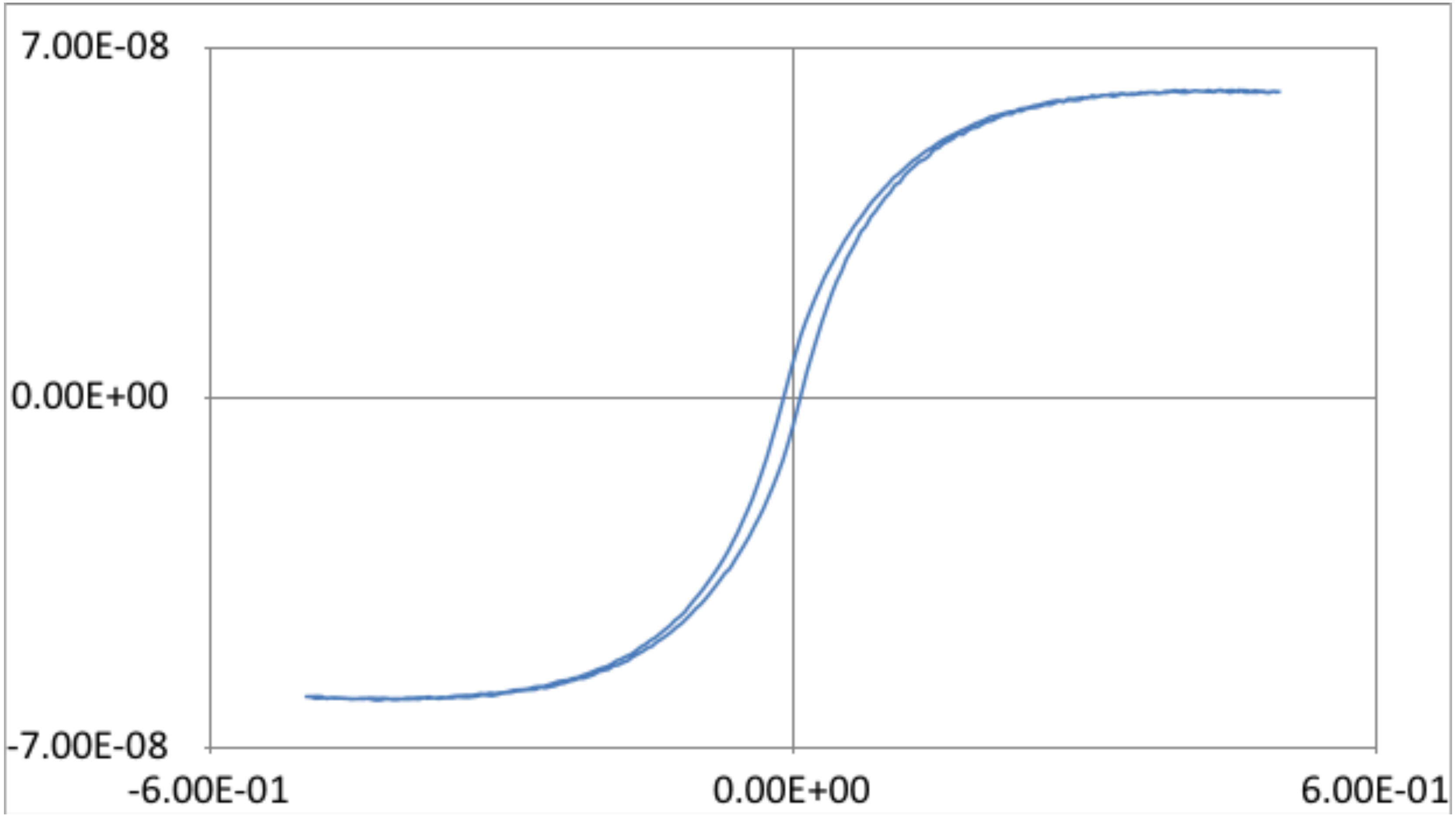
7.00E-08
0.00E+00
-7.00E-08
-6.00E-01
0.00E+00
6.00E-01

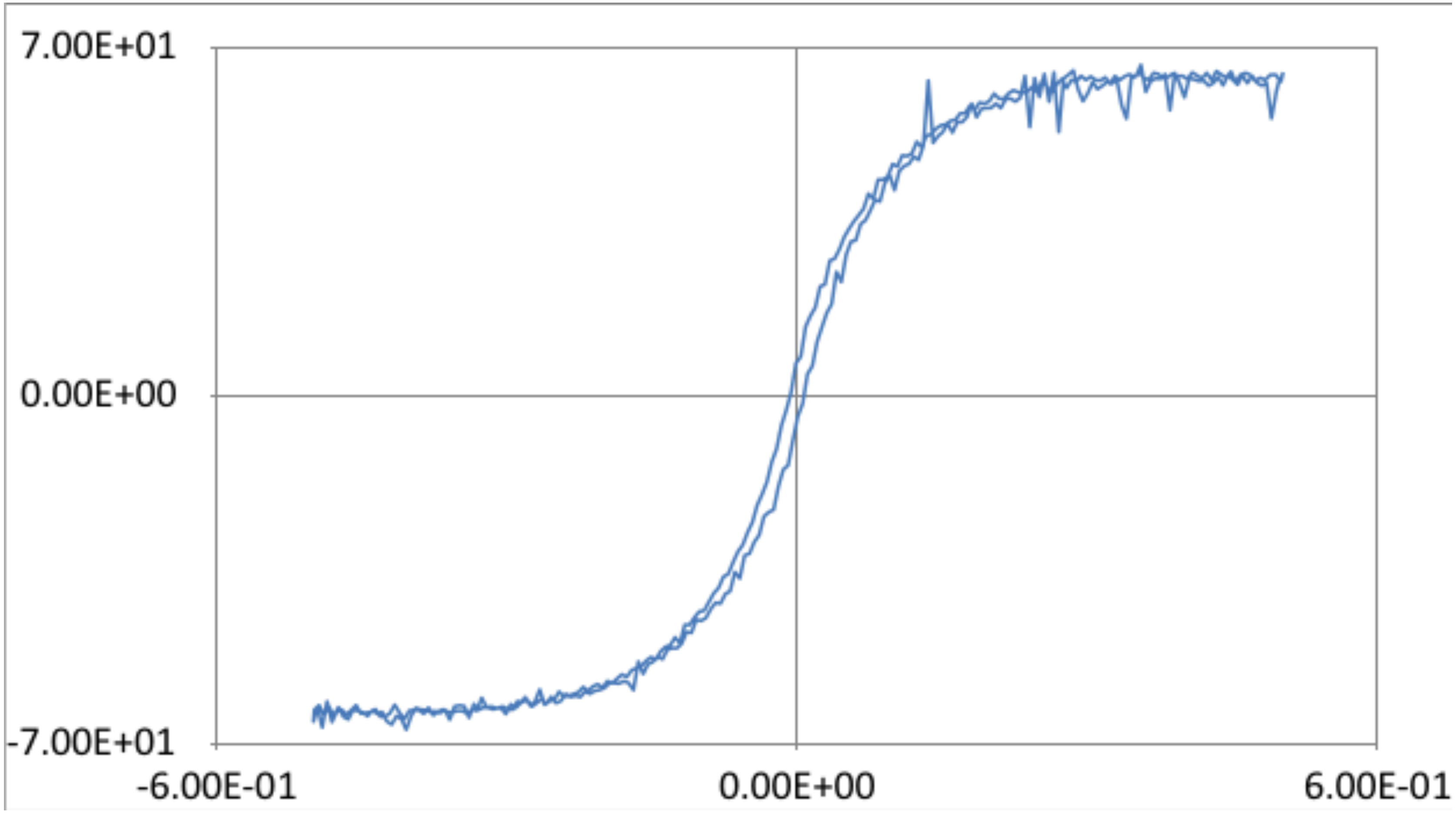
7.00E+01
0.00E+00
-7.00E+01
-6.00E-01
0.00E+00
6.00E-01

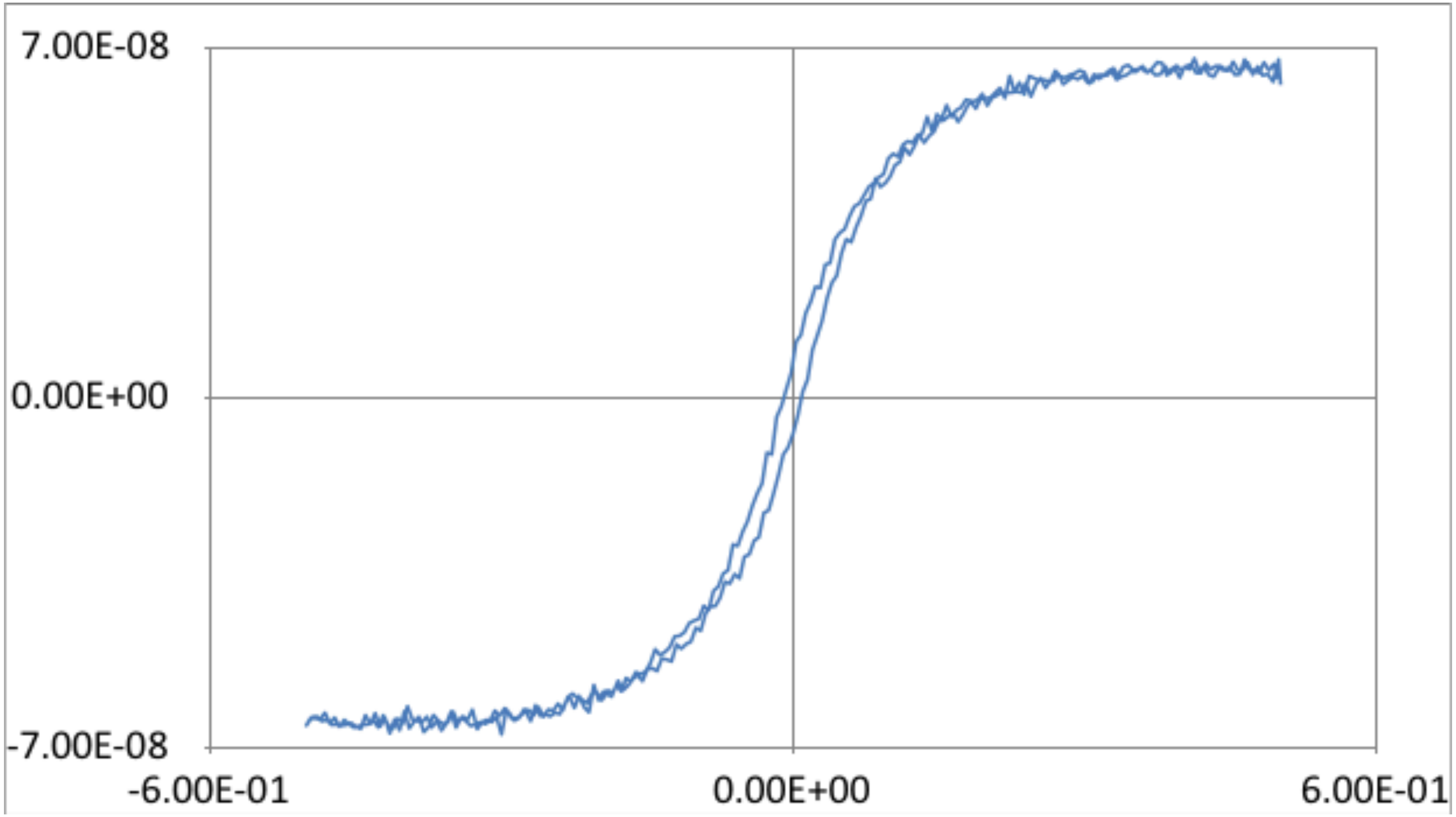
7.00E-08
0.00E+00
-7.00E-08
-6.00E-01
0.00E+00
6.00E-01

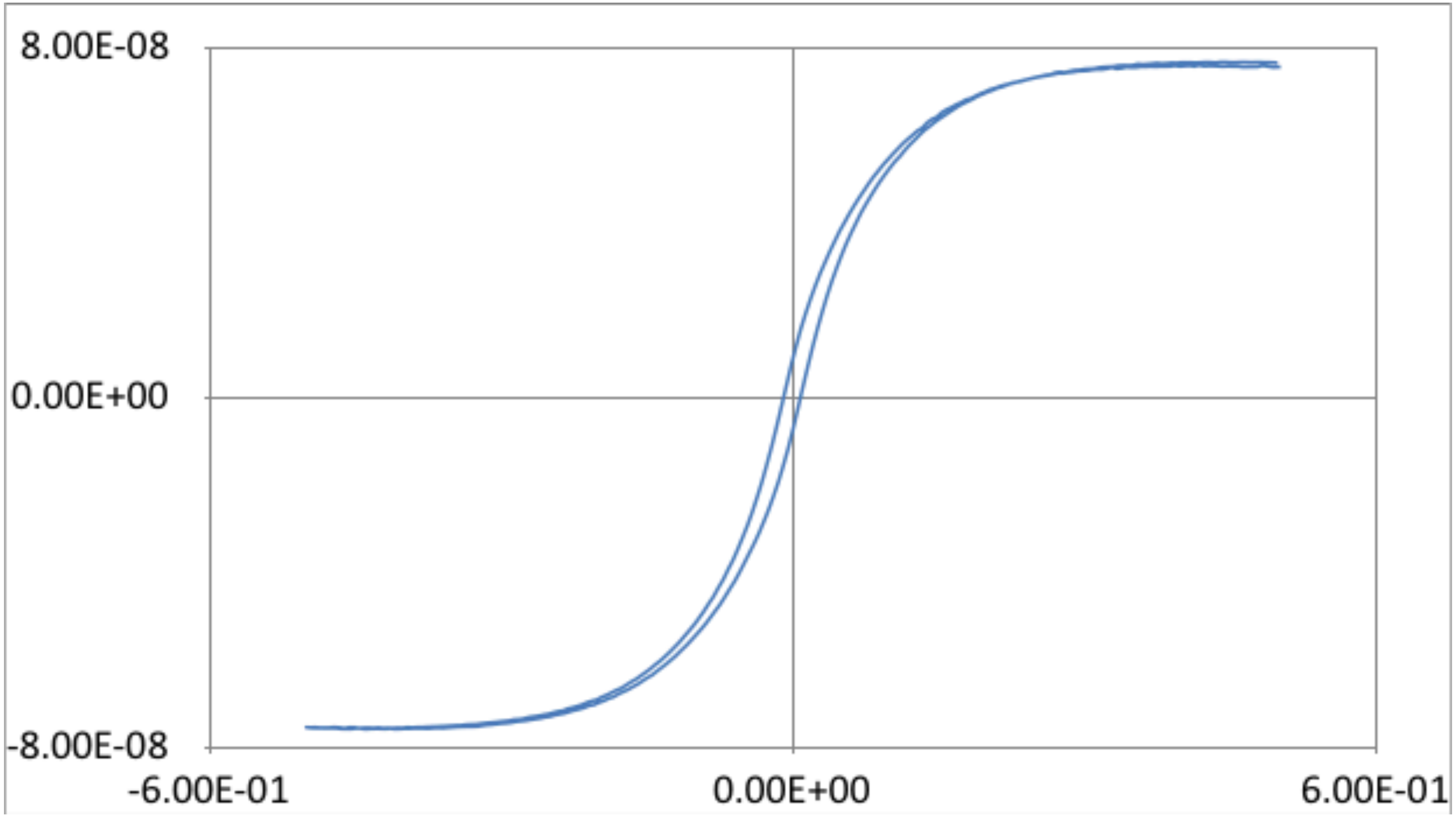
8.00E-08
0.00E+00
-8.00E-08
-6.00E-01
0.00E+00
6.00E-01